Microvascular monitoring in the ICU using high-resolution near-infrared spectroscopy

Amirali Mirsajadi

A Thesis submitted to the Faculty of Graduate Studies of The University of Manitoba in partial fulfillment of the requirements of the degree of

MASTER OF SCIENCE

Graduate Program in Biomedical Engineering

University of Manitoba

Winnipeg

Abstract

Circulatory shock, particularly septic shock, is a life-threatening condition characterized by impaired tissue perfusion and a high risk of organ failure. Conventional intensive care monitoring focuses on macro-hemodynamic parameters such as mean arterial pressure (MAP), which may not reflect the state of microvascular perfusion. High-resolution near-infrared spectroscopy (hr-NIRS) enables continuous, non-invasive monitoring of tissue hemoglobin dynamics, offering potential insight into regional microvascular function. This thesis presents two complementary analyses using hr-NIRS in critically ill patients: (1) derivation of optimal MAP (MAPopt) from skeletal muscle autoregulation signals, and (2) wavelet-based quantification of microvascular and cardiac power from NIRS signals. The study included 15 mechanically ventilated ICU patients (MAPopt study) requiring vasopressors, and 43 critically ill patients (wavelet study), along with 14 healthy volunteers recruited from a parallel study. MAPopt was derived using correlation indices between arterial pressure and NIRS signals in both skeletal muscle and brain. Muscle-derived MAPopt values moderately correlated with cerebral MAPopt ($r = 0.76$, $p < 0.001$), demonstrating the feasibility of peripheral autoregulation assessment. Notably, most muscle MAPopt values were below the standard clinical threshold of 65 mmHg, suggesting that conventional MAP targets may overestimate optimal perfusion pressure in some patients. Wavelet analysis demonstrated that microvascular power was significantly lower in ICU patients compared to healthy controls ($p < 0.001$), while cardiac power did not differ significantly. Subgroup analyses revealed no statistically significant differences in microvascular or cardiac power between survivors and non-survivors or between septic and non-septic patients. However, patients receiving vasopressors on day 1 exhibited significantly reduced microvascular power compared to those not receiving pressors ($p < 0.05$), particularly early in their ICU stay. These findings support the feasibility of deriving MAPopt from skeletal muscle and highlight the value of wavelet-based microvascular metrics in distinguishing physiologic states. Together, these techniques offer a promising framework for individualized hemodynamic monitoring and may enhance resuscitation strategies in critical care.

Key words: circulatory shock, septic shock, microvascular autoregulation, near-infrared spectroscopy (NIRS), optimal mean arterial pressure (MAPopt), wavelet transform, microvascular power

Acknowledgment of Previously Published Material

Portions of the Methods, Results, and Discussion sections of this thesis have been adapted from our previously published work: Mirsajadi A, et al. Microvascular Autoregulation in Skeletal Muscle Using Near-Infrared Spectroscopy and Derivation of Optimal Mean Arterial Pressure in the ICU: Pilot Study and Comparison with Cerebral Near-Infrared Spectroscopy. Critical Care Explorations. 2024;6(7):e1111. Permission for the inclusion of this material has been granted under the copyright policy of the journal.

Acknowledgments

I am deeply grateful to my supervisor, Dr. Asher Mendelson, whose support has gone far beyond academic mentorship. He has been a constant source of encouragement, always ready to offer thoughtful advice, celebrate small victories, and challenge me to grow. His dedication and belief in my work made the toughest moments manageable, and for that, I will always be thankful.

My sincere thanks also go to my co-advisor, Dr. Frederick Zeiler. His incredibly prompt feedback and sharp insights made a world of difference throughout this project.

I would also like to extend my appreciation to my committee members, Dr. Zahra Moussavi, Dr. Sherif Sherif, and Dr. Amir Ravandi. Their constructive feedback and thought-provoking questions brought valuable perspectives to my research.

A special shoutout goes to our wonderful team at Microvascular Monitoring in Circulatory Shock and Sepsis (MiMICSS). Raju Majumdar, Dustin Erickson, and Sumaya Alias were instrumental in the data collection process, and I couldn't have asked for better lab mates. Isuru Herath and Britney Blunderfield, thank you for your endless support, insightful discussions, and all the moments that made the journey so much brighter. I feel lucky to have worked alongside you.

I also want to acknowledge Dr. Zeiler's students, Logan Froese and Amanjyot Singh Sainbhi, who patiently introduced me to some of foundational concepts when I first started. Their generosity with their time and knowledge made those initial learning curves a little less steep.

Finally, to my parents, my family, and my friends – your unwavering support has meant everything to me. These past three years have been a whirlwind, and I couldn't have done it without your love and encouragement.

Thank you all for being part of this journey. I am forever grateful.

Table of Contents

List of Abbreviations

Abbreviation	Definition
ABP	Arterial Blood Pressure
bpm	Beats per Minute
CBF	Cerebral Blood Flow
CPP	Cerebral Perfusion Pressure
CCPopt	Optimal Cerebral Perfusion Pressure
CO	Cardiac Output
COx	Cerebral Tissue Saturation Index Correlation Index
CVP	Central Venous Pressure
CWT	Continuous Wavelet Transform
DPF	Differential Pathlength Factor
ECG	Electrocardiogram
Hb	Deoxyhemoglobin
HbO_2	Oxyhemoglobin
HbT	Total Hemoglobin
hr-NIRS	High-Resolution Near-Infrared Spectroscopy
ICP	Intracranial Pressure
ICU	Intensive Care Unit
ICM+	(Software for multimodal physiological monitoring)
MA	Microvascular Autoregulation
MAP	Mean Arterial Pressure
MAPopt	Optimal Mean Arterial Pressure
MiMICSS	Microvascular Monitoring in Circulatory Shock and Sepsis
MOx	Muscle Tissue Saturation Index Correlation Index
MVx	Muscle Total Hemoglobin Correlation Index
MV	Microvascular
NIRS	Near-Infrared Spectroscopy
SIRS	Systemic Inflammatory Response Syndrome
SOFA	Sequential [Sepsis-related] Organ Failure Assessment
SRS	Spatially Resolved Spectroscopy
StO_2	Tissue Oxygen Saturation
THx	Brain Total Hemoglobin Correlation Index
TSI	Tissue Saturation Index

List of Figures

List of Tables

1. Introduction

1.1. Background

Circulatory shock is a life-threatening condition defined by inadequate oxygen delivery to tissues, often resulting in multi-organ failure and death [1]. Septic shock, a subtype of distributive shock, is among the most common and deadly forms seen in the intensive care unit (ICU) [2]. It is caused by a dysregulated host response to infection and is characterized by profound circulatory, cellular, and metabolic abnormalities that significantly increase the risk of mortality [3].

Despite improvements in ICU care, septic shock remains challenging to manage. Current treatment protocols focus on restoring systemic hemodynamics using fluid resuscitation, vasopressors, and inotropes. Clinical monitoring typically relies on macro-hemodynamic indicators, such as mean arterial pressure (MAP), cardiac output (CO), central venous pressure (CVP), and serum lactate [4], [5]. However, there is growing recognition that these parameters may not adequately reflect regional tissue perfusion, especially at the microvascular level, where oxygen delivery and exchange occur [6].

The mismatch between global hemodynamic targets and microvascular perfusion is particularly problematic in sepsis, where systemic inflammation disrupts endothelial integrity, causes vasodilation, and impairs microvascular autoregulation. This can lead to a phenomenon known as "loss of hemodynamic coherence," in which patients may meet systemic blood pressure targets but still suffer from inadequate oxygen delivery at the tissue level [7]. Persistent microvascular dysfunction is associated with poor outcomes, including organ failure and death [8].

The microcirculation comprises small vessels, including arterioles, capillaries, and venules, responsible for delivering oxygen and nutrients to tissues. In conditions like septic shock, microvascular dysfunction is common and contributes significantly to organ failure. Restoration of macro-hemodynamic parameters does not guarantee microvascular recovery, and evidence suggests that persistent microvascular impairment is associated with poor outcomes [6].

Despite its importance, microvascular perfusion is not routinely monitored in the ICU. Clinical tools that provide real-time information about microcirculatory dynamics are limited,

and there is a growing need for non-invasive, bedside-compatible technologies that can bridge this gap.

Recent advances in near-infrared spectroscopy (NIRS), an optical technique that measures tissue oxygenation by detecting light absorption changes in hemoglobin, allow for the non-invasive assessment of microvascular function, offering real-time insights into regional perfusion. Tissue hemoglobin oxygen saturation (StO2) and total hemoglobin content (HbT) have been proposed as potential markers for tissue hypoxia and systemic perfusion adequacy [9]. Additionally, patient-specific optimal MAP (MAPopt), derived from correlation indices between MAP and NIRS-derived hemoglobin fluctuations, has been proposed as a more physiologically relevant target for individualized blood pressure management [10].

Despite these advancements, significant gaps remain in understanding the relationship between microvascular function, MAPopt, and patient outcomes in critical illness. Furthermore, the role of wavelet-based microvascular power (MV power) as an outcome predictor in septic and non-septic shock has not been fully explored. This thesis aims to address these gaps by evaluating the NIRS-derived microvascular power, MAPopt, and patient survival in the ICU.

1.2. Research Problem

Traditional monitoring techniques often rely on macro-hemodynamic parameters like MAP to guide resuscitation, but these metrics can fail to capture the state of the microvasculature, which is vital for oxygen delivery at the cellular level [11]. Impaired microvascular autoregulation in various forms of shock can result in tissue hypoxia, even when global hemodynamic parameters appear normalized [12]. This study addresses the need for advanced monitoring techniques that account for both macrocirculation and microvascular function to improve the understanding and management of critically ill patients experiencing shock.

Current hemodynamic monitoring tools, including traditional MAP targets, also fail to account for individual variations in microvascular perfusion and autoregulation [13]. Although interventions such as vasoactive medications are utilized to maintain MAP, they do not directly assess or optimize microvascular function, which is critical for determining outcomes in septic shock [14]. A significant gap in knowledge exists regarding the lack of methods to establish an

individualized MAPopt that ensures adequate microvascular perfusion. Notably, skeletal muscle MAPopt in humans has not been studied at all, highlighting a crucial area for exploration. Additionally, there is an absence of robust techniques for non-invasively monitoring microvascular dynamics in the ICU. Existing research primarily focuses on macrocirculatory parameters, leading to under-monitoring of microvasculature, and does not adequately investigate how wavelet-transform-based analysis of microvascular signals could provide deeper insights into patient-specific hemodynamics [15].

1.3. Two Complementary Studies in This Thesis

This thesis investigates two independent but complementary approaches for leveraging hr-NIRS to improve physiological monitoring in the ICU:

Study 1 – MAPopt from Skeletal Muscle Autoregulation:

This study explores whether an individualized optimal MAP (MAPopt) can be derived from skeletal muscle NIRS signals using autoregulatory indices. While MAPopt derived from cerebral NIRS has shown promise, its calculation from peripheral tissues remains largely unexplored. Establishing muscle-derived MAPopt could offer a non-invasive, regionally relevant perfusion target.

Study 2 – Wavelet-Based Microvascular and Cardiac Power:

This study applies continuous wavelet transform (CWT) to hr-NIRS signals to extract frequency-specific power in the microvascular (about 0.005–0.02 Hz) and cardiac (about 0.5–2 Hz) bands. The aim is to evaluate whether these metrics can differentiate between healthy individuals and critically ill patients, and whether they relate to clinical states such as vasopressor requirement, sepsis, or survival.

Together, these studies aim to advance the field of personalized perfusion monitoring by introducing new tools for assessing microvascular function at the bedside.

1.4. Knowledge Gap

There is currently no widely accepted method for real-time, individualized monitoring of microvascular perfusion in critically ill patients. While cerebral MAPopt monitoring has gained traction, no prior study has evaluated MAPopt using skeletal muscle NIRS in the ICU. Moreover, traditional signal analysis techniques fail to capture the dynamic, frequency-specific nature of microvascular signals.

The application of wavelet analysis to hr-NIRS is novel and may uncover features that are invisible to time-domain or spectral averaging approaches. However, the clinical utility of wavelet-derived microvascular and cardiac power remains unexplored in ICU patients.

1.5. Objectives and Hypotheses

This thesis investigates two independent but complementary approaches to microvascular monitoring in critically ill patients using high-resolution near-infrared spectroscopy (hr-NIRS):

(1) derivation of optimal mean arterial pressure (MAPopt) from skeletal muscle autoregulation signals, and

(2) application of wavelet-based analysis to quantify microvascular and cardiac power from NIRS signals.

MAPopt Study Objectives and Hypotheses

1. To evaluate skeletal muscle microvascular autoregulation in critically ill patients requiring vasoactive medications and mechanical ventilation using high-resolution near-infrared spectroscopy (hr-NIRS) and arterial blood pressure (ABP) signals. This objective arises from the need to better understand microvascular function in critically ill patients, as systemic hemodynamic measures often fail to capture localized perfusion abnormalities. By studying skeletal muscle autoregulation, we can assess how well the microcirculation adapts to physiological stressors and whether this adaptation can inform patient management.

Hypothesis 1: Skeletal muscle MAPopt can be feasibly calculated from hr-NIRS and ABP signals in most ICU patients.

2. To compare skeletal muscle-derived MAPopt values with the standardized mean arterial pressure (MAP) target of 65 mmHg used in ICU clinical practice. Standard ICU resuscitation protocols are typically based on fixed MAP goals (e.g., 65 mmHg), yet emerging evidence indicates that these may not be optimal for all patients. By determining whether muscle MAPopt values deviate from the standard threshold, this objective seeks to explore the need for individualized blood pressure targets.

Hypothesis 2: The individualized optimal mean arterial pressure (MAPopt) derived from skeletal muscle values in septic shock patients will differ significantly from standard MAP targets used in ICU practice

3. To examine the correlation between optimal MAP values derived from skeletal muscle and those derived from cerebral hr-NIRS signals. While brain NIRS has been used to estimate MAPopt in neurocritical care, peripheral muscle signals are more accessible and may reflect systemic autoregulatory status. By comparing muscle and cerebral MAPopt, we aim to evaluate the consistency and potential clinical interchangeability of the two monitoring sites.

Hypothesis 3: There is a significant positive correlation between skeletal muscle and brain-derived MAPopt in ICU patients, indicating that peripheral autoregulation monitoring may provide a valid surrogate for cerebral measurements.

Wavelet Study Objectives and Hypotheses

4. To evaluate differences in wavelet-derived microvascular and cardiac power between critically ill ICU patients and healthy controls using hr-NIRS signals. Conventional static measures of perfusion often fail to capture dynamic features of vascular tone and flow. Wavelet analysis enables the decomposition of NIRS signals into frequency bands associated with specific physiological mechanisms. This objective aims to assess whether critically ill patients exhibit impaired power in the microvascular and cardiac frequency bands compared to healthy individuals.

Hypothesis 4: ICU patients with septic shock will show lower microvascular power and greater variability in microvascular autoregulation compared to healthy controls.

5. To assess the relationship between wavelet-derived microvascular power and clinical outcomes, including survival and sepsis status, using hr-NIRS signals. Microvascular dysfunction is a hallmark of poor prognosis in critical illness. This objective evaluates whether wavelet-based power metrics from hr-NIRS signals can distinguish survivors from non-survivors and differentiate septic from non-septic patients.

Hypothesis 5: Microvascular power will be significantly higher in patients who survived and in those without septic shock.

6. To investigate temporal changes in wavelet-derived microvascular power between day 1 and day 3 of ICU admission, based on hr-NIRS signal analysis, and assess their association with patient outcomes. Critical illness is a dynamic process, and microvascular recovery or deterioration may evolve over time. This objective explores whether changes in microvascular power derived from hr-NIRS signals over multiple days can help differentiate patients with improving versus worsening physiology.

Hypothesis 6: Microvascular power derived from hr-NIRS signals will increase over time in ICU survivors but remain low or decline in non-survivors.

1.6. Thesis Outline

This thesis consists of six chapters, beginning with the introduction and culminating in the discussion of key findings and future research directions.

The second chapter provides a comprehensive review of the literature relevant to this study. It explores the pathophysiology of circulatory shock, particularly focusing on septic shock and its microvascular implications. The chapter also covers current methods of hemodynamic monitoring in critical care, highlighting the limitations of macrovascular-based strategies and the emerging role of near-infrared spectroscopy (NIRS). Furthermore, it delves

into the principles of physiological signal analysis, with particular emphasis on wavelet-based techniques for assessing microvascular dynamics.

Chapter three describes the study design and data acquisition protocols, including patient recruitment, inclusion/exclusion criteria, and the recording and preprocessing of NIRS and arterial blood pressure (ABP) signals. The chapter details the overall framework for preparing signals for MAPopt and wavelet studies, along with the general pre-processing methods employed.

Chapter four focuses specifically on MAPopt analysis in skeletal muscle. It explains the methods used to quantify microvascular autoregulation and derive MAPopt, followed by results highlighting its clinical relevance.

Chapter five presents the wavelet-based signal processing and the derivation of microvascular and cardiac powers from the muscle NIRS signals. The chapter reports on temporal changes and comparisons between patient subgroups, examining the relationship between microvascular spectral features, vasopressor therapy, and survival.

The final chapter combines discussion and conclusions, synthesizing the study's key findings and situating them within the broader critical care literature. It critically compares the results with previous studies, emphasizing their clinical and theoretical implications. Additionally, this chapter highlights study limitations, identifies potential biases, and discusses areas for future research. The chapter concludes with revisiting study's hypotheses and comparing them with the results.

2. Literature Review

2.1. Circulatory Shock

Circulatory shock is a life-threatening condition characterized by an imbalance between oxygen supply and demand [16]. It can be caused by various factors, including hypovolemia, cardiogenic issues, obstructive conditions, and distributive problems [17]. Early diagnosis and prompt treatment are crucial for a positive outcome [18]. Treatment typically involves interventions to increase oxygen delivery and address the underlying cause [16]. Despite ongoing research, the condition remains a significant challenge in critical care, with mortality estimates of approximately 50% [19].

2.1.1. Definition

Shock can be described as a critical, widespread state of acute circulatory failure, linked to insufficient oxygen uptake by cellular structures [2]. The term 'shock' was first used in English by surgeon George Guthrie in 1827 to describe the physiological response to injury [20]. Throughout its history, the study of shock has evolved from focusing on traumatic shock to emphasizing distinguishing between various clinical syndromes and their clinical and pathological features [21].

Currently, the term "shock" is applied to critically ill patients experiencing various distinct pathophysiological states, like significant cardiac dysfunction or major infections, which all result in inadequate tissue perfusion and oxygen delivery, as well as aberrant cellular oxygen utilization [22]. This compromised microcirculation can lead to certain clinical manifestations, such as mottling of the skin, acrocyanosis, and prolonged capillary refill time [2].

2.1.2. Pathophysiology

Shock can originate from any of four fundamental pathophysiological origins: significant fluid depletion either within or external to the body (hypovolemic shock), cardiac influences including heart attacks or irregular rhythms (cardiogenic shock), blockages like blood clots in the lungs or compression of the heart (obstructive shock), and systemic vasodilation as observed in intense infections or allergic reactions (distributive shock) [1].

The progression of shock occurs through several sequential stages. It starts with the early stage and moves towards the compensatory phase, during which the body utilizes intrinsic mechanisms to enhance blood flow and preserve stability. As shock progresses, compensatory mechanisms become overwhelmed, leading to progressive deterioration characterized by metabolic acidosis and tissue damage. In the absence of prompt therapeutic measures, shock can enter a refractory stage, leading to permanent cellular impairment, multiple organ dysfunction, and substantially increased mortality risk [23], [24].

2.1.2.1. Hypovolemic Shock

Hypovolemic shock can arise due to blood loss that is either external or internal, such as gastrointestinal or urinary tract hemorrhage, a hemothorax, or a hematoma in soft tissues, as well as from the depletion of fluid into third spaces, examples of which include ileus and peritonitis [25]. This medical condition is systematically categorized into four levels depending on the percentage of circulatory blood volume that is lost, ranging from mild shock at less than 15% to severe shock when the loss exceeds 40% [26].

A severe shock can impair essential organs like the brain and heart. Hypovolemic shock induces a series of physiological reactions, including the constriction of blood vessels to sustain blood pressure and the perfusion of tissues. Early symptoms may include restlessness, cool skin, and mild rapid heartbeat, while late signs include confusion, low blood pressure, and rapid heartbeat [27].

2.1.2.2. Cardiogenic Shock

Cardiogenic shock arises when the heart fails to pump sufficiently, causing insufficient perfusion of tissues, often because of an acute myocardial infarction. Clinically, it's defined by reduced cardiac output and tissue oxygen deprivation despite adequate blood volume [28]. Initially, the body tries to compensate by narrowing blood vessels to improve blood flow, but this puts extra strain on the already damaged heart. Inflammation worsens the situation by causing abnormal widening of blood vessels, which further affects heart function. In some cases, right ventricular failure occurs, where the right side of the heart can't pump blood effectively, leading to poor blood flow to organs and increased pressure in the veins [29].

2.1.2.3. Obstructive Shock

Obstructive shock involves blockage in the cardiovascular system, leading to problems with heart filling or increased pressure against which the heart must pump. This blockage reduces the heart's ability to pump blood effectively, resulting in inadequate oxygen delivery. Causes include tension pneumothorax, cardiac tamponade, and pulmonary embolism [30], [31].

2.1.2.4. Distributive (Septic) Shock

Distributive shock represents the predominant form of circulatory shock. Often, sepsis serves as the precipitating factor for distributive shock (septic shock); however, disturbances in immune, neurological, and endocrinological systems may also play a role in the development of this severe condition [32]. Sepsis has classically been defined as a systemic inflammatory response syndrome (SIRS) caused by infection, characterized by the invasion of normally sterile tissue or body cavities by pathogenic microorganisms. Severe sepsis was diagnosed when sepsis was accompanied by hypoperfusion or organ dysfunction [33]. However, these definitions have evolved over time.

The Third International Consensus Definitions for Sepsis and Septic Shock (Sepsis-3) now define sepsis as 'life-threatening organ dysfunction caused by a dysregulated host response to infection'. Organ dysfunction is operationalized as an acute increase in the Sequential [Sepsis-related] Organ Failure Assessment (SOFA) score by 2 points or more, which correlates with a significant risk of mortality. The Sepsis-3 task force further concluded that the term severe sepsis is redundant, as sepsis inherently involves life-threatening organ dysfunction. This update reflects a deeper understanding of sepsis pathobiology and improves its clinical identification [3].

While bacterial infections are the most common cause of sepsis, it can also result from other infections such as viruses (e.g. SARS-CoV-2, influenza), parasites, or fungi. When pathogens invade the body, the immune system initiates a response by releasing pro-inflammatory cytokines, including tumor necrosis factor (TNF) and interleukins (IL-1 and IL-6). While these mediators are essential for combating infections, they can also trigger excessive systemic inflammation, resulting in endothelial dysfunction, increased vascular permeability, and vasodilation. The extreme dilation of blood vessels and leakage of capillaries into the interstitial space leads to hypoperfusion and inadequate oxygen and

nutrient delivery to tissues. This vasodilation contributes to low blood pressure, which is further aggravated by a decrease in vascular tone and the inability of blood vessels to properly constrict. Nitric oxide and other vasodilatory substances play a key role in sustaining this reduced vascular tone. Additionally, the injury to endothelial cells impairs microvascular function, further contributing to tissue hypoxia and organ dysfunction. [34].

According to the Sepsis-3 definition, septic shock is defined as 'a subset of sepsis in which underlying circulatory, cellular, and metabolic abnormalities are profound enough to substantially increase mortality'. Clinically, septic shock is identified by the requirement of vasopressors to maintain a mean arterial pressure (MAP) of 65 mmHg or greater, along with a serum lactate level greater than 2 mmol/L despite adequate fluid resuscitation, which is associated with a mortality rate exceeding 40%. This definition emphasizes the severity spectrum of sepsis, differentiating septic shock as the most life-threatening form of the condition [3]. In septic shock, the cardiovascular system fails to maintain sufficient blood pressure due to reduced systemic vascular resistance (SVR) and myocardial depression. Additionally, sepsis-induced myocardial dysfunction impairs the heart's ability to pump effectively, further contributing to circulatory failure. This combination of low SVR, cardiac dysfunction, and capillary leakage results in refractory hypotension, hypoperfusion, and ultimately multi-organ failure if left untreated [35], [36].

2.1.3. Epidemiology

The epidemiology of circulatory shock includes a broad range of research undertaken in different geographic areas and medical environments. Such research offers a critical understanding concerning the incidence, causes, and consequences related to circulatory shock. In the SOAP study conducted in European countries in 2002, involving 3,147 patients, 33.6% experienced shock at some point, and among these patients, septic shock accounted for 14.7% of cases, representing the largest proportion of shock patients. The ICU mortality rate for patients with shock was 38.3%, while hospital mortality reached 44.6%. Importantly, mortality rates were even higher in patients with septic shock, with an ICU mortality rate of 47.4% and a hospital mortality rate of 54.1%, compared to non-septic shock cases, where ICU and hospital mortality rates were 31.2% and 37.2%, respectively [37].

A cross-sectional study conducted in Egypt in 2017 examined 4,997 patients admitted to medical ICUs. Among them, 13.9% were diagnosed with circulatory shock. Hypovolemic shock was the most common subtype (51.4%), followed by septic shock (36.5%) and cardiogenic shock (12.1%) [38]. Data from the Critical Care Cardiology Trials Network (CCCTN) Registry, which included 3,048 cardiac ICU admissions in the US and Canada from September 2017 to September 2018, highlighted a 22% prevalence of shock meeting clinical criteria. Cardiogenic shock was the predominant subtype (68%), with a mortality rate of 28% in cardiogenic patients [39].

In the United States, severe sepsis is estimated to occur in approximately 300 cases per 100,000 population [40]. Mortality rates for septic shock have improved in recent years, now ranging from approximately 30-40%, according to a meta-analysis and national database studies [41], [42]. Risk factors for severe sepsis include older age, male gender, black race, and a higher burden of chronic health conditions [40]. A study conducted in England from January 2011 to December 2015, involving 654,918 admissions to adult general ICUs, reported a 30.2% prevalence of sepsis or septic shock. The mortality rate for septic shock decreased from 37% in 2011 to 33% in 2015 [43]. Independent risk factors for acute hospital mortality included increasing age, male gender, severe comorbidities, increasing dependency, and worsening APACHE II acute physiology score [43].

2.1.4. Diagnosis

Diagnosis and monitoring of acute circulatory failure rely on assessing arterial hypotension alongside signs indicating altered tissue perfusion. Key clinical features include altered mental status, reduced capillary refill, and oliguria, complemented by hemodynamic parameters and tissue hypoxia monitors for a comprehensive evaluation [44]. The traditional definition of shock has been closely associated with hypotension; however, recent insights suggest that this criterion may not be sufficient for a comprehensive characterization of shock states [45].

Despite normal or maintained arterial blood pressure, markers of inadequate tissue perfusion such as elevated blood lactate levels, reduced mixed venous oxygen saturation (SvO2), and low central venous oxygen saturation (ScvO2) can be indicative of underlying

shock. This recognition of other markers has led to the exclusion of hypotension from the mandatory criteria for defining shock, except in the case of septic shock [45].

Elevated blood lactate levels are a critical biomarker for diagnosing and monitoring shock, particularly in sepsis. Lactate is produced from pyruvate through glycolysis and reflects a balance between its production and clearance. In sepsis, hyperlactatemia arises from multiple mechanisms, including adrenergic-driven increases in glycolysis (aerobic processes), mitochondrial dysfunction, and impaired clearance by the liver and kidneys. Anaerobic glycolysis due to tissue hypoxia and hypoperfusion remains a contributing factor, especially in cases of severe microvascular dysfunction, but recent evidence highlights the predominant role of aerobic pathways as part of the stress response [5], [46]. Elevated lactate levels, typically defined as greater than 2 mmol/L, are associated with metabolic stress, illness severity, and poor outcomes in septic patients. Persistent hyperlactatemia has been strongly linked to increased mortality, underscoring its importance in the clinical management of sepsis [47].

Beyond the common symptoms shared among all shock subtypes, each category of shock has distinct diagnostic indicators. Hypovolemic shock is identified by a patient's pale appearance, poor perfusion, and cold, clammy skin. Cardiogenic shock diagnosis includes observing signs of left ventricular dysfunction, such as pulmonary crepitations, a weak volume pulse, and a gallop rhythm, often accompanied by raised jugular venous pressure and peripheral edema. Obstructive shock is diagnosed through specific signs like pulsus paradoxus, a significant drop in systolic blood pressure upon inspiration, and elevated jugular venous pressure. Distributive shock, which can be warm or cold, is initially diagnosed by bounding pulses and a change in skin temperature, with progression to poor perfusion and hypovolemia [48].

2.1.5. Treatment

Effective management of circulatory shock hinges on two pivotal actions: addressing the root cause and restoring blood flow and oxygen delivery to tissues. For instance, in hemorrhagic shock, it is crucial to halt bleeding, while cardiogenic shock from a heart attack may require clot-dissolving drugs or procedures like angioplasty and coronary stenting. Obstructive shock caused by fluid around the heart necessitates drainage, and for shock due to a pulmonary embolism, removing the blockage through medical or interventional means is key.

In cases of septic shock, prompt antibiotic treatment and elimination of the infection source are essential [49]. Once the underlying cause is addressed, resuscitation aims to restore tissue perfusion and oxygen delivery. This often involves ventilation, fluid infusion, and vasopressor and inotropes [20].

2.1.5.1. Ventilation

Immediate oxygen administration is crucial for enhancing oxygen delivery. Endotracheal intubation is recommended for most patients experiencing severe respiratory distress or acidemia, as it not only aids in breathing but also reduces cardiac stress. However, the initiation of invasive ventilation requires careful monitoring for potential hypovolemia, and sedative use should be minimized to prevent further cardiovascular compromise [1].

A prospective multicenter observational study aimed to investigate the timing and setting for tracheal intubation and mechanical ventilation in septic shock patients. A total of 859 patients from 30 ICUs in France and Spain were included. The study found that 24% of patients were intubated by hour 8 and 38% by hour 72 of their ICU stay [50].

2.1.5.2. Fluid Therapy

Fluid repletion is a common necessity in shock patients, primarily aimed at reversing hypovolemia. Regardless of the cause, restoring adequate cardiac output and arterial pressure through volume repletion is crucial for normal perfusion of vital organs and tissues. While fluid repletion is generally more effective in restoring circulation during early hypovolemic states, its efficacy diminishes in later stages. However, over-resuscitation and excessive fluid administration are associated with poor outcomes, including increased mortality, pulmonary edema, coagulopathy, and abdominal compartment syndrome [51].

Excess fluid can also contribute to tissue edema, impairing oxygen delivery and exacerbating organ dysfunction. Crystalloids, such as 0.9% saline, distribute widely in extracellular space but have limited volume-stabilizing effects, necessitating repeated boluses. Excessive use of crystalloids can lead to hyperchloremic acidosis and renal dysfunction. Colloids, while expanding plasma volume more rapidly with smaller doses, are costlier and associated with side effects such as impaired coagulation, anaphylactic

reactions, and renal dysfunction (especially with hydroxyethyl starch). Thus, fluid administration must be carefully titrated to avoid volume overload and achieve resuscitation endpoints [52].

2.1.5.3. Vasopressors and Inotropes

Vasopressors and inotropes are types of drugs that are administered to constrict blood vessels or to enhance the heart's pumping strength, respectively [53]. Ahlquist's work in 1948 identified alpha- and beta-adrenergic receptors, which influenced how drugs are classified. Alpha-agonists like phenylephrine and methoxamine primarily raise blood pressure by constricting arteries. Beta-agonists like isoproterenol increase heart output and rate but can raise oxygen demand. Adrenergic drugs such as epinephrine and norepinephrine affect both alpha and beta receptors, impacting arterial resistance and heart function differently [54].

Choosing the right vasopressor in septic shock is challenging. Norepinephrine and dopamine are commonly used, with dopamine having stronger inotropic effects. Norepinephrine is often combined with dobutamine due to its weaker inotropic. Epinephrine, which combines vasopressor and inotropic effects, is another option. Phenylephrine, mainly a vasopressor, is occasionally used as well [55].

Defining appropriate blood pressure targets is crucial in managing septic shock to optimize patient outcomes. Mean arterial pressure (MAP) is commonly used as a target for vasopressor therapy in septic shock, with the Surviving Sepsis Guidelines recommending an initial target of MAP $\geq$ 65 mmHg to ensure adequate organ perfusion during resuscitation [56].

However, evidence indicates that blood pressure targets should not follow a “one-size-fits-all” approach, especially in the diverse ICU population. Asfar et al. compared two MAP targets in septic shock patients, randomizing them to either a high MAP target (80-85 mmHg) or the standard target (65-70 mmHg). The trial found no significant difference in mortality between the groups, though the higher target was linked to increased vasopressor use and a higher risk of atrial fibrillation. Subgroups, such as patients with chronic hypertension, benefited from higher MAP targets due to pre-existing vascular adaptations [4].

2.2. Critical Care and Microvascular Monitoring

Critical illness represents a complex state where vital organ dysfunction poses an immediate threat to life, necessitating swift and comprehensive care to support organ functions and increase the chances of reversibility [57]. This complex state is often manifested through syndromes like sepsis, acute respiratory distress syndrome (ARDS), and delirium, which are identified by their clinical presentations rather than distinct biological markers and can vary greatly in their triggers and patient responses [58]. In Manitoba, the data shows that 0.5% of adults require intensive care annually, pointing to the significant role these conditions play within the healthcare framework [59].

2.2.1. Hemodynamic Monitoring

Hemodynamic monitoring is a vital aspect of critical care that involves evaluating cardiovascular function to ensure adequate blood flow and oxygenation to the tissues [60]. This includes a range of techniques, from basic clinical assessments to advanced invasive methods, aimed at assessing the patient's cardiovascular status and guiding therapeutic interventions [61]. Common monitoring methods include central venous catheters, pulmonary artery catheters, invasive arterial monitoring, and ultrasonography [60], [61].

Recent advances in technology have led to the development of non-invasive and minimally invasive techniques to assess various cardiovascular parameters. These include pulse-wave analysis for evaluating cardiac output derived from arterial blood pressure tracing, thoracic bioimpedance for estimating cardiac output by measuring the thorax's electrical conductivity, and esophageal doppler, which employs ultrasound technology to measure blood flow velocity in the descending aorta using an esophageal probe [62]. By integrating various hemodynamic parameters and monitoring techniques, clinicians can determine a patient's cardiovascular condition and develop appropriate treatment strategies [63].

The Cecconi consensus emphasizes the importance of tailoring hemodynamic monitoring strategies to individual patient needs. It advocates for the use of dynamic over static variables, like stroke volume variation and pulse pressure variation, to predict fluid responsiveness. The consensus also highlights echocardiography as the preferred modality for initial assessment of shock, given its ability to rapidly identify the type of circulatory failure [2], [64]

2.2.2. Microcirculation and Microvascular Monitoring

Microcirculation plays a pivotal role in maintaining tissue nutrition, oxygen delivery, and organ function [65]. It encompasses the terminal vascular bed, comprised of vessels less than 150μ in diameter, responsible for oxygen transfer, waste removal, permeability, and various regulatory functions [66]. The microcirculation maintains adequate blood flow through autoregulation, stabilizing capillary pressure despite fluctuations in arterial perfusion pressure [65]. This system is crucial for meeting cellular energy requirements, supporting functional activity, and maintaining homeostasis over a wide physiological range of systemic perfusion [66]. The microcirculation represents the smallest functional unit of the cardiovascular system, offering a unique perspective on disease processes and bridging the gap between clinical and molecular medicine [67].

Recent studies have focused on the effects of diseases, drugs, and fluids on this critical system [66]. Monitoring microvascular circulation is of great importance in critical care as it provides valuable insights into tissue perfusion and oxygenation. There are various bedside techniques available for evaluating microcirculation in critically ill patients, such as laser Doppler fluxmetry, venous congestion plethysmography, intravital microscopy, and gastrointestinal pCO2-tonometry [68].

Although side-stream dark field (SDF) imaging devices can visualize microvascular blood flow, automated analysis methods are being developed to improve reliability [69]. Alterations in microvascular perfusion have been observed in patients with sepsis, cardiogenic shock, and high-risk surgery, often characterized by heterogeneity of flow [70]. These alterations are associated with organ dysfunction and poor patient outcomes [71].

In a study conducted by De Backer et al. the proportion of perfused small vessels (< 20 μm) was significantly reduced in patients with cardiac failure and cardiogenic shock (63% and 49%, respectively) compared to control patients (92%). Moreover, patients who survived had a higher proportion of perfused vessels (90% in all vessels and 64% in small vessels) compared to non-survivors (81% and 43%, respectively) [72].

Another study by De Backer et al. using orthogonal polarization spectral imaging demonstrated significant microcirculatory changes in patients with severe sepsis, which were not observed in healthy volunteers or non-septic critically ill patients. The density of all vessels was markedly reduced in patients with sepsis (median: 4.5 vessels/mm) compared to healthy

volunteers (median: 5.4 vessels/mm, $p < 0.01$). The proportion of perfused small vessels (<20 μm) was also significantly lower in septic patients (48% versus 90% in healthy controls, $p < 0.001$), and these alterations were even more pronounced in non-survivors [73].

Monitoring microcirculation may provide a more physiological approach to understanding pathogenesis, diagnosis, and treatment in critical care, especially when there is a loss of hemodynamic coherence between macrocirculation and microcirculation [74]. Capillary refill time (CRT) and peripheral perfusion are straightforward bedside tools for assessing microcirculatory status. CRT measures the time for color to return to blanched skin after pressure, with prolonged CRT indicating impaired peripheral perfusion. Peripheral perfusion assessments, including skin temperature and mottling, provide early warnings of microcirculation deterioration, especially in septic or shock patients. These indicators correlate with outcomes, as poor peripheral perfusion is linked to higher mortality in critically ill patients [75].

The ANDROMEDA study (2019) examined peripheral perfusion-guided resuscitation in septic shock, comparing resuscitation targeting lactate levels versus CRT. It found that CRT-targeted resuscitation resulted in lower mortality compared to lactate-guided resuscitation. This underscores the importance of directly monitoring microcirculation and peripheral perfusion in managing shock patients. The study supports perfusion-guided resuscitation, emphasizing tissue-level perfusion over global hemodynamic parameters like lactate clearance or blood pressure [76].

The different technologies available for microvascular monitoring each have unique benefits and limitations, summarized in Table 2.1. Among these methods, near-infrared spectroscopy (NIRS) offers a non-invasive, continuous, and quantitative approach to assessing tissue oxygenation, making it highly suitable for clinical and research applications in critically ill patients. In this study, NIRS was chosen because it allows for the assessment of regional oxygenation in real time, providing valuable insights into microvascular function and its coherence with macrocirculation. This method aligns with the study's aim to evaluate microvascular autoregulation and its implications for patient outcomes in septic shock and other critical conditions.

Table 2.1 Overview of Microvascular Monitoring Techniques, Their Benefits, and Limitations

Technique	Description	Benefits	Limitations
Laser Doppler Fluxmetry	Measures blood flow by detecting frequency shifts in laser light reflected by moving red blood cells.	Non-invasive, continuous monitoring, good for superficial tissues.	Limited to surface tissues; does not provide direct visualization of microvasculature.
Venous Congestion Plethysmography	Measures changes in blood volume in a limb or organ to assess venous outflow and microvascular function.	Non-invasive, useful for functional assessments.	Not widely available; challenging in critically ill patients due to movement artifacts.
Intravital Microscopy	Direct visualization of microvascular blood flow using a microscope.	High-resolution, detailed evaluation of microcirculation dynamics.	Invasive; primarily used in research; not suitable for routine clinical use.
Gastrointestinal pCO2-Tonometry	Assesses regional gut perfusion by measuring carbon dioxide levels in the gastrointestinal mucosa.	Provides information on splanchnic perfusion; useful in abdominal surgery or septic shock.	Invasive, operator-dependent, and susceptible to measurement variability.
Side-stream Dark Field (SDF) Imaging	Visualizes microvascular flow in real time using reflected light.	Portable, bedside visualization of microcirculation.	Requires manual analysis; limited tissue penetration; affected by motion artifacts.
Orthogonal Polarization Spectral (OPS) Imaging	Like SDF, it uses polarized light to visualize microvascular blood flow.	Portable and provides high-resolution images of microcirculation.	Expensive, requires training; prone to inter-observer variability.
Near-Infrared Spectroscopy (NIRS)	Measures tissue oxygenation by detecting light absorption in hemoglobin.	Non-invasive, continuous monitoring; useful in cerebral and muscle oxygenation.	Provides indirect assessment of microvascular function; influenced by tissue heterogeneity.
Capillary Refill Time (CRT)	Measures time taken for color to return to blanched skin after pressure application.	Simple, inexpensive bedside tool; provides early indicator of peripheral perfusion impairment.	Subjective; influenced by skin color, ambient temperature, and inter-observer variability.
Peripheral Perfusion (e.g., skin mottling, temperature)	Assesses skin temperature, color, and mottling score.	Easy to perform, correlates with clinical outcomes in septic or shock patients.	Lacks quantitative precision; subjective and dependent on observer expertise.

2.3. Near-Infrared Spectroscopy

Near-infrared spectroscopy (NIRS) is a non-invasive technique that can provide valuable information in the ICU. It has been used to monitor cerebral oxygenation in severely brain-injured patients [77], tissue oxygenation in pediatric cardiac surgery and the cardiac ICU [78], and peripheral tissue perfusion in critically ill patients [79]. NIRS has also shown promise in the surgical/trauma ICU for shock management and as a prognostic tool [80].

2.3.1. Principles of NIRS

The fundamental principle of near-infrared spectroscopy (NIRS) lies in the differential absorption of near-infrared light by various chromophores, such as oxygenated and deoxygenated hemoglobin, within the tissue. As the near-infrared light diffuses into the tissue, it interacts with these chromophores, and the reflected and scattered light is detected by the NIRS device [81].

2.3.1.1. Physics of Light Absorption and Biological Absorbers

The physics and mathematics behind NIRS technology are rooted in the "Beer-Lambert law," which asserts that light traveling through a solution with a chromophore will partially be absorbed, thereby diminishing the intensity of the transmitted light. This law can be expressed as follows:

$$\mathrm{A} = \log\left(\frac{l_0}{l}\right) = \varepsilon c d$$

where A is the optical density (log of the ratio of incident to transmitted light intensities), ε its extinction coefficient, c the chromophore concentration, and d the thickness (optical path length) of the solution [80]. The use of an optical window ranging from 700 to 900 nanometers enables light to penetrate through the skin or bone to reach the underlying tissue. By considering the differential absorption of at least two different wavelengths of light and employing a dual-detector system that can diminish the impact of shallow signals, a Near-Infrared Spectroscopy (NIRS) device can continuously and noninvasively determine the oxygen saturation level of hemoglobin in deep tissues beyond the sensor. The depth of the optical field is roughly half the distance between the source and detector, which is typically 4 centimeters in most used devices [78].

Near-infrared light (700–900 nm) used by NIRS devices is largely transparent to skin, bone, and connective tissue and interacts with hemoglobin through absorption, reflection, scattering, and transmission. Transmitted and absorbed light do not return to the sensor, while some reflected light does, along with a smaller amount scattered by blood flow in arteries. During typical NIRS recordings, tissue structure remains constant, resulting in stable reflection, transmission, and scattering. Thus, the only variable is absorption, influenced by oxygen saturation and tissue hemoglobin levels. Oxy- and deoxyhemoglobin have distinct absorption spectra in the near-infrared range. Oxy- and deoxyhemoglobin have distinct absorption spectra in the near-infrared range, as shown in Figure 2.1. Using light of at least two wavelengths (above and below 810 nm) on the tissue, the modified Beer–Lambert law estimates the relative concentrations of oxygenated and deoxygenated hemoglobin, providing a tissue oxygenation index [81].

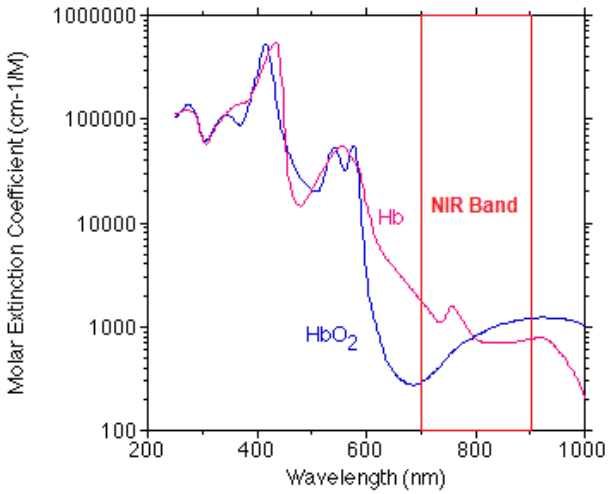

Figure 2.1 Diagram of Extinction Coefficients of Oxyhemoglobin (HbO2) and Deoxyhemoglobin (Hb) across the visible and near-infrared (NIR) spectrum. The NIR band (highlighted in red) is commonly used in Near-Infrared Spectroscopy (NIRS) for non-invasive tissue oxygenation monitoring [82]

2.3.1.2. Scattering and Differential Pathlength Factor

Scattering in tissue significantly influences light travel, as light traverses a greater distance than the direct path between the source and detector. Understanding the actual distance light travels in tissue is necessary to quantify changes in chromophore concentration. This increased travel distance due to scattering is quantified by the differential pathlength factor (DPF), which represents the real distance light travels. With

this information, changes in chromophore concentration can be measured in mol/litre of tissue.

As a result, tissue spectrometers can display real-time changes in cerebral Hb and HbO2 concentrations, as well as their sum, the total cerebral haemoglobin (HbT) concentration. The interpretation of NIRS data significantly depends on the chosen DPF value. Typically derived from studies on healthy adults, DPF can vary in different contexts and with the light wavelength used. Pathological conditions like cerebral edema or ischemia have not been studied, and current clinical practice uses these "normal" values [83]. Considering the DPF, we can express the modified Beer-Lambert law in the following manner:

$$\Delta A(\lambda) = \Delta\mu_a(\lambda) d\ell_{DPF}(\lambda) = [\varepsilon_{HbO2}(\lambda)\Delta[HbO_2] + \varepsilon_{HbR}(\lambda)\Delta[HbR]] d\ell_{DPF}(\lambda)$$

Where $\Delta A(\lambda)$ is the change in optical density assessed at a specific wavelength, $\Delta\mu_a(\lambda)$ is the corresponding change in tissue absorption, d is the distance between the source and detector, and $\ell_{DPF}(\lambda)$ is the differential pathlength factor. The change in absorption is also linked to changes in the chromophore concentrations of oxyhemoglobin ($\Delta[HbO_2]$) and deoxyhemoglobin ($\Delta[HbR]$) by the extinction coefficients $\varepsilon_{HbO2}(\lambda)$ and $\varepsilon_{HbR}(\lambda)$, which are dependent on wavelength. From measurements of $\Delta A(\lambda)$ at two wavelengths, the concentration changes can be calculated [84].

2.3.1.3. Spatially Resolved NIRS

The modified Beer-Lambert law is specifically designed for calculating the relative concentration changes of oxygenated and deoxygenated hemoglobin. To obtain absolute concentrations which is necessary for calculating tissue oxygen saturation, spatial resolved spectroscopy (SRS) must be used. In SRS, the intensity of the light reflected from the transmitter is measured as a function of the distance from the transmitter. This function's shape is directly related to the absorption coefficient (μ_a) of the tissue, which allows for the calculation of both the absolute hemoglobin concentrations and the tissue saturation index (TSI) [85], [86]. Figure 2.2 illustrates this technique.

The amount of light received by a receiver depends on the source-detector distance and the absorption and scattering coefficients of the tissue. By using at least two transmitters, the slope of light attenuation versus distance ($\partial A/\partial d$) can be determined, which allows for the calculation of the absorption coefficient. However, certain key

assumptions must be made, such as tissue homogeneity and wavelength-independent scattering during measurement. Additionally, using two wavelengths enables the calculation of oxygenated and deoxygenated hemoglobin. The tissue saturation index (TSI) estimates tissue oxygen saturation (StO2) as follows [86], [87]:

$$TSI = \frac{[HbO_2]}{[HbO_2] + [HbR]} \times 100$$

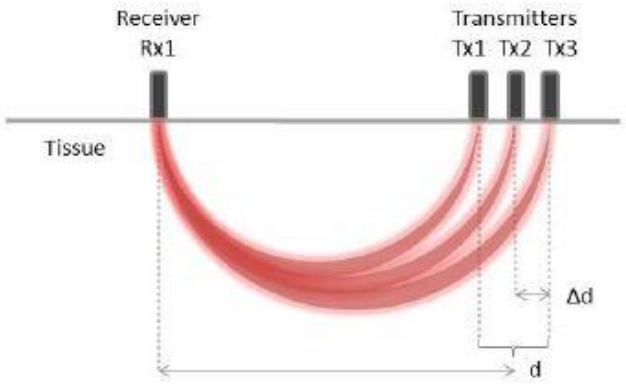

Figure 2.2 Principle of Spatially Resolved Spectroscopy (SRS). Light emitted from multiple transmitters (Tx1, Tx2, Tx3) penetrates tissue and is detected at a receiver (Rx1). The intensity of reflected light varies as a function of the source-detector distance (d), enabling the calculation of the absorption coefficient (μ_a) and, subsequently, absolute hemoglobin concentrations and tissue oxygen saturation [86]

2.3.2. Clinical applications of NIRS

NIRS has proven to be a valuable non-invasive tool with diverse clinical applications. It has shown promise in detecting intracranial hematomas and monitoring intracranial pressure and brain oxygenation in traumatic brain injury [88]. Moreover, it has been employed in neurorehabilitation to investigate functional recovery mechanisms and as a potential therapeutic tool for brain-computer interfaces and neurofeedback [89].

NIRS has also been applied in cardiac surgery to monitor cerebral oxygenation, and some studies suggest that NIRS-guided protocols may reduce perioperative neurological complications [90]. Additionally, NIRS has contributed to our understanding of early brain development and language acquisition in infants [91]. NIRS is also a promising technology for critical care settings due to its ability to provide high-resolution monitoring of tissue oxygenation and hemodynamics. Animal studies conducted in the past on hemorrhagic shock revealed a strong correlation between S_tO_2 and global blood flow, suggesting that NIRS could be used as a non-invasive method to detect progressive hypovolemia. Subsequent human

studies on central hypovolemia demonstrated that declines in S_tO_2 and the tissue hemoglobin index were effective in identifying blood volume losses of 400-500 cc before the onset of tachycardia or hypotension [92].

Clinical trials on StO2 levels in septic patients have yielded conflicting results about its predictive value. While some studies report similar S_tO_2 values in healthy and septic patients, others find lower values in septic shock patients. This discrepancy may stem from different resuscitation methods and measurement timings. However, recent prospective observational research indicates that S_tO_2 levels below 70% within the first 8 hours of ICU admission correlate with poor outcomes, such as organ dysfunction [79].

A study review of 18 individual studies on patients with circulatory shock and NIRS-derived S_tO_2 showed promising results for NIRS as a tissue perfusion monitoring technique in shock states, without any reported negative side effects. Although high-quality data on NIRS-guided treatment for circulatory shock patients are limited, baseline S_tO_2 appears to be a predictor of mortality and may help identify severe shock cases [93].

While tissue oxygen saturation measurement is well-studied, the influence of total hemoglobin concentration (HbT) from NIRS on critical care outcomes remains under-researched. In 2021, Mendelson et al. demonstrated that high-resolution NIRS can continuously measure microvascular hemoglobin content (MHC) in peripheral tissue in the ICU, reflecting hemoglobin distribution variability in the microcirculation. The study also found that mechanical ventilation directly impacts peripheral tissue MHC. These findings suggest the need for further evaluation of this hemodynamic metric for diagnosing microvascular dysfunction and monitoring peripheral perfusion [15].

2.4. Microvascular Autoregulation

Microvascular autoregulation (MA) is a vital process that helps maintain consistent microvascular blood flow, even when blood pressure changes occur. This process is essential for ensuring proper tissue perfusion and oxygen delivery, which is crucial for the proper functioning of various brain functions. NIRS can be used to measure autoregulation non-invasively in the microvasculature, which offers potential for localized monitoring [94].

MA is frequently disrupted during critical illness and contributes to organ failure. This concept has been most widely studied in the field of neurocritical care, where cerebral MA has been measured as the correlation between blood pressure and invasive (e.g., intracranial pressure monitoring) and non-invasive (e.g., NIRS) modalities [95].

Disrupted cerebral MA is a significant factor in subarachnoid hemorrhage-induced brain injury, highlighting the need for targeted therapeutic interventions [96]. It is well-established that impaired cerebral MA plays a critical role in the pathophysiology of traumatic brain injury (TBI). Zeiler et al. have demonstrated that continuous MA monitoring facilitates personalized therapeutic strategies, which are more effective than traditional uniform treatment protocols [97]. Monitoring cerebral autoregulation can help identify optimal blood pressure targets in various clinical scenarios. In cardiopulmonary bypass patients, the average optimal MAP was 78 ± 11 mmHg, with individual variation [98]. For sepsis-associated encephalopathy, near-infrared spectroscopy-derived cerebral oximetry identified patient-specific optimal MAP ranges between 55-115 mmHg [10]. In post-cardiac arrest patients, pressure reactivity index monitoring suggested a mean optimal MAP of 89 ± 11 mmHg [99]. Individualized blood pressure management based on autoregulation monitoring may improve outcomes in critical conditions.

2.4.1. Cerebral MA and CCPopt

Cerebral MA maintains constant cerebral blood flow (CBF) despite fluctuations in MAP or cerebral perfusion pressure (CPP, defined as MAP minus intracranial pressure). Historically, Lassen's autoregulation curve illustrated a plateau in CBF across a MAP range of approximately 60–150 mmHg, derived from data pooled across independent studies [100]. However, with advancements in intracranial pressure monitoring, it has become clear that applying a fixed CPP range (often cited as 50–150 mmHg) oversimplifies the complex and highly variable nature of cerebral autoregulation. Modern evidence challenges the traditional dogmatic view by demonstrating significant inter-individual variability and emphasizing that microvascular autoregulation offers a dynamic, localized assessment of CBF regulation [101]. Assessing the boundaries and efficacy of this autoregulatory plateau is vital because impaired autoregulation increases the risk of cerebral ischemia and brain injury. Therefore, a comprehensive evaluation that integrates both classical principles and contemporary

measurement techniques is essential for optimizing patient care [94]. Figure 2.3 is the contemporary illustration of MAP vs CBF curve with lower and upper limits that can vary between individuals.

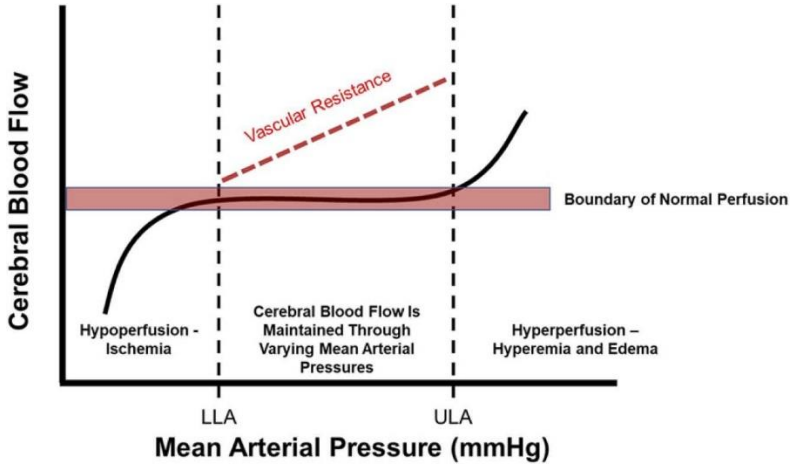

Figure 2.3 Autoregulation curve illustrating the relationship between cerebral blood flow (CBF) and mean arterial pressure (MAP). The plateau region represents the autoregulatory range where CBF remains stable despite fluctuations in MAP. The lower limit of autoregulation (LLA) and upper limit of autoregulation (ULA) define the boundaries beyond which cerebral perfusion becomes pressure-dependent, leading to hypoperfusion (ischemia) or hyperperfusion (edema). Modern research suggests that these boundaries vary significantly between individuals [102]

2.4.1.1. Physiology of Cerebral MA

Cerebral blood flow is regulated through four primary mechanisms: myogenic, neurogenic, endothelial, and metabolic regulation. These mechanisms work together to maintain stable blood flow despite changes in pressure, neural activity, and metabolic demand.

The myogenic mechanism is an automatic response of blood vessels to changes in pressure. When blood pressure increases, smooth muscle cells in the vessel walls contract, causing vasoconstriction, which prevents excessive blood flow. Conversely, when pressure decreases, the vessels relax and dilate, allowing more blood to flow and preventing ischemia. This process is driven by stretch-sensitive ion channels, which detect changes in vessel wall tension and regulate calcium influx, controlling muscle contraction [103], [104]. The myogenic response acts as a first-line defense against sudden blood pressure fluctuations. Disorders like CADASIL, which impair smooth muscle function, disrupt this regulation and increase the risk of cerebrovascular events [105].

The neurogenic mechanism involves the nervous system's control over blood vessel diameter through neurotransmitter release. Sympathetic nerve activity generally promotes vasoconstriction by releasing norepinephrine, reducing blood flow when necessary. In contrast, parasympathetic stimulation releases acetylcholine and nitric oxide, leading to vasodilation and increased blood flow. Additionally, local brain activity influences vessel diameter, a process known as neurovascular coupling, ensuring that active regions of the brain receive more oxygen and nutrients [103], [106]. This regulation is crucial for maintaining blood flow during sudden changes in neural activity. Conditions such as posterior reversible encephalopathy syndrome (PRES) are thought to involve dysfunction in neurogenic control, leading to abnormal blood pressure regulation in the brain [105], [106].

The endothelial mechanism is driven by substances released by the endothelial cells lining blood vessels, allowing for localized and precise control of vascular tone. Nitric oxide (NO) and prostacyclin (PGI_2) act as vasodilators, increasing blood flow, while endothelin-1 and thromboxane A_2 promote vasoconstriction. This system plays a key role in maintaining vascular flexibility, responding to changes in shear stress and inflammation [103], [107]. Statins have been shown to enhance nitric oxide production, improving endothelial function and supporting blood flow regulation [105], [107]. Endothelial dysfunction, seen in conditions like hypertension and atherosclerosis, can impair this mechanism, contributing to cerebral blood flow instability [103].

The metabolic mechanism regulates blood flow based on the brain’s metabolic needs. When neurons are highly active, they produce more carbon dioxide (CO_2), hydrogen ions (H^+), and lactate, which cause vasodilation, increasing oxygen and nutrient delivery. Conversely, when activity is low, blood flow decreases to prevent excess perfusion [105]. Carbonic anhydrase plays a role in converting CO_2 into protons, further influencing vessel tone. However, this process takes longer than the other three mechanisms, as it relies on the accumulation of metabolic byproducts over seconds to minutes [103]. Because of this slower response, metabolic regulation is not the primary driver of cerebral autoregulation under normal conditions. Instead, it becomes more prominent in conditions like traumatic brain injury (TBI) or prolonged ischemia, where persistent edema and neuroinflammation impair the faster-acting myogenic, neurogenic, and endothelial responses [108]. In these

cases, metabolic changes can significantly influence blood flow, as autoregulation shifts to compensate for prolonged tissue damage and energy deficits [108].

2.4.1.2. Impaired Autoregulation

The neurocritical care community has developed continuous CA measurement metrics using physiological data such as MAP and intracranial pressure (ICP) to recognize the critical role of impaired cerebral MA in secondary brain injury following moderate/severe traumatic brain injury (TBI). One such metric is the pressure reactivity index (PRx), which was developed in the late 1990s and assesses Cerebral MA using the moving Pearson correlation between MAP/CPP and ICP. PRx ranges from +1 (impaired CA) to -1 (intact CA), with higher values correlating with poor long-term outcomes and increased mortality. Impaired CA in moderate to severe TBI is associated with secondary brain damage, unfavorable outcomes, and higher mortality rates at 6 and 12 months post-TBI. PRx thresholds of +0.05, +0.25, and +0.35 have been identified for favorable outcomes, unfavorable outcomes, and mortality, respectively, particularly in patients without decompressive hemicraniectomy. The burden of PRx values above these thresholds correlates with the 6-month Glasgow Outcome Score [97].

2.4.1.3. Optimal Cerebral Perfusion Pressure

Optimal CPP (CPPopt) refers to the CPP that best maintains cerebral MA for a patient, aiming to improve outcomes by tailoring CPP management. Developed almost two decades ago, CPPopt is identified by plotting mean PRx against CPP (in 5 mmHg intervals) for TBI patients, forming a U-shaped curve where the nadir indicates the optimal CPP. Continuous automated CPPopt derivation has facilitated its clinical use, and retrospective studies suggest better 6-month outcomes when CPP aligns with CPPopt. The COGITATE study demonstrated the feasibility and safety of CPPopt use, but a phase III trial is needed to confirm its clinical benefits. TBI's heterogeneity complicates CA, and PRx offers a global cerebral MA average. The acute TBI phase includes biochemical changes affecting cerebral MA independently of CPP, complicating CPPopt calculations. While CPPopt is promising for personalized TBI management, further research and trials are needed for widespread clinical adoption [97], [109].

2.4.2. Non-Cerebral MA

Autoregulation is a process that occurs in various organs of the body, including the brain, spinal cord, heart, kidneys, skeletal muscle, and visceral organs, and each organ exhibits unique capacities for autoregulation. The degree of heterogeneity and variability in autoregulation is influenced by factors such as age, sex, chronic hypertension, diabetes, metabolic rate, cardiac output, hemodilution, CO_2 levels, drugs, anesthesia, and sympathetic tone. Clinically, organs with weaker autoregulation are more susceptible to injury from changes in blood pressure, making it essential to understand the different levels of autoregulation in organs.

In 1902, Bayliss initiated research on autoregulation, which led to the development of three-point scale classifying organs as having robust (brain, spinal cord, heart, kidney), moderate (skeletal muscle), or weak (splanchnic organs) autoregulatory capacities. This scale, which has been validated through animal studies due to the limited research on non-cerebral organ autoregulation in humans, evaluates the slope of the autoregulatory plateau, the identifiability of limits, and reproducibility, emphasizing the importance of personalized clinical approaches to manage blood pressure-related risks [110].

2.4.2.1. MA in skeletal muscles

Few studies have examined the activity of MA in human skeletal muscles. In a prospective case-control study conducted in a surgical ICU, researchers assessed microvascular function, regulation, oxygenation, and cellular metabolism in patients with septic shock. The study included 26 individuals, comprising 13 patients with septic shock and 13 non-septic postoperative individuals, as well as 15 healthy volunteers. Using NIRS on the brachioradial muscle, they measured tissue hemoglobin concentrations, blood volume, hemoglobin re-saturation time, microvascular compliance, and O2 consumption. The results indicated that septic shock patients exhibited higher tissue blood volumes, lower microvascular compliance, prolonged hemoglobin re-saturation times, and reduced O2 consumption compared to healthy controls [111].

However, it is important to note that the correlation between NIRS and arterial blood pressure (ABP) in skeletal muscles, particularly in ICU patients, has not been studied. This presents a significant gap in the current understanding of microvascular regulation in

critically ill patients, and exploring this relationship could provide valuable insights into optimizing hemodynamic monitoring.

2.5. Physiological Signals Analysis

Signal processing in physiological waveforms, particularly in the context of the ICU and critical care for conditions such as circulatory shock and sepsis, involves both time and frequency domains analyses. Time-domain analysis examines changes over time within the signal itself, while frequency-domain analysis decomposes the signal into its constituent frequencies, providing insight into the periodic components of the waveform.

2.5.1. Time domain Analysis vs Frequency Analysis

Biomedical signal processing in critical care involves various time-domain analysis techniques to assess physiological signals. Time-domain methods are particularly useful for analyzing signals such as ECGs, which are critical for monitoring cardiac function in ICUs [112]. For instance, the Pervasive Patient Timeline, as described in Braga et al. (2017), integrates time-domain data such as vital signs and laboratory results to support decision-making in ICUs [113].

Similarly, the novel vital signs viewer system evaluated in Yang et al. (2023) provides at-a-glance summaries of physiological data, including time-domain representations of vital signs, to assist clinicians in prioritizing care for critically ill patients [114]. It can be inferred from literature that methods such as waveform analysis, peak detection, and temporal pattern recognition are likely to be employed, given their relevance to the types of signals and the clinical objectives mentioned [112], [113], [114].

Frequency analysis is also pivotal in processing physiological signals within critical care environments. For instance, the Fast Fourier Transform (FFT) is utilized to optimize the computational process of the Discrete Fourier Transform (DFT) for the analysis of electrocardiogram (ECG) and electroencephalogram (EEG) signals, aiding in the diagnosis of arrhythmias and the analysis of sleep quality [115].

Additionally, the continuous Fourier transform is applied in multiresolution signal processing to detect the exact location of high-frequency signals, which is crucial for time-

frequency analysis of signals in critical care scenarios [116]. Toweill et al. (2000) presents an application of frequency-domain analysis in pediatric patients with sepsis and septic shock, using power spectral analysis to assess heart rate variability. The study found diminished low-frequency and high-frequency heart rate power in septic patients, indicating uncoupling of the autonomic and cardiovascular systems. This suggests that frequency-domain metrics can be useful in differentiating between sepsis, septic shock, and recovery states [117].

However, there are limitations to both approaches. Time-domain analysis may not adequately capture the complex interactions between different physiological systems, and frequency-domain analysis can be sensitive to non-stationarities in the signal, which are common in critically ill patients.

2.5.2. Wavelet Transform

Wavelet transforms separate signals into scale and space components by employing localized wavelet functions [118]. Unlike Fourier transforms, which are limited to stationary signals and are nonlocal, wavelet transforms excel in analyzing non-stationary signals [119]. They are commonly used in turbulence analysis, signal processing, image coding, and numerical analysis [118]. These transforms are useful in analyzing complex data, such as speech, music, and images, facilitating precise decomposition and reconstruction [119].

Wavelet transforms are effective for analyzing non-stationary biomedical signals, including electrocardiograms (ECG) and lung sounds [120]. In critical care, wavelet transforms are used to analyze physiological time series data, such as heart rhythm, chest volume, and blood oxygen saturation in sleep apnea patients [121]. A recent non-invasive intracranial pressure waveform monitoring technique correlated strongly with invasive methods [122]. Spectral analysis of systemic arterial pressure and heart rate signals has shown prognostic value in ICU patient outcomes, comparable to the APACHE II scoring system [123].

2.5.2.1. Advantages of Wavelet over Time-domain and Frequency-domain Analysis

Wavelet analysis offers several advantages over traditional time-domain and frequency-domain analysis methods. The wavelet transform (WT) is particularly well-suited for non-stationary signal analysis, as it provides a time-frequency representation of a signal with adjustable resolution [124]. This adaptability allows for a more precise analysis of transient and time-varying phenomena, which are common in physiological

signals. In contrast to the Fourier Transform (FT), which offers good frequency resolution but is inadequate for transient analysis, the WT can provide detailed information about the temporal evolution of spectral features [125]. This is crucial in critical care, where rapid changes in physiological signals can indicate significant clinical events. Additionally, the WT's ability to handle noise effectively is beneficial for analyzing physiological signals, which are often corrupted by various sources of noise [126]. The wavelet spectrum in Figure 2.4 highlights the presence of different frequency components and their evolution over time, demonstrating its superiority in capturing dynamic physiological signals.

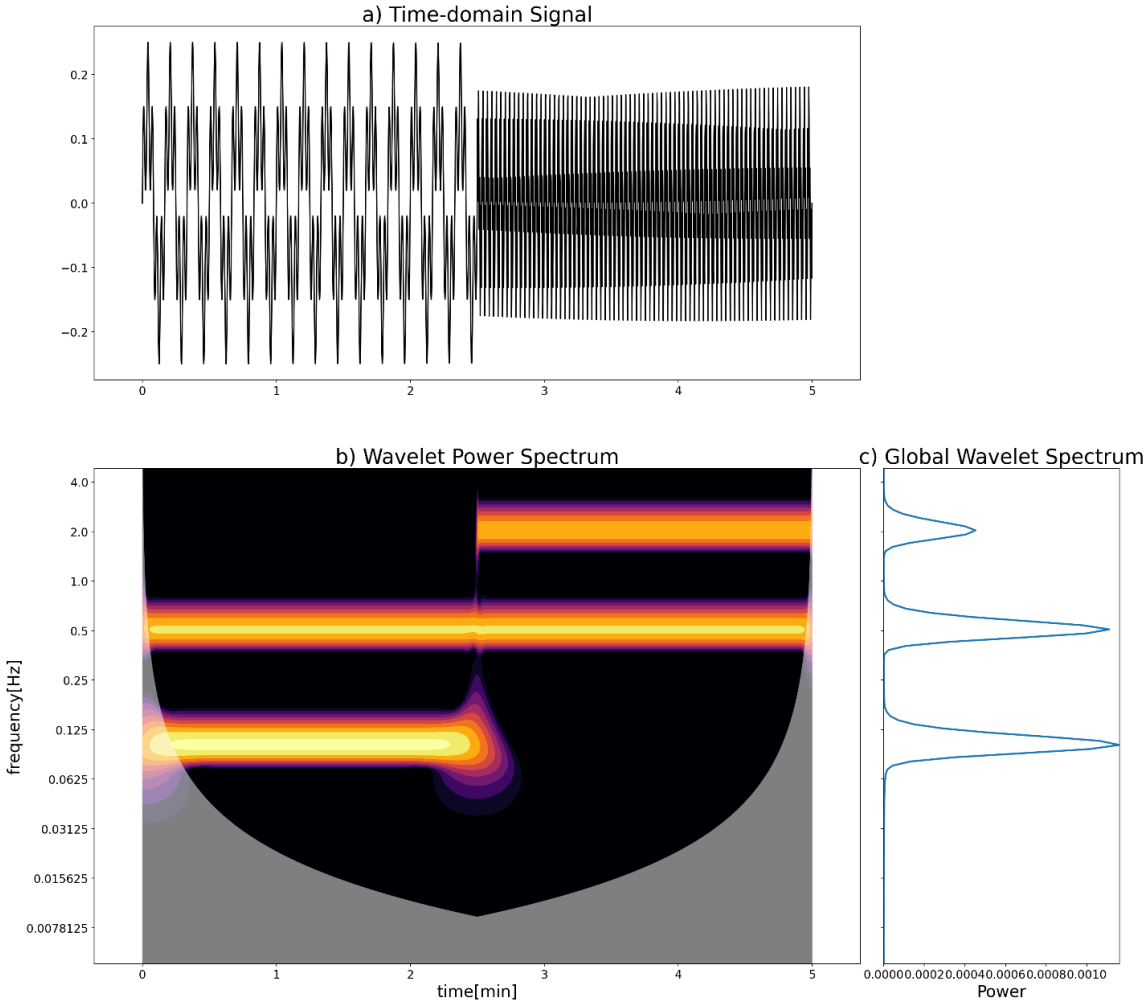

Figure 2.4 Continuous Wavelet Transform (CWT) analysis of a non-stationary signal. (Top) The original time-domain signal, consisting of two components: a constant low-frequency oscillation (0.5 Hz) and a piecewise frequency shift at t=150 seconds. Before the transition, the second component oscillates at 0.1 Hz, while after the transition, it shifts to 2 Hz with a lower amplitude. (Bottom Left) The wavelet power spectrum using the Morlet wavelet, showing the time-frequency localization of the dominant oscillatory components. (Bottom Right) The global wavelet spectrum, representing the overall power distribution across different frequencies.

Furthermore, the wavelet analysis can be tailored to specific signal characteristics, as demonstrated by the adaptive mode separation-based wavelet transform (AMSWT), which offers superior time-frequency resolution and can precisely highlight relevant features in nonstationary seismic signals [127]. This adaptability can be translated into the analysis of physiological signals, where the ability to focus on signal components can enhance the detection and interpretation of critical care events.

2.5.2.2. Continuous Wavelet Transform

Wavelet transform is a mathematical technique that transforms a signal into a more compact form, revealing its hidden characteristics. Unlike a smooth, continuous wave, a wavelet is a small, oscillating wave with energy concentrated in time. Mathematically, a wavelet $\psi(t)$ must satisfy the admissibility condition.

$$\int_{-\infty}^{\infty} \frac{|\Psi(\mathrm{f})|^2}{|f|} df < \infty$$

where $\Psi(\mathrm{f})$ is the Fourier transform of $\psi(t)$. This condition implies that $\Psi(0) = 0$, indicating the wavelet's average value is zero:

$$\int_{-\infty}^{\infty} \psi(t)\, dt = 0$$

Through dilation (stretching or squeezing the wavelet function by $1/s$) and translation (shifting along the time axis by τ), a family of scaled and translated wavelets can be created as:

$$\psi_{s,\tau}(t) = \frac{1}{\sqrt{s}} \psi\left(\frac{t-\tau}{s}\right), \quad s > 0, \quad \tau \in R$$

$\psi\left(\frac{t-\tau}{s}\right)$ is the scaled and shifted version of the original (mother) wavelet $\psi(t)$. The factor $\frac{1}{\sqrt{s}}$ ensures that the energy of the wavelet family remains consistent across different scales. The wavelet transform can be represented in continuous form (continuous wavelet transform, CWT) as well as in discrete forms (discrete wavelet transform). The CWT of a signal $x(t)$ is defined as:

$$wt(s,\tau) = \frac{1}{\sqrt{s}} \int_{-\infty}^{\infty} x(t) \psi^*\left(\frac{t-\tau}{s}\right) dt$$

The CWT is similar to the Fourier Transform as it involves integration. However, CWT uses two parameters, scale and translation, to transform a signal with a wavelet basis onto a two-dimensional time-scale plane, unlike the one-dimensional frequency domain of the Fourier Transform. The wavelet's localization enables capturing features in the time-scale plane that are not evident in the original signal, such as specific spectral components related to bearing defects at certain times [128].

2.5.2.3. The Selection of Mother Wavelet

There are various types of mother wavelets that are employed in CWT, such as the Mexican hat wavelet, Morlet wavelet, Gaussian wavelet, Frequency B-spline wavelet, and Shannon wavelet. Each type possesses a distinct equation and form. The primary challenge in wavelet analysis is selecting the optimal mother wavelet. Both qualitative and quantitative approaches have been proposed and applied in various fields for this purpose, with most methods focusing on the similarity between the signal and the mother wavelet. However, studies have shown that the most similar mother wavelet is not always the best choice for all wavelet-based processing tasks [129]. In the majority of critical care studies employing NIRS signals, researchers typically opt for Morlet wavelet as the mother wavelet for CWT [130]. The Morlet wavelet is defined as:

$$\psi_M(t) = \frac{1}{\sqrt{\pi f_b}} e^{j2\pi f_c t} e^{-\frac{t^2}{f_b}}$$

where f_b is the bandwidth parameter and f_c is the wavelet center frequency [128]. The Morlet wavelet is favored in those wavelet studies due to its optimal time-frequency compactness. This compactness, coupled with its simple geometry featuring a single smooth Gaussian bump, reduces component clutter in the transform domain, aiding in the separation of relevant components [130]. Figure 2.5 shows the real part of Morlet Wavelet.

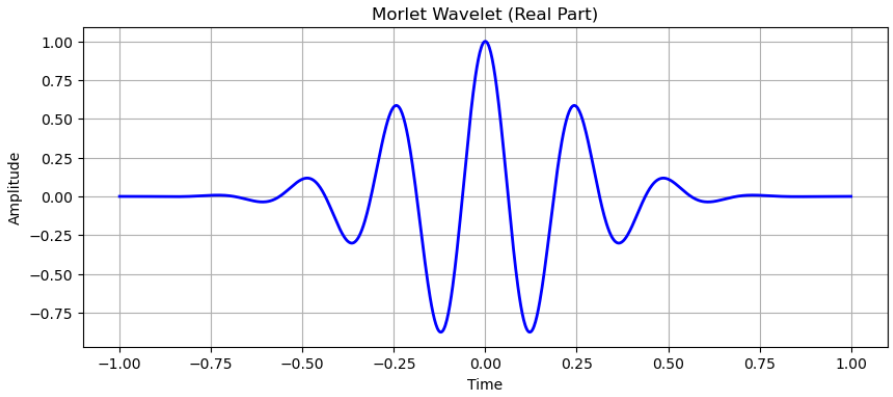

Figure 2.5 Real part of the Morlet wavelet. The Morlet Wavelet is a complex sinusoid modulated by a Gaussian envelope, making it well-suited for time-frequency analysis.

2.5.3. Wavelet in Critical Care

In this segment, we will explore various instances of employing CWT in critical care situations. The study conducted by Vasilios E Papaioannou et al. examines the intricacy of temperature in critically ill patients experiencing systemic inflammatory response syndrome (SIRS), sepsis, and septic shock. The researchers utilize wavelet transformation and multiscale entropy analysis to achieve this. Wavelet transformation divides temperature signals into various frequency components, which represent both neurogenic and metabolic influences. The research employs both discrete wavelet transform (DWT) and continuous wavelet transform (CWT), focusing on different frequency bands related to physiological events. The study found substantial differences in wavelet entropy and multiscale entropy among the patient groups, indicating potential diagnostic value in determining the severity of illness and differentiating between infectious and non-infectious conditions [131].

Saeed et al. [132] presented an Intelligent Patient Monitoring (IPM) system that incorporates wavelet analysis to evaluate and display trends in multiple parameters from critically ill patients. The study focused on heart rate (HR), arterial blood pressure (ABP), and pulmonary artery pressure (PAP) data from 58 patients in the MIMIC database and employed the Haar wavelet to identify physiological events and artifacts in long-term trends. Wavelet coefficients at different scales are calculated to detect changes in trends over specific time intervals, facilitating automated artifact detection and physiological event monitoring. The IPM framework integrates wavelet-based algorithms to enhance the monitoring and

interpretation of left ventricular hemodynamic function, ultimately supporting clinical decision-making in ICU settings [132].

A study by Zengyong Li et al. [133] focuses on assessing cerebral oxygenation oscillations in subjects with cerebral infarction (CI) using wavelet transform of NIRS signals. Conducted on twenty subjects, the research identified five frequency intervals through wavelet spectral analysis to analyze [HbO2] and [Hb] amplitudes. Significant reductions in amplitude were observed across several frequency intervals in CI subjects compared to normal controls, suggesting increased arterial stiffness. The Morlet wavelet was employed due to its optimal time-frequency localization capabilities. The findings highlight potential applications of spontaneous oscillations in assessing vascular health and atherosclerosis risk using NIRS-based wavelet analysis [133].

2.6. Rationale for This Study

Critically ill patients in the ICU face severe physiological challenges, often experiencing conditions such as septic shock, respiratory failure, cardiovascular collapse, and multi-organ dysfunction. Regardless of the underlying disease, most of these patients suffer from impaired or non-optimal cardiovascular perfusion, particularly at the microvascular level. The ICU team employs standardized resuscitation strategies, including fluid therapy, vasopressors, and mechanical ventilation, to restore hemodynamic stability [134]. These approaches have been refined over decades and remain the foundation of critical care. However, there is always a need for more personalized and efficient strategies to optimize patient management and reduce ICU length of stay, morbidity, and long-term complications such as ICU-acquired weakness and ventilator dependency [135].

With advances in biomedical monitoring, we now have a real-time, non-invasive method to assess microvascular perfusion using Near-Infrared Spectroscopy. This technology allows for the measurement of total hemoglobin concentration in tissues, providing insight into regional blood flow and oxygenation [79]. The next step is determining how to use this information to improve ICU care. This study explores two distinct but complementary approaches to applying NIRS data in critical care settings: the MAPopt Study and the Wavelet Study.

2.6.1. MAPopt Study

When a critically ill patient arrives in the ICU, one of the most immediate priorities is stabilizing blood pressure to prevent hypoperfusion and organ failure. Current clinical guidelines recommend maintaining a mean arterial pressure of at least 65 mmHg [134], but there is ongoing debate about whether this universal target is optimal for all patients. Some researchers suggest that individualized MAP targets, tailored to each patient's own autoregulatory mechanisms, may lead to better outcomes [136].

This study aims to investigate whether skeletal muscle-derived MAPopt can serve as a personalized hemodynamic target. The concept is inspired by research in traumatic brain injury, where an optimal cerebral perfusion pressure, known as CPPopt, is calculated to maintain brain autoregulation. Studies have shown that cerebral autoregulation is most effective at a specific CPP, ensuring that cerebral blood flow remains stable despite fluctuations in systemic pressure [137]. Since microvascular autoregulation is not exclusive to the brain but exists in other organs, including skeletal muscle, it is reasonable to hypothesize that a similar optimal MAP can be identified for skeletal muscle [110]. If there exists a mean pressure at which skeletal muscle blood flow has minimal correlation with systemic blood pressure, this could indicate a pressure at which autoregulation is functioning at its best.

The primary goal of this study is to determine whether MAPopt can be calculated for skeletal muscle and whether it correlates with brain-derived MAPopt. Establishing this relationship would provide insight into whether skeletal muscle and brain autoregulation function in parallel or whether skeletal muscle has its own distinct optimal perfusion pressure. By comparing MAPopt values from both skeletal muscle and the brain, we aim to understand whether there is consistency in their response to systemic blood pressure changes. If a meaningful difference is found, it would suggest that skeletal muscle has an independent autoregulatory threshold that could be used as a personalized target for critically ill patients, particularly those in shock and septic states.

2.6.2. Wavelet Study

In addition to investigating personalized MAP targets, this study explores an alternative approach to utilizing NIRS-derived blood perfusion data by introducing a new variable to quantify microvascular power. This builds upon the previous work of Mendelson, who

investigated hemodynamic fluctuations in critical illness [15]. While ICU monitoring routinely includes macrocirculatory metrics such as cardiac output, stroke volume, and pulse pressure variation, there is currently no variable that directly quantifies microvascular activity [138]. However, the microvascular network plays a crucial role in perfusion, regulated by myogenic, neurogenic, and endothelial mechanisms, many of which operate at lower frequency ranges. These low-frequency oscillations in blood flow are not easily analyzed using conventional signal processing methods [139].

Wavelet transform offers a powerful tool for analyzing these signals, as it allows for the decomposition of NIRS signals into different frequency components, isolating contributions from cardiac, respiratory, and microvascular activity. Another advantage of wavelet transform is its ability to calculate power variables over flexible time durations, whether for an entire recording session, for hourly intervals, or even as a time-varying signal. This flexibility makes wavelet-derived variables useful not only for the current study but also for potential future research applications in ICU monitoring.

This study aims to demonstrate that it is possible to derive a clinically meaningful measure of microvascular power in ICU patients using wavelet analysis. The first objective is to establish the feasibility of creating such a variable and to validate its measurement. The next step is to determine whether critically ill patients exhibit lower microvascular activity than healthy individuals, which would indicate that the variable reflects an important physiological process. Beyond this, the study will investigate whether microvascular power can serve as a predictive indicator of ICU outcomes, such as mortality or sepsis diagnosis. Since patient recordings are taken over multiple ICU days whenever possible, we also aim to analyze whether temporal changes in microvascular power provide additional insights into the progression or resolution of critical illness.

3. Study Design and Signal Acquisition

3.1. Study Design

This prospective observational cohort study, titled MiMICSS (Microvascular Monitoring in Circulatory Shock in Sepsis), was conducted at the Winnipeg Health Science Center Medical and Surgical Intensive Care Units (ICUs) between May 2022 and July 2024. The study protocol was approved by the University of Manitoba Biomedical Research Ethics Board (HS25043, September 15, 2021) and the Shared Health Approval Committee (SH2021-147, November 21, 2021), following the Declaration of Helsinki. The study was registered at clinicaltrials.gov (NCT05985525).

The primary objective was to investigate microvascular monitoring in critically ill patients with circulatory shock and sepsis. Eligibility criteria included ICU admission on Day 1 and requirement for mechanical ventilation. The study was divided into two sub-studies:

MAPopt study: Enrolled patients requiring vasoactive medications to maintain mean arterial pressure (MAP) above 65 mmHg and who had invasive arterial blood pressure (ABP) monitoring.

Wavelet study: Included a broader cohort of critically ill patients regardless of vasopressor use or invasive monitoring status.

By July 2023, 34 ICU patients had been recorded, of whom 15 met the MAPopt study inclusion criteria. By July 2024, 54 patients were recorded, with 43 included in the Wavelet study. Some patients participated in both studies, others in one or none.

A healthy control group was recruited via posters and email advertisements at the University of Manitoba, without specific age or gender matching. These participants provided baseline microvascular data for comparison.

3.2. Experimental Procedure

A deferred consent approach was utilized for ICU patients. Upon identification of an eligible candidate, recordings were initiated immediately. Subsequently, written informed consent was obtained from the patient or their legally authorized representative, typically the next of kin, by trained research staff.

Healthy control participants provided written informed consent prior to testing.

Healthy adults were recruited through posted notices and email invitations circulated within the University community. Participants were screened to exclude any history of cardiovascular, metabolic, or neurological disorders. Exclusion criteria followed ATS Safety Guidelines, including resting blood pressure over 160/90 mmHg or heart rate exceeding 100 bpm.

All physiological recordings were conducted by trained research assistants from our laboratory. For ICU patients, measurements were performed bedside in the ICU using portable high-resolution near-infrared spectroscopy (hr-NIRS) and invasive arterial pressure monitors (where applicable). Healthy participants were assessed at the Active Living Center (ALC) in a controlled laboratory environment.

- ICU patients (MAPopt and Wavelet studies): Measurements were collected on Day 1 (D1) of ICU admission and repeated on Day 3 (D3) and Day 8 (D8), contingent on patient availability and clinical stability.
- Healthy controls: Underwent a single assessment session lasting approximately two hours, during which anthropometrics, baseline blood pressure, heart rate, and microvascular NIRS data were collected.

3.3. Patients Demographics

A total of 383 ICU patients were screened for eligibility between May 2022 and July 2024. Of these, 54 patients were enrolled in the study, with their demographic characteristics summarized in Table 3.1. Eight participants were later excluded due to withdrawal of consent. The MAPopt analysis included 15 patients who met specific criteria (including vasopressor use and invasive arterial blood pressure monitoring) from among the first 34 enrolled patients at the time of analysis. The wavelet analysis included 43 patients with usable recordings. A flow diagram outlining the screening, enrollment, and inclusion in each sub-study is shown in Figure 3.1.

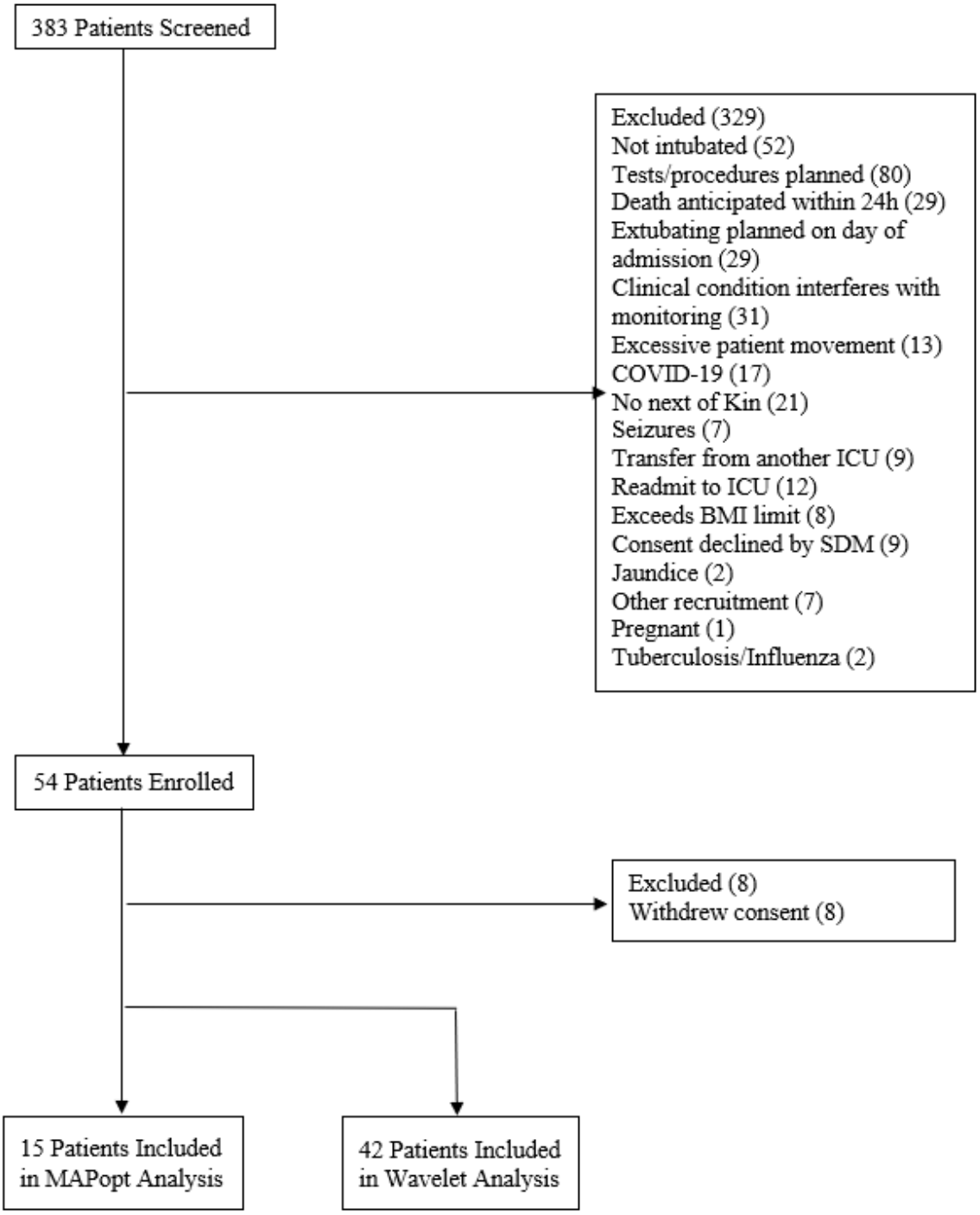

Figure 3.1 Flow diagram of the ICU recruitment

Table 3.1 Summary of demographic and clinical characteristics for ICU patients and healthy controls. The MAPopt study included 15 patients; the wavelet analysis involved 43 patients contributing 70 signal segments from different ICU days (D1, D3, D8). The healthy control group included 14 participants. Data are presented as mean ± SD, count (n/N), or median (IQR), as appropriate.

Patient Demographic	ICU Cohort		Healthy Control n=14
	MAPopt Study n=15	Wavelet Study n=43 patients N=70 signals	
Age (year)	63 ± 14	63 ± 16	42 ± 20
Female	4/15	21/43	4/14
Sepsis	10/15	21/43	N/A
Norepinephrine dose (µg/kg/min)	0.13 (0.08-0.17)	0.04 (0-0.14) N=70	N/A
Vasopressin	9/15	38/43	N/A
Lactate	1.8 (1.45–3.00)	1.8 (1.1-2.6) N=70	N/A
Acute Physiology and Chronic Health Evaluation II score	19 (15.5–23)	16 (13-19) N=70	N/A
Capillary refill time less than 3s	12/15	38/43	14/14
Mean arterial pressure (mm Hg)	74 ± 3	N/A	N/A
Heart rate	90 ± 19	90 ± 20 N=69	72 ± 11
Arterial blood pressure range (mm Hg)	38 (29.5–46.0)	N/A	N/A
Mortality	5/15	17/43	N/A

3.4. Microvascular Monitoring Using High-Resolution NIRS

This study utilized high-resolution near-infrared spectroscopy (hr-NIRS) to evaluate microvascular autoregulation and total hemoglobin concentration in the muscle tissue of critically ill patients. A NIRS device, specifically the PortaMon (Artinis Medical Systems, Netherlands), was positioned on the brachioradialis muscle to assess hemoglobin variability. The differential path length (DPF) was set to four for the muscle, while the DPF for the brain was determined based on age-recommended values from the manufacturer. The NIRS device setup is illustrated in Figure 3.2, demonstrating its application in both brain and muscle monitoring.

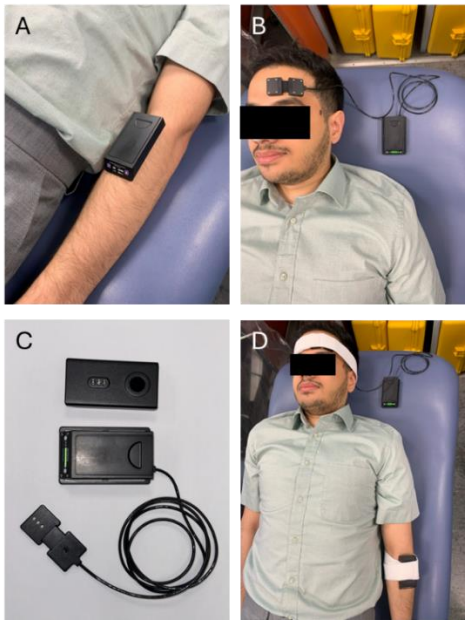

Figure 3.2 Near-Infrared Spectroscopy (NIRS) device placement for cerebral and skeletal muscle monitoring. (A) NIRS sensor positioned on the forearm for skeletal muscle oxygenation assessment. (B) NIRS sensor placed on the forehead for cerebral oxygenation monitoring. (C) Components of the NIRS device, including the sensor, control unit, and connection cables. (D) Experimental setup demonstrating simultaneous cerebral and skeletal muscle NIRS monitoring.

The spectrometers recorded data at a high temporal resolution of 10 Hz, employing a spatially resolved spectroscopy method using three light transmitters and one receiver, with distances of 30, 35, and 40 mm. Each transmitter-receiver pair measured the relative changes in oxyhemoglobin, deoxyhemoglobin, and total hemoglobin (HbT) concentrations. To maximize tissue penetration depth, the 40 mm distance was utilized for analysis. The use of all three transmitter-receiver pairs also allowed for the approximation of the tissue scattering coefficient and the calculation of the tissue saturation index (TSI), analogous to tissue oxygen saturation (StO2, rsO2) reported with similar NIRS systems.

NIRS data were transmitted via Bluetooth to the OxySoft software (Artinis Medical Systems) (Figure 3.5) and subsequently sent to the ICM+ software (Cambridge Enterprises, United Kingdom) for further processing. Before initiating recordings, the thickness of adipose tissue over the brachioradialis was measured using a standard ultrasound and linear probe (Sonosite, Canada) as shown in Figure 3.3, and the finger capillary refill test was conducted on each patient.

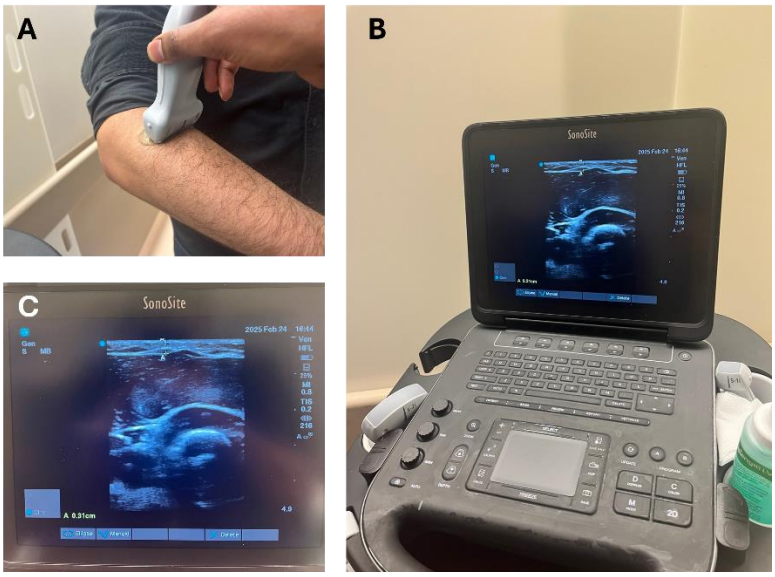

Figure 3.3 Ultrasound measurement of adipose tissue thickness over the brachioradialis muscle. (A) Ultrasound probe placement on the forearm. (B) Ultrasound device setup used for imaging. (C) Ultrasound measurement interface displaying adipose tissue thickness in millimeters.

Additionally, if available, arterial blood pressure (ABP) was measured via an invasive arterial catheter zeroed at the level of the right atrium, inserted by the clinical team as part of standard care, and continuously acquired using a DT9804 (Data Translation, United States) data acquisition module from the bedside ICU monitor at 100 Hz (Figure 3.4). All NIRS and ABP signals were merged and synthesized in ICM+ software for further analysis (Figure 3.6).

Figure 3.4 Bedside ICU monitor displaying real-time hemodynamic parameters, including arterial blood pressure (ABP) and electrocardiogram (ECG). These values were continuously recorded and acquired for analysis as part of the study.

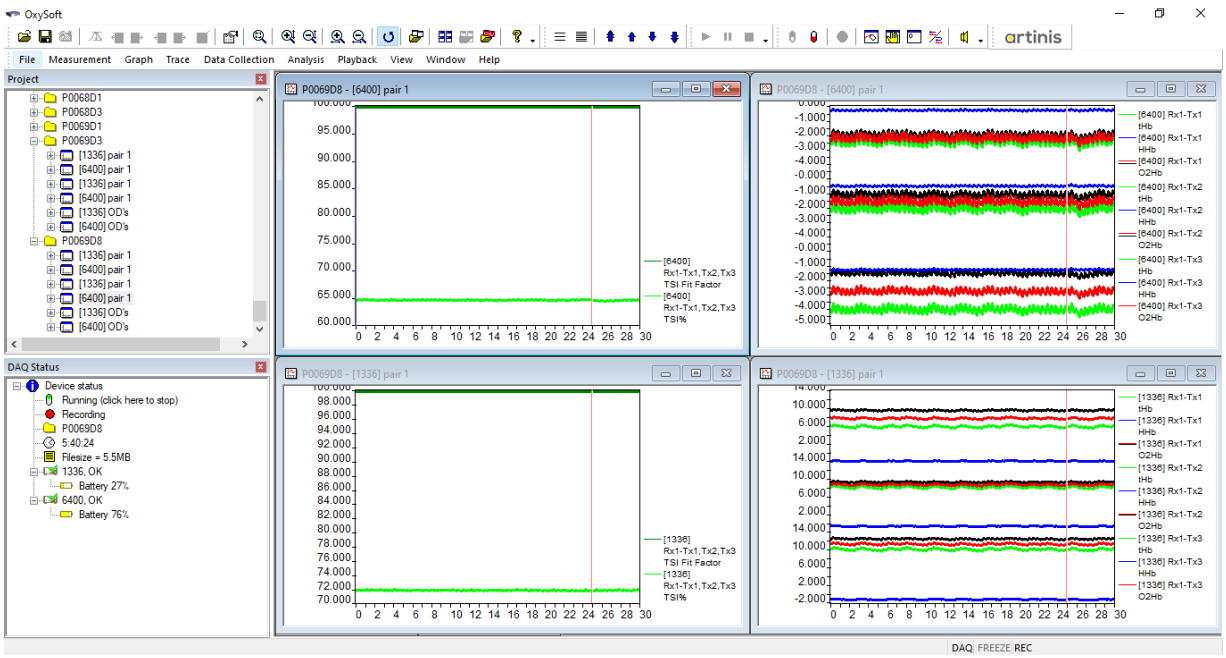

Figure 3.5 OxySoft software interface used for real-time acquisition and monitoring of NIRS signals. The display shows recorded oxygenation data from different source-detector pairs, with signal quality indicators and device status.

Figure 3.6 ICM+ software interface displaying real-time hemodynamic and NIRS-derived parameters. The monitored signals include arterial blood pressure (ABP), electrocardiogram (ECG), total hemoglobin concentration (tHb), and tissue saturation index (TSI). ICM+ was used for synchronized multimodal physiological data collection and analysis during the study.

The microvascular monitoring procedure in the healthy control study mirrored that of the ICU cohort, utilizing hr-NIRS to assess hemoglobin variability in the brachioradialis muscle. The same PortaMon device and configuration of light transmitters and receiver distances (30, 35, and 40 mm) with a DPF of 4 were used. Monitoring in healthy participants was performed while they were at rest in a horizontal position for 60 minutes.

3.5. Removing Motion Artifact

Raw NIRS and ABP signals were manually inspected, and motion artifacts were removed using the ICM+ artifact cleaning tool. These artifacts often manifest as abrupt signal spikes, dropouts, or baseline shifts caused by patient movement, probe adjustment, or external interference. While automated filtering techniques can be useful, they may fail to reliably distinguish physiological variations from noise in real-time clinical signals. Therefore, manual review served as a critical quality control step to ensure the integrity of the time-series data. Three examples of these artifacts are shown in Figure 3.7. Panel A displays frequent, high-amplitude transients that completely distort the signal, likely due to continuous probe movement or vibration. In Panel B, the signal initially shows usable physiological fluctuations, but then a sudden upward shift in baseline occurs, likely from a brief probe displacement. Panel C shows a more gradual baseline drift and contains clear motion artifacts such as abrupt spikes that need to be removed. These types of segments were excluded from further analysis to avoid distortion in time- and frequency-domain features.

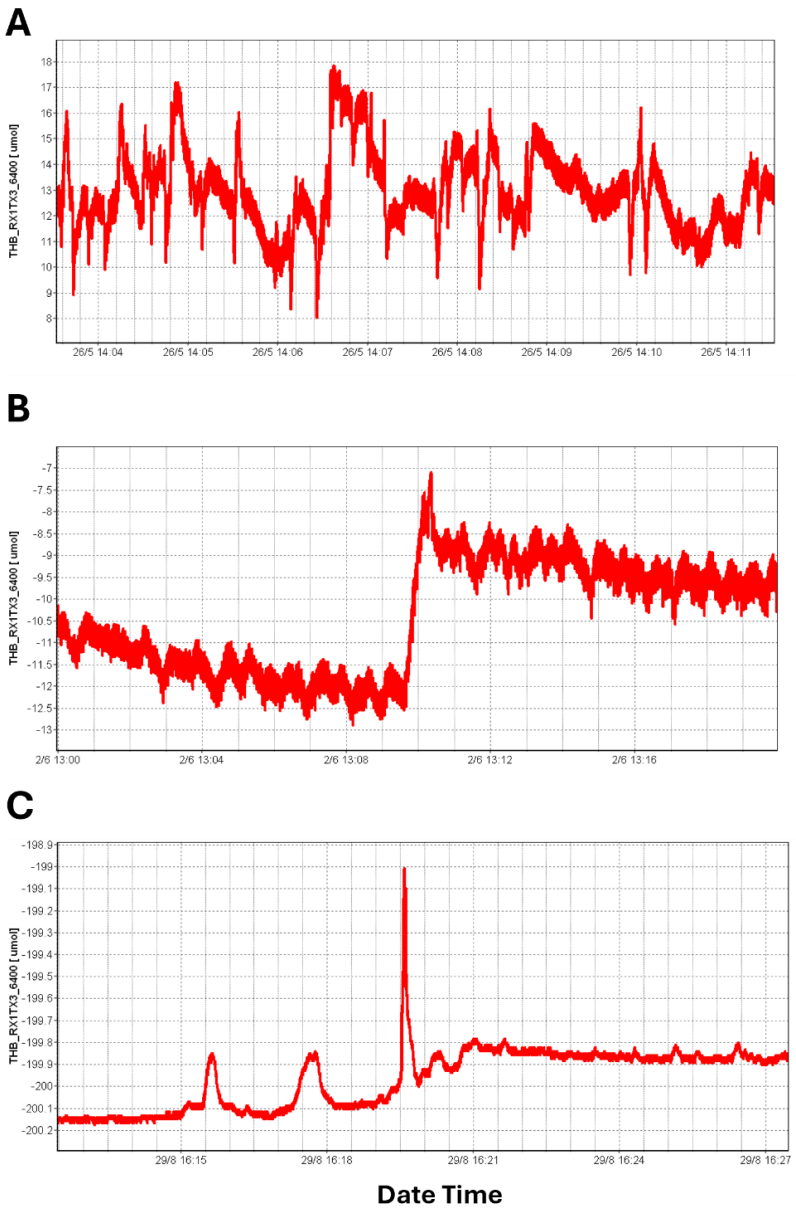

Figure 3.7 Examples of motion artifacts in raw NIRS signals. (A) Frequent, high-amplitude transients caused by continuous probe movement. (B) Sudden baseline shift following a period of clean signal, likely due to brief displacement. (C) Motion-induced spikes superimposed on a slow baseline drift.

4. MAPopt in Skeletal Muscle: Methods and Results

This chapter presents the methodology and findings of the MAPopt sub-study within the MiMICSS project. The primary aim of this sub-study was to evaluate skeletal muscle microvascular autoregulation in critically ill patients by deriving an individualized optimal mean arterial pressure (MAPopt) based on near-infrared spectroscopy (NIRS) signals. By adapting previously established techniques from cerebral autoregulation research, this study sought to determine the pressure range associated with the most favorable microvascular function in the peripheral circulation. The analysis focused on high-resolution recordings acquired on the first day of ICU admission in a subset of patients who met specific inclusion criteria, including the use of vasopressors and availability of invasive arterial blood pressure monitoring.

4.1. Microvascular autoregulation and derivation of optimal mean arterial pressure (MAPopt)

Only the data from day 1 signals were utilized in the subsequent analysis. MA was determined based on the correlation between the NIRS signal and ABP, as has been described previously for cerebral NIRS [140]. To minimize the influence of high-frequency components of respiratory and cardiac activities, as well as focus on the microvascular frequencies, a 10-second moving average was applied to the signals [141].

Subsequently, the averaged ABP was designated as mean arterial pressure (MAP). A Pearson correlation analysis was then conducted between MAP and each of the four NIRS signals within a 5-minute window, with updates every minute. These correlation coefficients are denoted as MVx (muscle HbT), THx (brain HbT), MOx (muscle TSI), and COx (brain TSI) as shown in Table 4.1. This is a standard approach in similar studies to calculate autoregulation indices [141], [142], [143]. Under normal conditions, correlation indices are presumed to have a low or negative value, reflecting intact MA; in disease conditions, these indices become strongly positive reflecting a pressure-passive system with loss of MA [95].

Table 4.1 Correlation indices used to assess the relationship between arterial blood pressure (ABP) and NIRS-derived signals

Source Signal	Correlation Indices (vs ABP)
Muscle HbT	MVx
Brain HbT	THx
Muscle TSI	MOx
Brain TSI	COx

MAPopt was determined using the four correlation indices listed above – MVx, THx, MOx, and COx. The processing procedure for calculating MAPopt was executed using ICM+ software. MAPopt is calculated by initially preprocessing correlation coefficients using the Fisher Transform to achieve normal distribution. Then data is divided into MAP-based bins, and an error bar chart illustrates the relationship between correlation signals and MAP. Adjustments to the default ICM+ configuration for MAP bins and error thresholds can be made, such as reducing the exclusion threshold to 2% of the data or modifying the binning settings using 4 mm Hg instead of 5 mm Hg increments.

The algorithm aims to fit a curve, ideally forming a smooth U-shaped pattern, to this plot. It follows specific criteria to ensure the quality of the curve fit, including the exclusion of outlier bins, representing at least 50% of all data points within the analyzed window period, and accounting for a minimum of 20 mm Hg of MAP fluctuation. If the criteria are met, the algorithm stops, returning the minimum of the fitted curve as the MAPopt value, which is the MAP with the best-preserved MA. In some scenarios, only the monotonically ascending or descending section of the curve may be available within the given MAP range, and the minimum value of these curves is then reported as the MAPopt [142].

Figure 4.1 and Figure 4.2 illustrate examples of the MAPopt calculation process using ICM+ software. Both figures display the MAP signal alongside brain and muscle total hemoglobin (THb) signals, as well as their corresponding correlation indices (THx for the brain and MVx for muscle). The error bar charts in these figures depict the correlation indices binned across different MAP values, facilitating the curve-fitting process used to derive MAPopt.

In Figure 4.1, a U-shaped curve was successfully fitted for the THx index, allowing the nadir of the curve to be identified as the optimal MAP (MAPopt). However, for the MVx index,

a U-shaped curve could not be obtained, and instead, the data followed an ascending trend. Conversely, in Figure 4.2, the opposite pattern was observed—neither THx nor MVx formed a complete U-shaped curve. Instead, both indices exhibited a descending trend, requiring the minimum value in the available range to be reported as MAPopt.

Additionally, an adjustment was necessary in the processing of the MVx index. The standard binning interval of 5 mmHg did not allow for an adequate curve fit; therefore, the bin width was manually refined to 4.7 mmHg.

Because of the relatively short length of our recording (hours), this algorithm was executed on a fixed window spanning the entire duration of each recording session for each patient, as described originally by Steiner and colleagues for the CPPopt method [144]. However, we also explored newer methodologies, including the optimal flex window method [145], and with various window sizes (1-8 hours) and MAP bin widths (2-5 mm Hg).

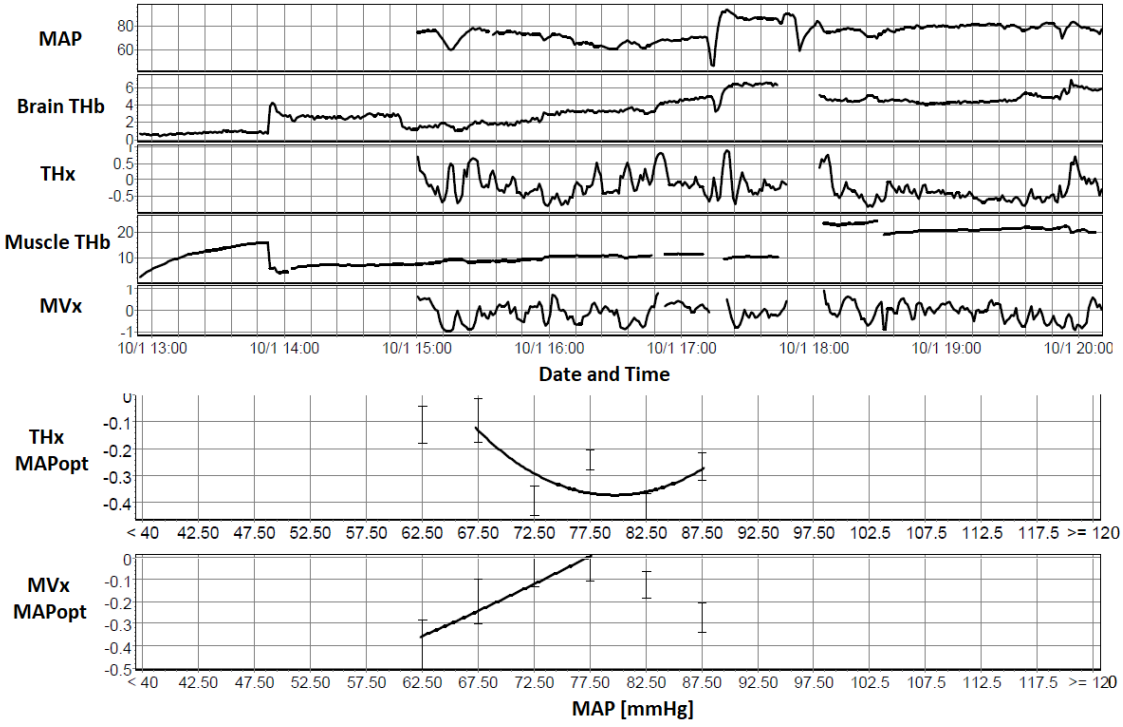

Figure 4.1 MAPopt calculation using ICM+ software. Shown are MAP, brain THb, and muscle THb signals, along with their respective autoregulation indices: THx (brain) and MVx (muscle). A U-shaped curve was successfully fitted to THx while MVx showed an ascending trend, with their minimum indicating MAPopt.

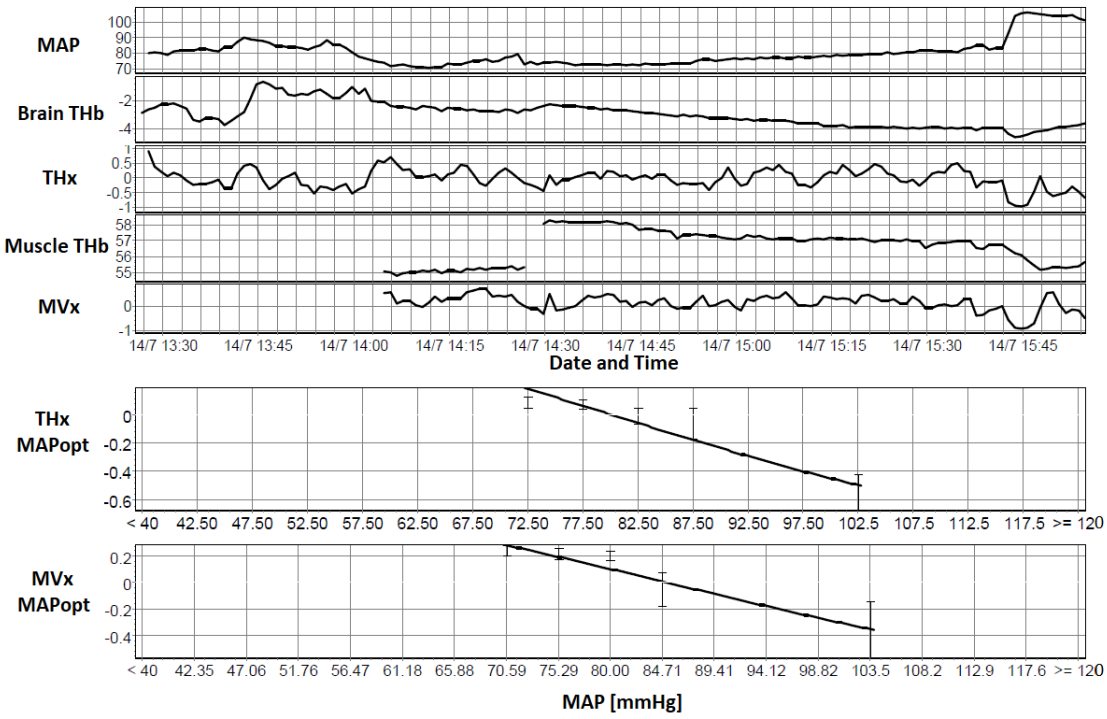

Figure 4.2 MAPopt calculation example where both THx and MVx displayed descending trends. No U-shaped curves were observed. MAPopt was taken as the lowest MAP in range. MVx bin width was adjusted to 4.7 mmHg to improve curve resolution.

4.2. Statistical Analysis

Statistical analyses were performed using GraphPad Prism (GraphPad Software Inc., United States). Continuous variables are reported as mean ± standard deviation or median (interquartile range), as appropriate.

For the MAPopt sub-study, descriptive statistics were used to summarize microvascular autoregulation (MA) indices, including median, interquartile range (IQR), and coefficient of variation. The duration, percentage of total recording time, and norepinephrine dose per hour were quantified for periods during which the MA correlation indices exceeded a predefined threshold of 0.3—previously established as an indicator of impaired autoregulatory function.

MAPopt values were computed per patient for each MA index. Additionally, the percentage of time spent below MAPopt was calculated, which may reflect compromised autoregulation, consistent with literature from traumatic brain injury studies. Pearson correlation was used to evaluate associations between MAPopt values derived from different NIRS signals (HbT vs. TSI) and between brain and muscle recordings. A significance level of 5% was used for all analyses.

4.3. Patient Characteristics and Signal Quality

In the MAPopt cohort, the average duration of patient recordings was 394 ± 229 minutes. After excluding segments with motion artifacts, the average usable signal duration was 329 ± 168 minutes. The cohort included 15 patients, of whom 4 (27%) were female, with a mean age of 63 ± 14 years. Ten patients (67%) had a diagnosis of sepsis, and the same number had at least one preexisting cardiovascular condition, such as hypertension, diabetes, vascular disease, or heart failure.

During the recording period, the median norepinephrine dose was 0.13 (0.09) µg/kg/min, and 9 patients (60%) also received vasopressin. Median serum lactate levels were 1.8 (1.55) mmol/L, and capillary refill time was normal (<3 seconds) in 12 patients (80%). The average adipose tissue thickness over the brachioradialis muscle was 3.4 ± 1.0 mm (n = 13; data missing for 2 patients).

NIRS sensors were placed on both the forearm and forehead. In 11 patients, the placements were ipsilateral (same side), while in 3 patients they were contralateral (opposite sides). This variation in sensor positioning was due to practical constraints at the bedside (e.g., available space, wounds, or medical equipment), which occasionally necessitated alternate placement.

4.4. MAPopt Study Results

4.4.1. Impaired microvascular autoregulation in critically ill patients in skeletal muscle and brain

The correlation indices between each NIRS and MAP signal provide an evaluation of MA within skeletal muscle and brain. The median (IQR) value of each index is computed as follows: MVx: -0.02 (0.15), THx: -0.02 (0.31), MOx: 0.12 (0.25), and COx: 0.11 (0.16). These correlation indices also exhibit notable fluctuations within the same patient recording, with coefficients of variation of 1445% for MVx, 617% for THx, 1017% for MOx, and 418% for COx. To evaluate the extent of autoregulation impairment in patients, the percentage of time during which the correlation index of each signal exceeds the threshold of 0.3 is calculated. These values are reported as median (IQR): MVx: 29.7% (11.35%), THx: 24.5% (28.15%), MOx: 33.9% (31.1%), COx: 34.9% (16.05%), as shown in Figure 4.3. Furthermore, to assess

the magnitude of autoregulation impairment, the dose for which each signal remains above the 0.3 threshold per hour is computed.

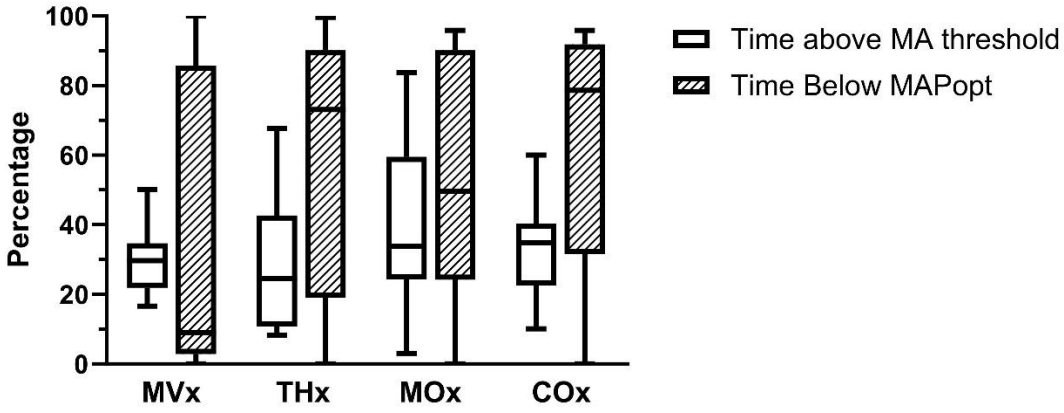

Figure 4.3 The percentage of time that each microvascular autoregulation (MA) correlation index exceeds the impairment threshold of 0.3 and the percentage of time that mean arterial pressure (MAP) is below the calculated optimal MAP (MAPopt). Plots represent the median, interquartile range, and minimum maximum for the cohort. COx = brain tissue saturation index, MOx = muscle tissue saturation index, MVx = muscle total hemoglobin, THx = brain total hemoglobin.

4.4.2. Derived MAPopt from skeletal muscle and cerebral NIRS signals

The MAPopt values were successfully determined for each correlation coefficient across all patients. 24/60 signals required adjustment to default ICM+ settings. Figure 4.4 serves as an illustrative example of ICM+ output, showcasing the process of calculating MAPopt. This figure displays the MAP, Brain HbT, THx, Muscle HbT, and MVx signals recorded over an approximately 8-hour session. Areas with no data correspond to segments where motion artifacts were removed. The figure also demonstrates the mean values of THx and MVx plotted in 5 mm Hg bins of MAP, fitted by a U-shaped curve that identifies the MAPopt at its nadir. As shown in Figure 4.5, the calculated MAPopt values for the cohort are presented as median (IQR): MVx-MAPopt 62.35 (17.33) mm Hg; THx-MAPopt 76.14 (12.25) mm Hg; MOx-MAPopt 75.98 (12.55) mm Hg; and COx-MAPopt 77.65 (8.11) mm Hg.

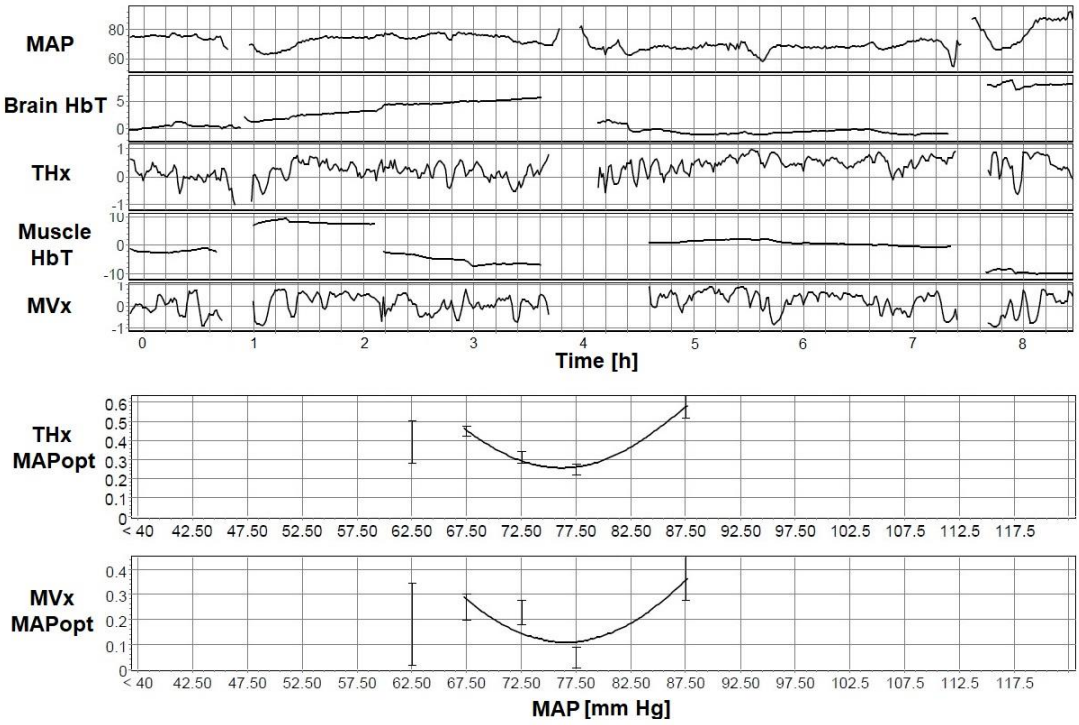

Figure 4.4 Derivation of optimal mean arterial pressure (MAPopt) from a representative time series from a single patient. Near-infrared spectroscopy signals from brain total hemoglobin (HbT) (THx) and muscle HbT (MVx), with the removal of motion artifacts and 10-s moving average filter, are used to derive a correlation index with arterial blood pressure denoted as THx and MVx, respectively. The error bar charts of THx and MVx vs. mean arterial pressure (MAP) bins are used to fit a U-shaped curve that calculates the nadir as MAPopt; this is the MAP with the best preservation of microvascular autoregulation. In this particular patient, the fitted MAPopt curves derived from the brain and muscle exhibit a high degree of similarity, despite differences in the correlation indices for each MAP bin between the two organs.

MAPopt values for each correlation index were above 65 mmHg for 7 patients (47%), 13 patients (87%), 12 patients (80%), and 14 patients (93%) for MVx, THx, MOx, and COx respectively. Among the 60 MAPopt values analyzed in this study – 4 values for each MA index per patient - 30 signals (50.0%) exhibited a U-shaped curve in their plot of MA index versus MAP. Sixteen signals (26.7%) demonstrated a descending curve along the MAP axis, and fourteen signals (23.3%) displayed an ascending curve. We also explored various algorithm configurations, involving window lengths of 1, 2, 4, and 8 hours, as well as bin widths of 3-, 4-, and 5-mm Hg.

The median MAPopt, interquartile range (IQR), and yield percentage for each configuration were calculated; overall there was good low variability between each of these configurations with only modest differences in derived MAPopt. The proportion of time during which blood pressure remained below the determined MAPopt is also assessed, represented as

median (IQR): 9.0 (74.5) % for MVx, 73.1 (62) % for THx, 49.7 (61.4) % for MOx, and 78.6 (42.8) % for COx, as shown in Figure 4.3.

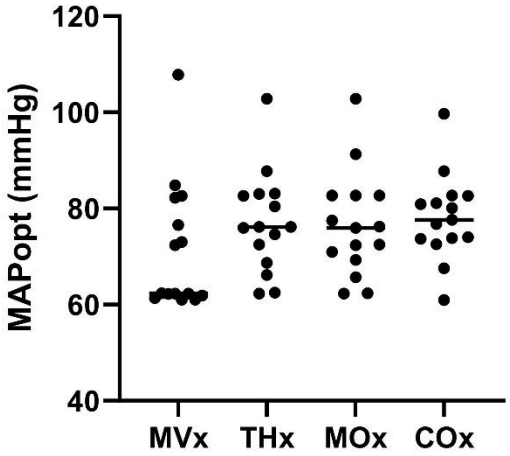

Figure 4.5 Optimal mean arterial pressure (MAPopt) values of the cohort derived from each of the four microvascular autoregulation (MA) indices. MA indices reflect the correlation between arterial blood pressure and muscle total hemoglobin (MVx), brain total hemoglobin (THx), muscle tissue saturation index (MOx), and brain tissue saturation index (COx). Line represents the median value.

4.4.3. Correlation and comparison of MAPopt Values Derived from skeletal muscle and brain NIRS

The correlation between skeletal muscle and brain-derived MAPopt is shown in Figure 4.6. Pearson correlation coefficient between MVx-MAPopt and THx-MAPopt is $r = 0.76$ ($p < 0.001$, CI = [0.41, 0.92]), and between MOx-MAPopt and COx-MAPopt is $r = 0.69$ ($p = 0.005$, CI = [0.27, 0.89]), suggesting a moderate correlation between MAPopt values derived from muscle and brain HbT and TSI signals. However, the difference between the calculated HbT-MAPopt values and the TSI-MAPopt values of the muscle and brain shows some notable differences. As shown in Figure 4.7, these calculations yielded a median (IQR) difference of -1.27 (9.67) mmHg and 0.05 (9.72) mmHg, respectively. The correlation between HbT and TSI derived MAPopt values for the same patient was also calculated: MVx-MOx correlation is $r = 0.58$ ($p = 0.022$, CI = [0.1, 0.84]), and THx-COx correlation is $r = 0.65$ ($p = 0.009$, CI = [0.21, 0.87]).

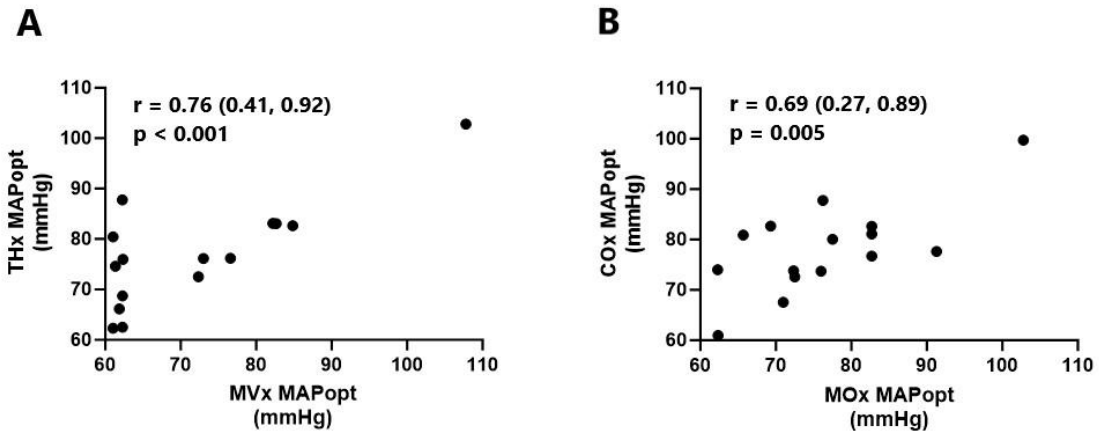

Figure 4.6 Correlation between optimal mean arterial pressure (MAPopt) values obtained from muscle and brain near-infrared spectroscopy (NIRS) for each patient in the cohort, derived from correlation indices from NIRS total hemoglobin (muscle total hemoglobin [MVx], brain total hemoglobin [THx]) and tissue saturation index (muscle tissue saturation index [MOx], brain tissue saturation index [COx]). A: Correlation between MVx–MAPopt and THx–MAPopt. B: Correlation between MOx–MAPopt and COx– MAPopt. Values represent the Pearson correlation coefficient (95% CI).

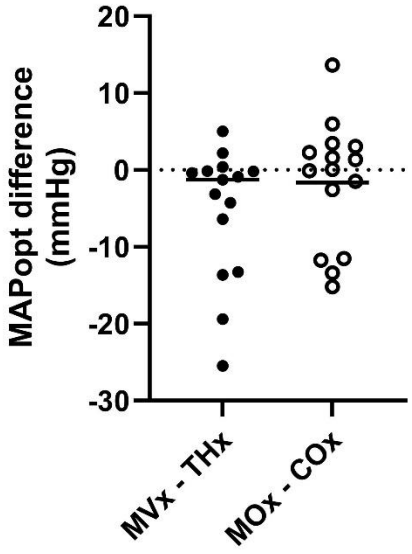

Figure 4.7 The difference between optimal mean arterial pressure (MAPopt) values of muscle and brain using near-infrared spectroscopy signals for total hemoglobin (muscle total hemoglobin [MVx]– brain total hemoglobin [THx]) and tissue saturation index (muscle tissue saturation index [MOx]–brain tissue saturation index [COx]) for each patient in the cohort. Across the cohort, MAPopt in skeletal muscle can get higher, lower, or nearly identical to the MAPopt in the brain. The line represents the median value.

5. Wavelet-derived Microvascular Power: Methods and Results

This chapter presents the methodology and findings from the wavelet-based analysis of near-infrared spectroscopy (NIRS) signals in critically ill patients. The primary objective was to quantify the frequency-specific power of microvascular and cardiac components within the tissue hemoglobin signal (HbT) and to explore their association with patient outcomes and vasopressor therapy. Unlike the MAPopt analysis, which focused on autoregulatory function, this component of the study aimed to characterize the spectral features of the microcirculation and evaluate changes over time during ICU admission. The analysis included NIRS signals collected on days 1, 3, and 8, with careful preprocessing and artifact removal to ensure signal integrity.

5.1. Wavelet Signal Processing and derivation of Microvascular and Cardiac Powers

For the wavelet signal processing component of the study and the derivation of microvascular and cardiac powers from patients' signals, we exclusively utilized the muscle HbT signal, building on previous work by our group [15]. For this part of the study, all of the signals form day 1, day 3, and day 8 were analyzed. Artifact removal was implemented using the ICM+ artifact removal tool, which facilitated the detection and elimination of signal portions affected by distortions, sudden variations due to motion artifacts, electrical noise, or other interferences. This process segmented the signals into portions of varying lengths, with each segment being free of artifacts and suitable for subsequent analysis.

To facilitate the subsequent stages of signal processing, a graphical user interface (GUI) has been developed. This GUI allows for the importation and display of high-quality data segments, which we defined as having at least 20 minutes of continuous, uninterrupted clean data; this duration of length was chosen given that it is well above the longest period of the lowest frequency range, and 20 minutes is relatively protected from edge artifacts. Users can review each segment and select one to continue with or choose not to use any of them if desired. Subsequently, each segment will undergo a continuous wavelet transform (Figure 5.1).

The Morlet wavelet will serve as the mother wavelet for this transformation, with $\omega_0 = 6$. The parameter ω_0 determines the Morlet wavelet's central frequency and is associated with the number of wavelet cycles. Setting ω_0 to 6 typically results in the wavelet having about 6 oscillations within its shape [146]. This parameter influences the wavelet's width and form in both time and frequency domains. For a Morlet wavelet, the central frequency fc is approximated by the equation:

$$f_c = \frac{\omega_0}{2\pi}$$

Thus, when ω_0 equals 6, the central frequency is roughly 0.955 [147].

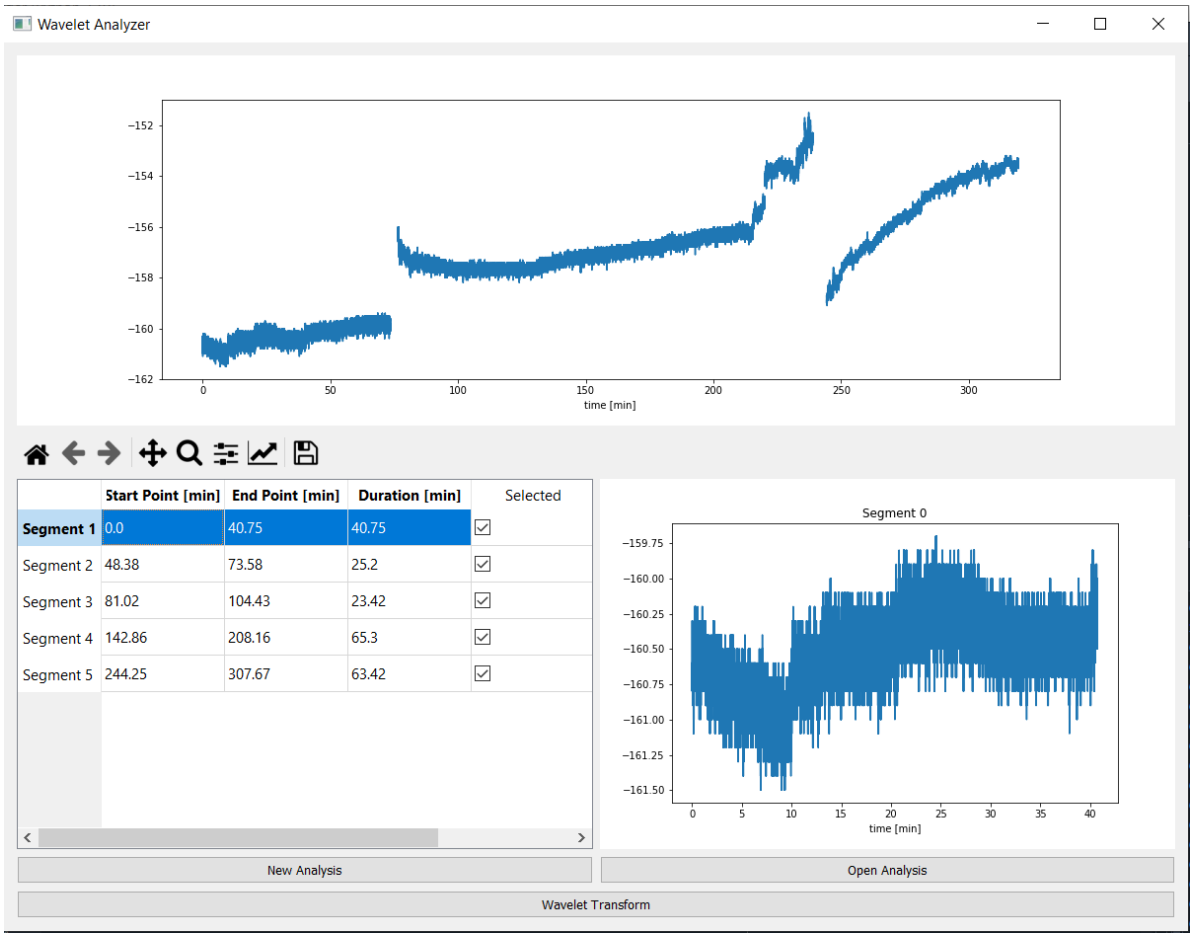

Figure 5.1 Interface of the Wavelet Analyzer tool designed for preprocessing time-series signals. The top panel shows the full signal over time, while the lower panel displays segmented data selections based on predefined time intervals. Each segment is analyzed independently to ensure the exclusion of motion artifacts and improve the reliability of wavelet-based power analysis.

The wavelet analysis employs 14 octaves and 12 sub-octaves within each octave set. In wavelet analysis, "octaves" and "sub-octaves" describe the distribution of wavelet scales across scale/frequency ranges. An octave signifies a scale doubling. For instance, if s_0 is the base scale factor, the subsequent octave encompasses scales from s_0 to $2s_0$, followed by $2s_0$ to $4s_0$, and so on. Sub-octaves are subdivisions within octaves, offering more detailed scales and frequency resolution. With 12 sub-octaves per octave, each octave is split into 12 smaller frequency bands, allowing for finer analysis.

The wavelet transform's frequency axis points correspond to frequencies calculated using the equation:

$$f_j = \frac{f_c}{s_j \times dt}$$

In this equation, f_c represents the Morlet transform's central frequency (approximately 0.955), s_j denotes the scale factor, and dt signifies the sampling time interval (0.1s). The initial scale factor in this instance is 2, which is influenced by the Nyquist law. This law states that the maximum detectable frequency is half the sampling rate. By selecting s_0 as 2 and knowing f_c is less than 1, we ensure that the highest frequency point will be slightly below but near 5 Hz. Subsequent scales are computed using the formula

$$s_j = s_0 \times 2^{\frac{j}{12}}$$

where j ranges from 0 to 168 (12×14).

The calculation of the power spectrum involves a time axis corresponding to the time domain signal points and a frequency axis spanning from low to high frequencies. At each point, the power for a specific scale s and time t is determined by squaring the magnitude of the wavelet coefficients:

$$Power(s,t) = |W(s,t)|^2$$

Which, $W(s,t)$ represents the complex wavelet coefficient at scale s and time t, resulting from the Continuous Wavelet Transform. While the power spectrum can be represented in both scale-time and frequency-time domains, this study utilized the frequency-time domain. This choice was made to facilitate the extraction of two distinct frequency bands: the cardiac band and the microvascular band, for which the frequencies are known.

The selection of bands will depend on the literature, and each band will have a specific frequency range. The microvascular band will encompass frequencies from 0.0095 Hz to 0.16

Hz, while the respiratory band will range from 0.16 Hz to 0.667 Hz. Lastly, the cardiac band will have a frequency range of 0.667 Hz to 3.1 Hz [15]. While these default values will be used as a starting point, adjustments may be necessary for individual signals.

To facilitate this, a tool has been created in the graphical user interface to modify the upper and lower boundaries of the bands in the spectrum (Figure 5.2). Visual cues are integrated into the interface to assist in identifying the bands accurately. One key feature is the identification of the prominent cardiac band second harmonics, often referred to as the "echo" feature. These second harmonics are distinct peaks in the frequency spectrum that arise due to the doubling of the primary cardiac frequency. While they are a normal artifact of the cardiac signal, they do not represent the primary cardiac activity and should not be included in the analysis of the cardiac band.

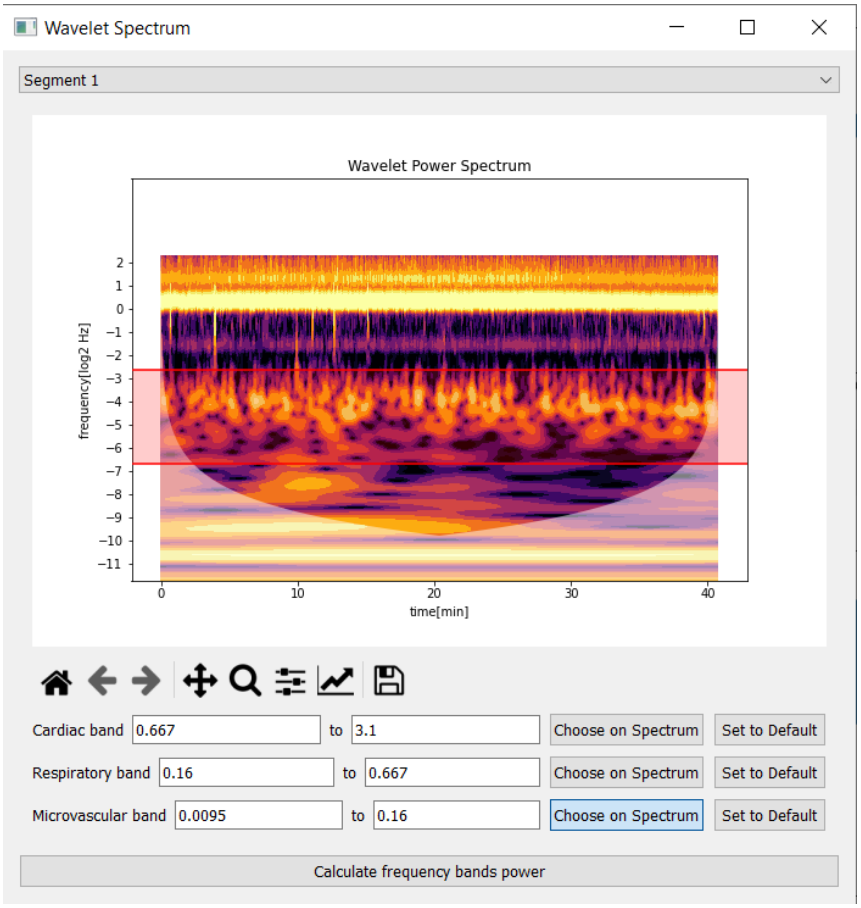

Figure 5.2 Example of a wavelet power spectrum for a selected segment. The color map represents the signal power across different frequencies and time. The red box highlights the microvascular frequency range (0.0095 - 0.16 Hz), where microvascular oscillations are analyzed.

GUI allows users to visually detect these echoes and exclude them from being calculated as part of the actual cardiac band. This ensures that the derived cardiac power is based solely on the primary cardiac frequency and not inflated by secondary harmonics. Similarly, the respiratory band, which is easily detectable between the cardiac and microvascular bands, is excluded from the target bands to maintain the focus on relevant physiological signals. By incorporating these tools and visual aids, the interface ensures precise identification and isolation of physiological signals, enabling accurate computation of microvascular and cardiac powers.

In the following step, we calculated the power of the cardiac and microvascular bands. To do this, we first calculated the sum of the powers of the frequencies within each band based on the limits of each band at each time point. Then, we produced a time series for both the cardiac and microvascular bands. To ensure consistency in the calculation and minimize the influence of secondary harmonics (echo), we carefully cropped the frequency intervals for both the cardiac and respiratory bands. Specifically, the cropping process excluded the second harmonics from the cardiac band and similar echoes from the respiratory band, ensuring that the calculated power reflected the primary physiological signals of interest. This approach ensures that the power in each band is based on well-defined and consistent frequency intervals, avoiding the need for normalization and maintaining comparability across patient groups. Figure 5.3 shows this process.

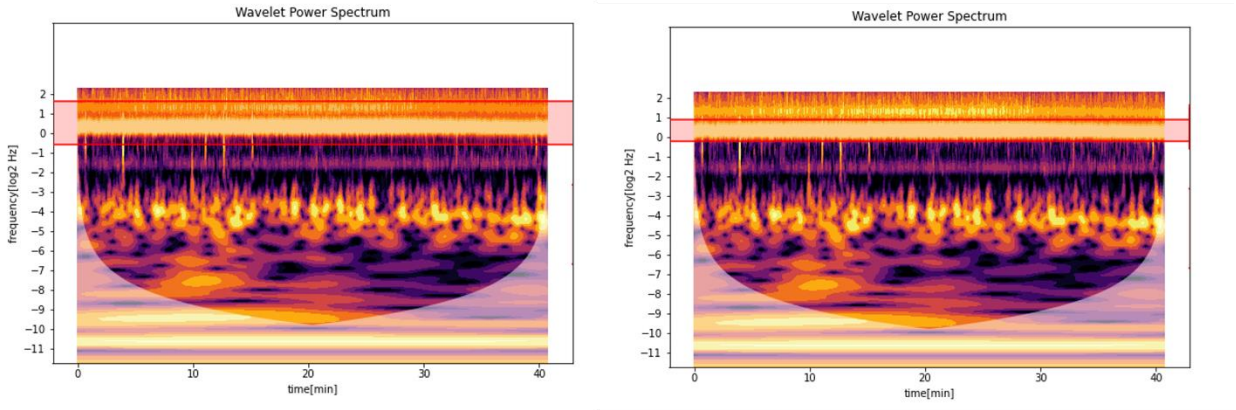

Figure 5.3 Wavelet power spectrum illustrating the selection of the cardiac frequency band and the presence of its harmonics. The left panel shows an initial band selection, while the right panel displays an adjusted range to better capture the dominant oscillations within the cardiac frequency domain. The red box in each plot marks the selected frequency range for power extraction. Additionally, multiple harmonics of the cardiac frequency can be observed as distinct parallel bands at higher frequencies, reflecting the nonlinear characteristics of physiological signals.

To determine the single-value power, we calculated the median of each time series and reported it as the power of each band. For recordings that were divided into multiple clean segments due to artifact removal, the segments were stitched together to form a continuous time series before calculating the median. This stitching process involved concatenating segments in the temporal order they occurred within the recording, ensuring no overlap or gaps between segments. Similarly, we applied the same approach to obtain the power of the respiratory band, which was not directly used in this study but was used to calculate the percentage of power of the cardiac and microvascular bands. The overall power was determined as the aggregate of the powers derived from the cardiac, respiratory, and microvascular bands, and the percentage of each power with respect to the total power was established as one of the variables. Figure 5.4 is the presentation of this part in the designed GUI.

Other variables were also defined here, such as the ratio of cardiac to microvascular power, and a variable referred to as mvP63, which is calculated in the following manner: it is the frequency at which the cumulative power in the microvascular band is 63% of the total power of the microvascular band. This method, inspired by the time constant of first-order LTI systems, is an effective indicator of the distribution of power across the frequencies of the microvascular band.

The same signal processing techniques were applied to the healthy control group data as described for the ICU cohort, including artifact removal, wavelet transform, and power spectrum analysis. The primary variables of interest, including microvascular power, cardiac power, and the ratio of cardiac to microvascular power, were calculated in both cohorts.

Figure 5.4 Output of the frequency band power analysis, showing extracted power values for cardiac, respiratory, and microvascular frequency bands. Signals are in time domain with the unit of minutes. The lower panel provides numerical values for median power and power percentage within each frequency band, allowing for quantitative comparisons across physiological oscillations.

5.2. Statistical Analysis

Statistical analyses were conducted using the PRISM software package (GraphPad Software Inc., United States). Data are reported as mean ± standard deviation or median (interquartile range), where appropriate.

For the wavelet analysis, a total of six variables were identified for each signal, including the logarithmic transformation of the power of the microvascular and cardiac bands, the percentage of power for each band, the ratio of cardiac to microvascular power, and mvP63. Two types of statistical analyses were performed: the first compared differences between these variables on Day 1 based on patient outcomes (survived or deceased) or the presence of septic

shock, while the second examined changes in these variables between Day 1 and Day 3 for patients who had data from both days to assess any differences following ICU admission and in relation to outcomes. The unpaired t-test (for log transformed parameters) and The Wilcoxon Mann-Whitney test (for remaining parameters: power percentages and MVP63) was employed to determine significance for these differences. The paired t-test was used to determine the differences between log-transformed variables in Day 1 and Day 3 for both survivors and non-survivors' groups.

An analysis was conducted to evaluate the relationship between microvascular (MV) power and cardiac power in relation to the administration of vasopressors during ICU care. To be classified in the "no-pressor" group, patients must have received no vasopressin, and either maintained an average norepinephrine dose below 0.04 μg/kg/min or had been weaned off norepinephrine during the recording session. To further examine the influence of vasopressor therapy over time, a subgroup analysis was performed on patients who had complete data available for both day 1 and day 3 of monitoring. Patients were categorized into three groups based on their vasopressor exposure: (1) Stayed on pressor – patients who received vasopressors on both day 1 and day 3; (2) Weaned off pressor – patients who received vasopressors on day 1 but not on day 3; and (3) Never on pressor – patients who did not receive any vasopressors on either day. Additionally, the Pearson correlation was calculated to assess associations between these variables and the mean norepinephrine dose. Finally, statistical comparisons between the ICU cohort and the healthy control group were made using Welch's t-test, with a significance level set at 5%.

5.3. Patient and Monitoring Characteristics

In the wavelet analysis, a total of 70 signals were processed (42 signals for Day 1, 23 signals for Day 3, and 5 signals for Day 8). The average duration of recordings after motion artifact removal was 352 ± 141 minutes, shortened to 201 ± 139 minutes after choosing high-quality segments. Of the 43 patients, 21 were female (49%), with an average age of 63 ± 16 years. Twenty-one participants (49%) were diagnosed with septic shock, and 34 patients (79%) had preexisting cardiovascular comorbidities. The median norepinephrine dose during the recording period was 0.04 μg/kg/min, ranging from 0 to 0.28 μg/kg/min. Additionally, 25 patients (58%) received vasopressin treatment on the first day in ICU, ranging from 1.2 to 2.4

U/min. The median serum lactate level was 1.8 mmol/L (range: 0.5 to 11.1 mmol/L), and the median capillary refill time was normal (less than 3 seconds) for 38 out of 43 patients (88%).

Regarding the healthy control group, 15 participants were recruited, with one participant excluded due to insufficient data. The demographic information is presented in

, with participants having a mean age of 30 years (SD 5), and 5 out of the 14 participants were female (35%). The average recording duration for the control group was 50 ± 20 minutes.

5.4. Wavelet Study Results

5.4.1. Segments and Signal Quality

As previously established, the objective was to identify segments in signals that contained a minimum of 20 minutes of high-quality data. A total of 79 signals were recorded, with a median 2 signals per patient. Of these 79 signals, 67 exhibited at least 20 minutes of high-quality data, and 3 contained at least one segment of either 15 or 20 minutes with a maximum one-minute gap between them. The remaining 9 signals lacked any high-quality components. These nine signals were excluded from the subsequent analysis and statistical calculations.

Table 5.1 summarizes the number of patient recordings included in the analysis across different days of monitoring. Of the full cohort, 43 patients had sufficient data quality and were included in the analysis: 42 had usable recordings on Day 1, 23 on Day 3, and 5 on Day 8. The number of patients available for analysis on ICU days 3 and 8 decreased due to various factors, including ICU discharge, in-hospital mortality, and excessive patient movement that prevented reliable data acquisition.

Table 5.1 Summary of Included Patient Recordings by Day

Recording Day	Number of Patients
Total Patients included	43
Day 1	42
Day 3	23
Day 8	5

While the mean ± standard deviation (SD) of recorded signals was 352 ± 138 minutes, the selected analyzed segments demonstrated a mean ± SD of 121 ± 91 minutes. This represented a mean ± SD percentage of 36% ± 24% of high-quality signal. On average, the high-quality segment duration for the control group was 40 ± 20 minutes, covering 83% ± 10% of the total recording duration.

On average, all the signals in ICU cohort exhibited of 3 ± 2 (mean ± SD) segments, while 18 of the 73 signals contained one segment. The mean values of each segment did not demonstrate substantial variation. We calculated the coefficient of variation (CV%) between the values of each segment in each signal. The mean CV% of cardio band segments in the signals with more than one segment was 32%, and the average CV% of microvascular band within the segments in signals with more than one segment was 36%. The bar diagram in Figure 5.5 shows the duration of each day 1 signal, along with the analyzed portions of each signal and their respective temporal positions.

5.4.2. Microvascular and Cardiac Power

The logarithmic transformation of the median power in the microvascular and cardiac band was calculated. To evaluate the relationship between these powers and ICU outcomes or septic shock presence. All parameters, including MV power [log], cardio power [log], MV power percentage, cardio power percentage, the ratio of cardio to MV power (c/Mv), and the frequency at which cumulative MV power reached 63% of its total power (MVP63), were examined to determine if there was a significant difference between patients who survived and those who died in the ICU. After applying the t-test on log-transformed parameters and the Wilcoxon test on other parameters, no significant difference was observed in the values of these parameters based on ICU mortality. Table 5.2 shows the values of these parameters for survived and deceased patients.

The same approach was applied to assess the presence of septic shock in patients, and again, no significant difference was found between the groups. Figure 5.6 illustrate the violin plots of selected parameters categorized by outcome and septic shock.

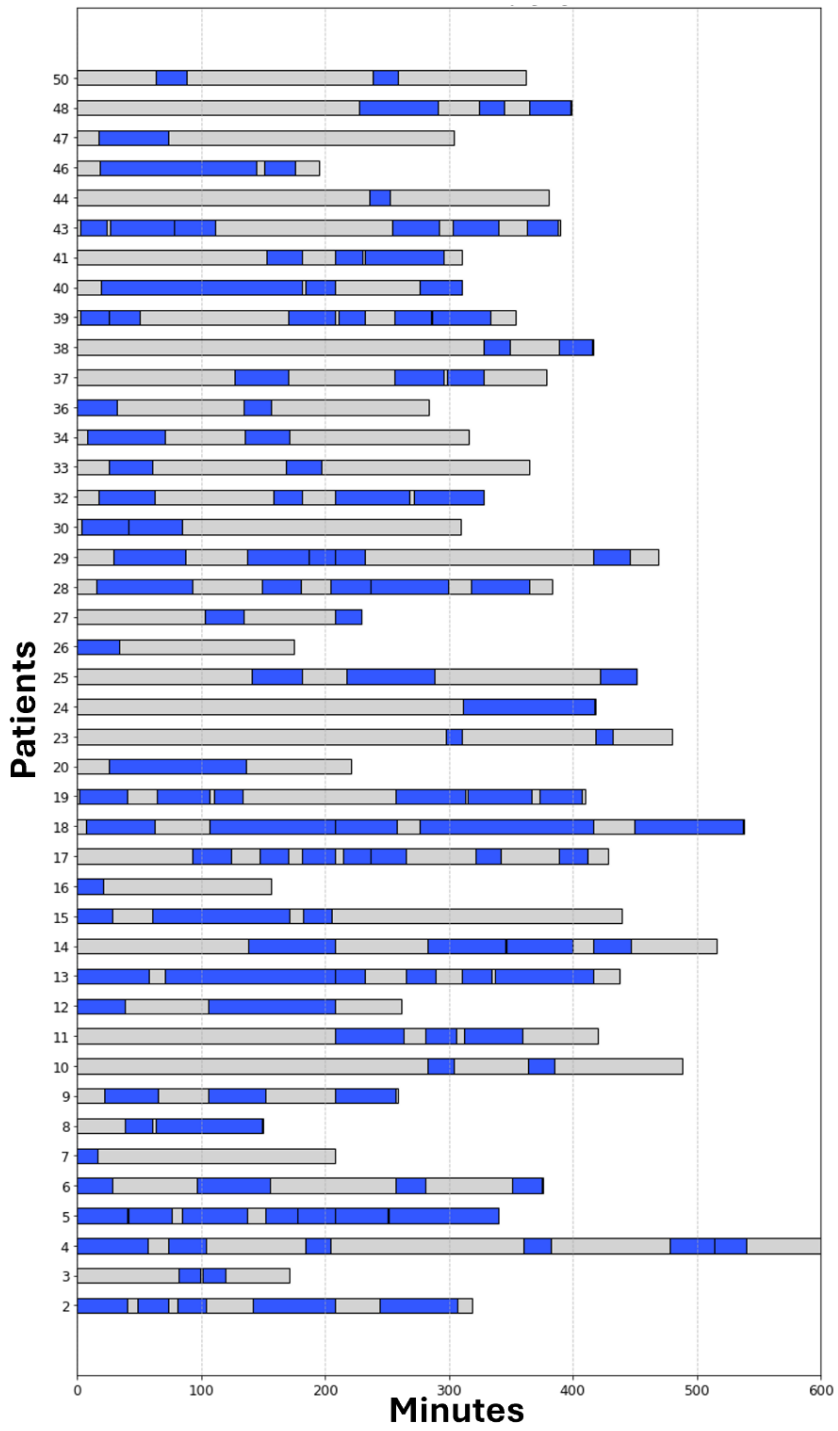

Figure 5.5 Bar diagram showing the duration of each Day 1 signal, highlighting the analyzed portions of each signal and their respective temporal positions within the recording periodEach bar represents the duration of the signal in minutes, with blue segments indicating portions selected for analysis and gray segments denoting areas excluded from further analysis due to insufficient signal quality.

Table 5.2 Wavelet derived parameters for patients in Day 1 of their ICU stay with the comparison of survivors and non-survivors; data is presented as mean ± std or median (q1-q3)

Parameter	Survivors (n=25)	Non-survivors (n=17)
MV [Log]	-0.38 ± 0.65	-0.44 ± 0.72
Cardio [Log]	-0.33 ± 0.46	-0.57 ± 0.76
c/Mv [Log]	0.04 ± 0.61	-0.12 ± 0.63
MV%	25.63 (12.55-42.42)	27.28 (23.04-39.26)
Cardio%	25.90 (22.41-43.46)	18.62 (10.58-48.47)
MVP63	0.04 (0.03-0.04)	0.04 (0.03-0.05)

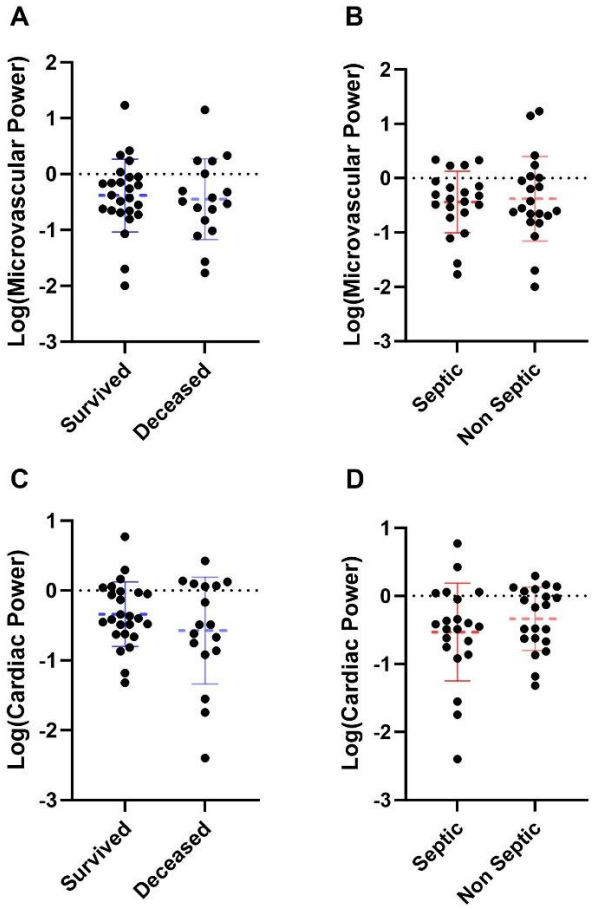

*Figure 5.6 Plots of the log-transformed microvascular (MV) power and cardiac power, categorized by patient outcome (survivor vs. non-survivor) and presence of septic shock. These plots display the distribution, density, and range of each parameter within the respective groups. **A**: No statistically significant difference in MV power was observed between patients who survived and those who did not survive. **B**: No statistically significant difference in MV power was observed between patients who were diagnosed with septic shock and those who were not. **C**: No statistically significant difference in cardiac power was observed between patients who survived and those who did not survive. **D**: No statistically significant difference in cardiac power was observed between patients who were diagnosed with septic shock and those who were not.*

To investigate the relationship between microvascular power and cardiac power with the use of pressors, two analytical approaches were employed.

The first approach focused on patients receiving norepinephrine, specifically examining the relationship between norepinephrine dosage and MV or cardiac power through a Pearson correlation analysis. This analysis, however, showed no significant correlation between norepinephrine dosage and MV power (R2=0.025; p=0.36), and the same lack of correlation was observed for cardiac power (R2=0.0002; p=0.93). Figure 5.7 illustrates the scatter plot of norepinephrine dosage and MV power and cardiac power, supporting these observations.

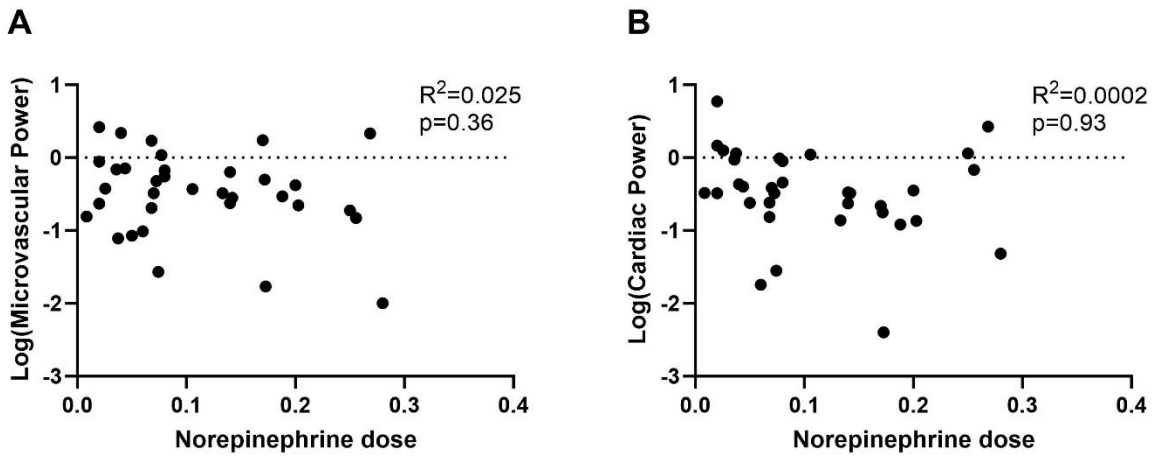

*Figure 5.7 **A**: Scatter plot showing the relationship between norepinephrine dosage and log-transformed MV power in patients receiving norepinephrine. **B**: Scatter plot showing the relationship between norepinephrine dosage and log-transformed Cardiac power in patients receiving norepinephrine.*

Secondly, a t-test compared log-transformed microvascular power and cardiac power between patients who didn't receive any form of pressors on day 1 (n=11) and those who received pressors on day 1 (n=31) based on criteria defined in 5.2. Table 5.3 shows the number of patients who received pressors on different days.

Table 5.3 Summary of patient numbers based on the presence of vasopressors in their ICU care

Days	On Pressor	Off Pressor
Day 1	31	11
Day 3	12	11
Day 8	1	4

The results demonstrated that MV power on day 1 was significantly higher in patients who did not require pressors (-0.03 ± 0.85 vs -0.54 ± 0.55; p=0.03) while no significant difference was observed on day 3 (-0.08 ± 0.43 vs -0.14 ± 0.46; p=0.72) as shown in Figure 5.8. The same results were observed in cardiac power, with a significantly higher power in patients without pressors on day 1 (-0.07 ± 0.31 vs -0.56 ± 0.63; p=0.02) and no difference on day 3 (-0.1 ± 0.47 vs -0.22 ± 0.56; p=0.59).

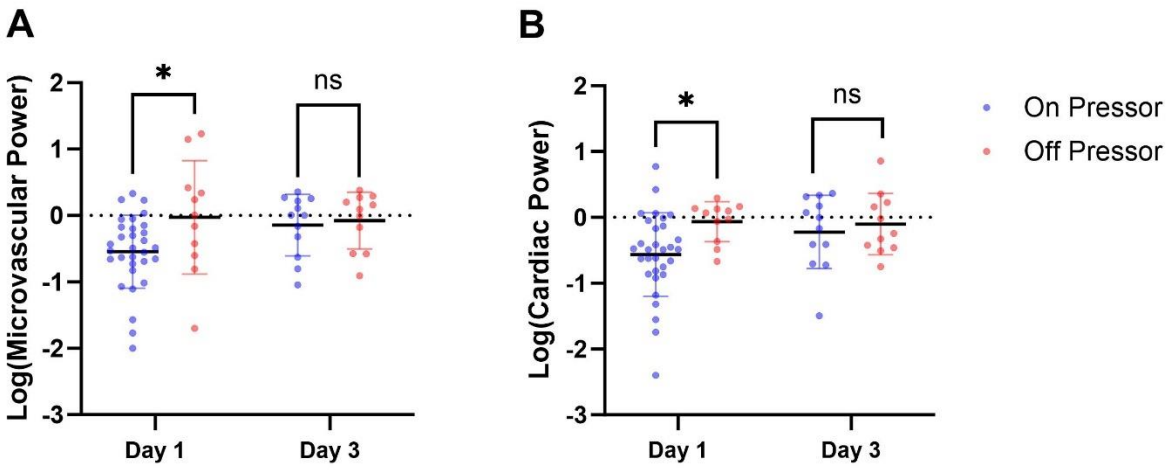

Figure 5.8 Comparison of log-transformed MV power and cardiac power between patients on pressors and those not on pressors. Plots represent each individual point and the mean of each category. ***A****: MV power was significantly higher in patients not requiring pressors on day 1 and no difference was found on day 3.* ***B****: Cardiac power was significantly higher in patients not requiring pressors on day 1 and no difference was found on day 3.*

To assess the temporal effects of vasopressor use on microvascular power, patients with data available on both day 1 and day 3 were divided into three groups: 9 patients in the "stayed on pressor" group, 4 in the "weaned off pressor" group, and 7 in the "never on pressor" group.

As shown in Figure 5.9A, on day 1, log-transformed MV power was significantly higher in both the "weaned off pressor" group and the "never on pressor" group compared to the "stayed on pressor" group, based on unpaired t-tests (-0.03 ± 0.43 vs -0.77 ± 0.41; p=0.01 and -0.06 ± 0.44 vs -0.77 ± 0.41; p=0.005, respectively). On day 3, MV power values were comparable across all groups (-0.09 ± 0.48 for "stayed on pressor", -0.41 ± 0.40 for "weaned off pressor", and 0.11 ± 0.32 for "never on pressor"). Within-group comparisons showed a significant increase in MV power from day 1 to day 3 only in the "stayed on pressor" group (-0.77 ± 0.41 vs -0.09 ± 0.48; p=0.03).

A similar trend was observed for cardiac power (Figure 5.9B), though the differences were less pronounced. On day 1, the "never on pressor" group had significantly higher cardiac power compared to the "stayed on pressor" group (-0.16 ± 0.34 vs -0.77 ± 0.57; p=0.03). The comparison between the "weaned off pressor" and "stayed on pressor" groups did not reach significance (-0.02 ± 0.73 vs -0.77 ± 0.57; p=0.07). Additionally, the increase in cardiac power from day 1 to day 3 in the "stayed on pressor" group was not statistically significant (-0.77 ± 0.57 vs -0.26 ± 0.59; p=0.09).

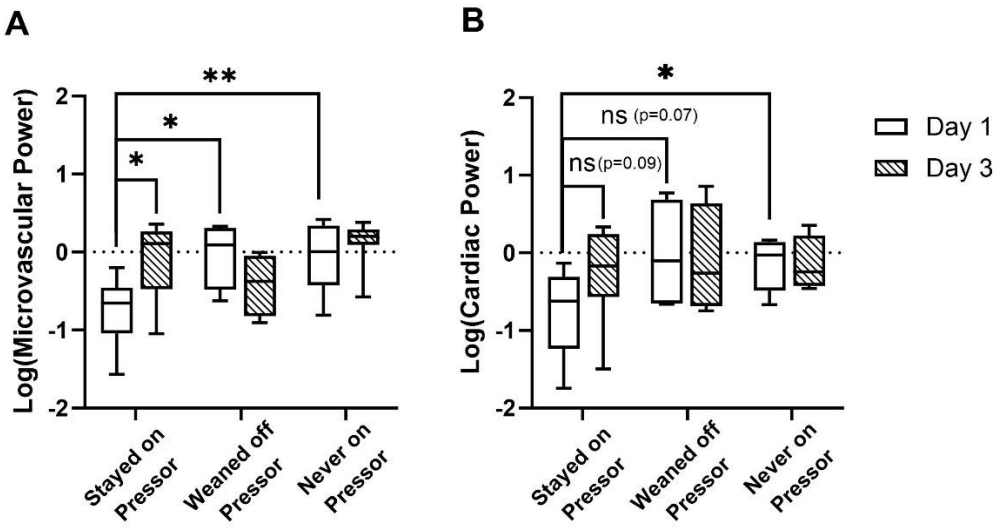

Figure 5.9 Log-transformed MV power (A) and cardiac power (B) on day 1 and day 3 across vasopressor status groups.

5.4.3. Day 1 and Day 3 Comparison

For patients who exhibited signals on both the first and third days, the wavelet-derived parameters were analyzed to explore patterns in their alteration over the patient's stay in the Intensive Care Unit (ICU). Figure 5.10 illustrates individual patient data (panels A and C) and mean log-transformed microvascular (MV) and cardiac power values (panels B and D) for the cohort on days 1, 3, and 8. Individual data points are connected by lines to provide a clear visualization of trends over time for each patient.

No statistically significant differences were observed between the wavelet-derived MV and cardiac power values on day 1 and day 3 when analyzed using paired t-tests (p=0.06 for MV and p=0.08 for cardio data). This was consistent across the entire cohort and in subgroup comparisons between survivors and non-survivors, as well as between patients with and without shock. Additionally, while Figure 5.10 includes day 8 data for context, statistical

analyses for this time point were excluded due to the limited number of patients (n=5) with available data.

The differences between day 1 and day 3 values were also calculated for each patient. These differences were further analyzed to assess whether changes in MV or cardiac power over time differed between subgroups, but no statistically significant findings were observed. The visualization provided in Figure 5.10 reinforces the lack of significant trends while emphasizing the heterogeneity in individual responses.

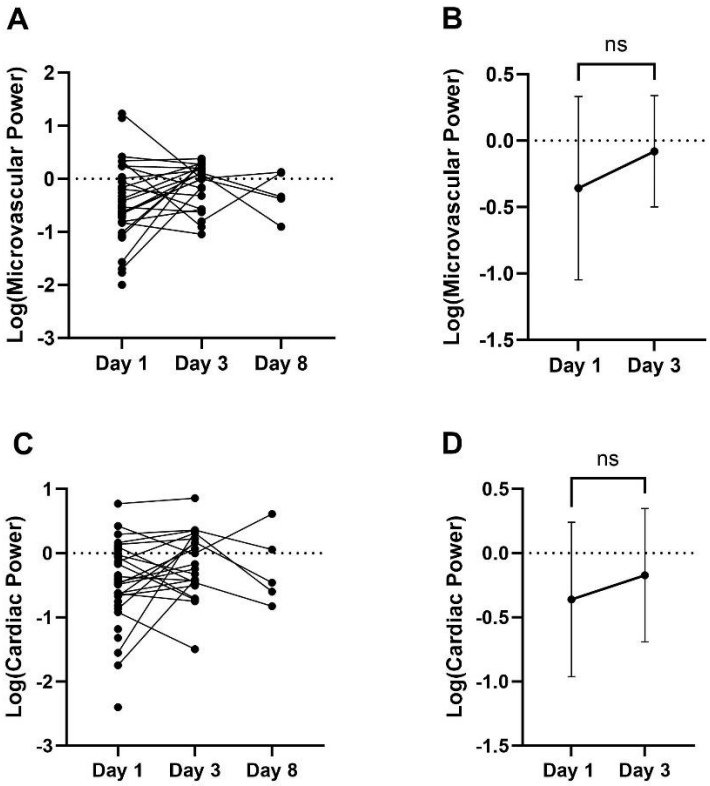

*Figure 5.10 : **A and C**: individual log-transformed MV and cardiac power values, respectively, with lines connecting data points for each patient on ICU days 1, 3, and 8; **B and D**: the mean values with standard deviation bars for the time points in which the data was available for both days 1 and 3.*

Figure 5.11 presents the data for Day 1 and Day 3, categorized by survival status. No statistically significant differences were observed within each subgroup over time in the ICU. While the mean values of microvascular power and cardiac power exhibited an increasing trend in survivors and non-survivors, these differences did not reach statistical significance. Furthermore, comparisons between survivors and non-survivors on both Day 1 and Day 3 did not reveal any significant differences.

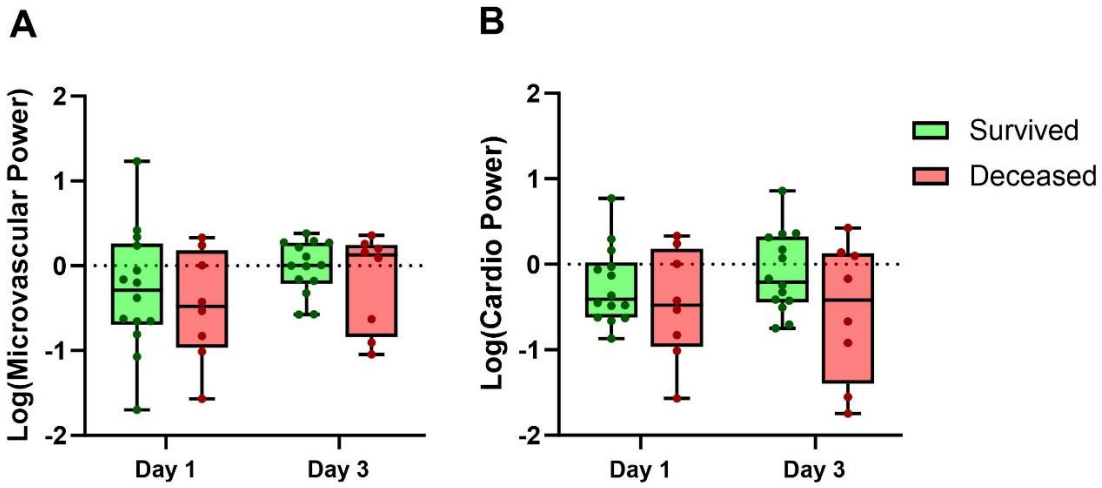

Figure 5.11 Microvascular (A) and Cardiac (B) Power on Day 1 and Day 3 in Survivors and Non-Survivors

5.4.4. ICU Patients and Healthy Control Comparison

To compare the ICU cohort with healthy participants, we analyzed day 1 data from the ICU group alongside the control group data. The key wavelet-derived parameters—MV power [Log], cardio power [Log], MV power percentage, cardio power percentage, the ratio of cardio to MV power (c/Mv[Log]), and the frequency at which cumulative MV power reached 63% (MVP63)—were examined. Healthy controls exhibited significantly higher microvascular power compared to ICU patients (Welch t-test: 0.48 ± 0.3 vs -0.41 ± 0.68; $p<0.001$) while cardiac power was not statistically different between the two groups (Welch t-test: -0.43 ± 0.58 vs -0.43 ± 0.6; $p=0.99$). c/Mv was significantly higher in ICU patients compared to healthy controls (t-test: -0.02 ± 0.62 vs -0.09 ± 0.59; $p<0.001$).

MV power percentage was significantly higher in healthy control (Man-Whitney test: 83.7% (76.2-91.4) vs 26.6% (13.7-41.3); $p<0.001$) and cardiac power percentage was significantly higher in ICU patients (Man-Whitney test: 25.4% (12.3-48.7) vs 13% (4.3-15.9); $p=0.005$). There was no significant difference in MVP63 values between ICU patients and healthy controls (Man-Whitney test: 0.038 Hz (0.03-0.048) vs 0.035 Hz (0.03-0.038); $p=0.41$). All variables are illustrated in Figure 5.12.

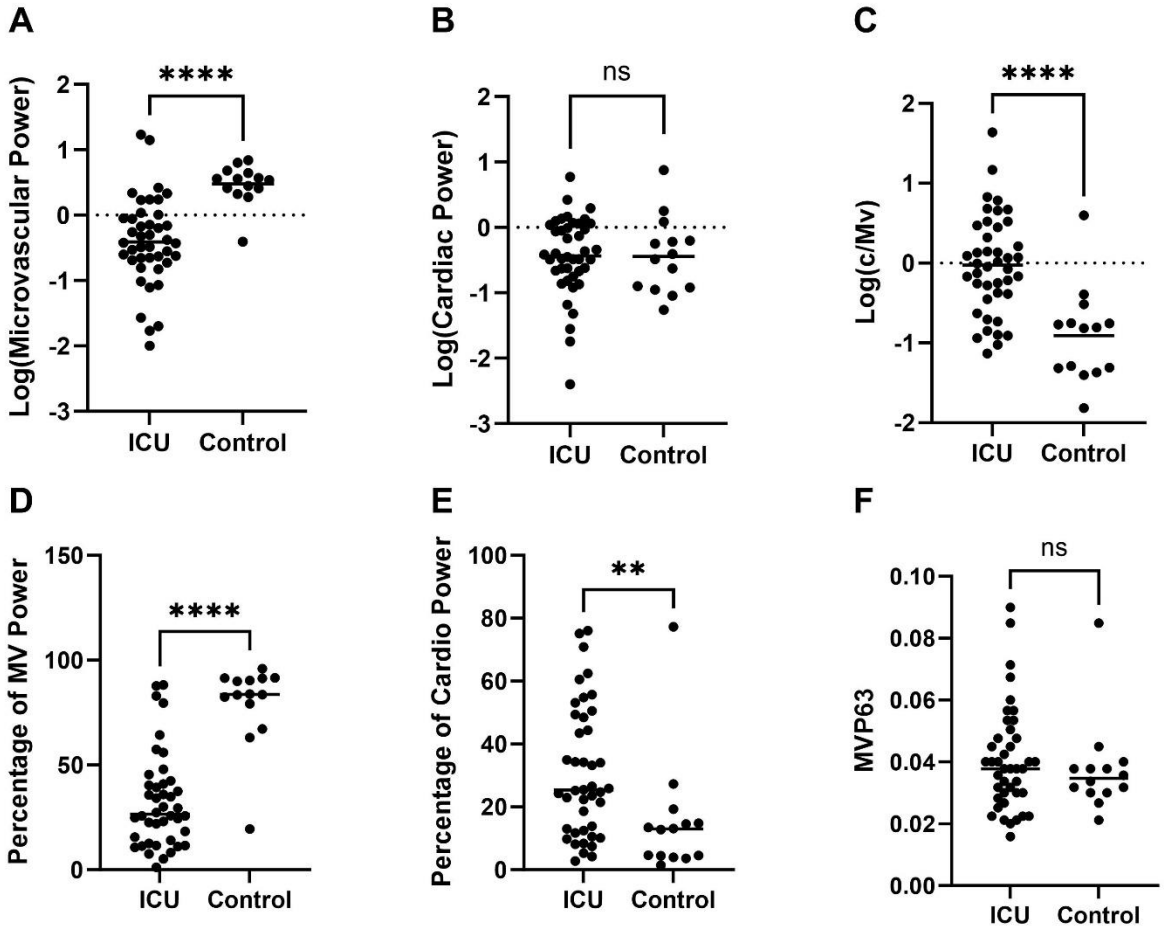

*Figure 5.12 Comparison of wavelet parameters between healthy controls and ICU patients. **A**: healthy controls exhibited significantly higher MV power than ICU patients; **B**: cardiac power remained comparable between the two groups; **C**: c/Mv was significantly higher in ICU patients; **D**: MV% is significantly higher in healthy control; **E**: Cardio% is significantly higher in ICU patients; **F**: MVP63 is similar in two groups*

Additionally, the control group demonstrated a lower coefficient of variation (CV%) for both MV and cardiac power compared to the ICU cohort. The mean CV% for MV power in the control group was 12%, compared to 36% in the ICU cohort ($p < 0.05$). This reflects more stable and homogenous microvascular responses in healthy individuals.

6. Discussion and Conclusion

6.1. Interpretation of Key Findings

In these observational studies, we used two complementary approaches—high-resolution NIRS-derived MAPopt analysis within the time domain and wavelet transform analysis of microvascular power within the frequency domain —to investigate microvascular dysfunction in ICU patients.

In the MAPopt study, we used high-resolution NIRS to simultaneously monitor microvascular perfusion in skeletal muscle (brachioradialis) and brain (frontal cortex) in mechanically ventilated ICU patients requiring vasoactive medication on the first day of ICU admission. We determined the correlation between arterial blood pressure and NIRS (HbT and TSI) at both sites and derived the optimal mean arterial pressure (MAPopt) that minimizes this correlation coefficient—proposed as the target MAP that preserves microvascular autoregulation (MA). To the best of our knowledge, this is the first study in humans to demonstrate MAP-dependent variation in skeletal muscle MA and the feasibility of deriving MAPopt for an organ outside the brain.

This study is also noteworthy for demonstrating that patients in a general ICU population experience a significant burden of microvascular dysfunction in both skeletal muscle and brain, as quantified by the proportion of time above the threshold of MA impairment (0.3) on the first day of ICU admission. Furthermore, MAPopt in skeletal muscle and brain can vary dramatically within the same patient, reflecting distinct autoregulatory mechanisms and regional perfusion requirements. These findings highlight the heterogeneity in MAPopt values, suggesting an opportunity for personalized hemodynamic management based on microvascular status in patients with circulatory shock [148], [149], as has been proposed with CPPopt in traumatic brain injury [150], [151], [152].

The comparison of MAPopt in skeletal muscle and brain represents a novel contribution of this study. While there is a correlation between MAPopt values for these two organs, targets can vary significantly depending on whether they are based on HbT- or TSI-derived indices. This variability suggests that universal resuscitation targets require not only patient-specific adjustments but also organ-specific considerations. Although MAP is a primary determinant of cerebral blood flow, MAP itself is determined by systemic vascular resistance in skeletal

muscle. Furthermore, skeletal muscle blood flow control is under a high degree of sympathetic tone [153] and a primary site of action for vasoactive medications, whereas cerebrovascular networks exhibit predominantly myogenic control [154], [155] and MA in the brain appears relatively insensitive to changes in vasopressor dosage [156]. Furthermore, the role of astrocytes and pericytes in microvascular flow regulation is well-described in the brain [157], [158], but corollary cell types and mechanisms in skeletal muscle are either absent or non-contributory. Prior studies have examined the discrepancies between effects for other organs.

In the second part of this study, wavelet analysis was applied to microvascular and cardiac power signals derived from high-resolution NIRS measurements.

Our findings demonstrate significantly lower microvascular power (log-transformed) in ICU patients compared to healthy controls. This underscores the profound alterations in microvascular regulation caused by critical illness. De Backer (2019) similarly observed that microvascular alterations in sepsis, including reduced capillary density and flow heterogeneity, are strongly associated with poor clinical outcomes [159]. This reinforces the role of microvascular metrics as critical indicators of disease severity. Interestingly, no significant difference was observed in cardiac power between the two groups, suggesting that systemic cardiac oscillations may be preserved even when microvascular function is impaired.

These results align with prior literature emphasizing the sensitivity of the microcirculation to hemodynamic disturbances. Mendelson et al. reported that microvascular power variability reflects dynamic adjustments to oxygen delivery in response to critical illness [15], and our study builds upon that foundational work by demonstrating markedly reduced microvascular power in ICU patients, likely reflecting impaired tissue perfusion. By incorporating a healthy control group, we quantify the extent of this impairment relative to baseline physiology, providing a broader context for understanding microvascular dysfunction. Additionally, the longitudinal analysis between Day 1 and Day 3 offers insights into temporal variability, expanding on prior single-timepoint observations in critically ill populations. Furthermore, by analyzing correlations between microvascular power metrics and clinical outcomes, our study extends Mendelson et al.'s findings to explore the prognostic significance of these parameters

Contrary to our initial hypothesis, microvascular and cardiac power metrics did not significantly differ between survivors and non-survivors or between patients with and without septic shock. However, patients receiving vasopressors had significantly lower microvascular

power, indicating a potential relationship between microvascular dysfunction and the severity of circulatory compromise. This finding supports the role of microvascular monitoring in identifying patients at higher risk of adverse outcomes.

Importantly, when analyzing changes from Day 1 to Day 3, patients who remained on vasopressors ("stayed" group) showed a modest increase in MV power over time. This group likely represents the sickest subset of the cohort — patients with the most severe circulatory dysfunction requiring ongoing vasopressor therapy. Their initially depressed MV power on Day 1 aligns with their clinical severity, and the observed increase on Day 3 may reflect gradual hemodynamic recovery or adaptation. These findings suggest that microvascular power is sensitive to both illness severity and therapeutic modulation.

The lack of significant differences in microvascular power between survivors and non-survivors may reflect the multifactorial nature of critical illness outcomes, where factors such as comorbidities, systemic inflammation, and metabolic disturbances play crucial roles. Sepsis, for instance, encompasses diverse phenotypes characterized by distinct organ dysfunction patterns and variable responses to interventions. Studies employing latent profile analysis have demonstrated that survival outcomes in sepsis are heavily influenced by subclass-specific pathophysiology, suggesting that a single microvascular metric may fail to capture the complexity of such heterogeneity [160].

Additionally, microvascular responses are known to be highly dynamic and influenced by early interventions. For example, fluid resuscitation or vasopressor administration can transiently improve microcirculatory flow, but these changes may not always translate into longer-term outcomes such as survival [161], [162]. Moreover, systemic resuscitation targets like MAP often fail to account for regional perfusion heterogeneity, as noted in the MAPopt study. This disconnects between systemic and microvascular parameters further complicates the interpretation of microvascular power as a prognostic marker.

Our repeated analysis over the 3 days revealed no consistent trends in microvascular or cardiac power between Day 1 and Day 3 of ICU admission. While some patients exhibited improvements in microvascular power, others experienced decreases, reflecting the heterogeneity within the cohort. Notably, these changes did not correlate with clinical outcomes such as survival, suggesting that day-to-day fluctuations in microvascular power may not fully capture the multifactorial drivers of critical illness outcomes. This variability

highlights the complexity of microvascular regulation in critically ill patients and underscores the need for future studies to explore whether specific patterns or thresholds of microvascular power are predictive of outcomes. Furthermore, the short follow-up duration limits our ability to assess longer-term trends, such as potential recovery or progressive dysfunction over time. Extended monitoring periods in larger cohorts are warranted to better understand the temporal dynamics of microvascular power and its clinical significance

6.2. Clinical Implications

The MAPopt targets derived for skeletal muscle and brain were commonly above the threshold of 65 mmHg uniformly prescribed for critically ill patients. This supports the growing recognition that standardized MAP thresholds may fail to address patient-specific needs. Kato and Pinsky (2015) highlighted the importance of tailoring MAP targets to individual profiles, particularly advocating for higher MAPs in hypertensive patients to reduce renal injury and improve outcomes [149]. While studies such as that by Asfar et al. [4] did not show a benefit to targeting a MAP of 80 mm Hg versus 65 mm Hg in septic patients, the application of uniform targets across heterogeneous populations likely limited its relevance to individual patients. For instance, evidence suggests that targeting higher MAPs, particularly in patients with pre-existing hypertension, can enhance microcirculatory flow and capillary density [163]. Although other studies have shown that increasing MAP beyond 65 mmHg, while beneficial for systemic parameters, has not consistently demonstrated improvements in microvascular blood flow [162]. These findings show the importance of tailoring MAP thresholds to individual patient profiles to improve microvascular perfusion and overall outcomes.

The ANDROMEDA investigators explored strategies like raising MAP with norepinephrine for patients with persistently abnormal CRT, but even patients with preserved CRT may benefit from advanced monitoring [76], [164]. Interestingly, 12 of 15 patients in our current study had normal CRT of less than 3 seconds, despite many remaining below their MAPopt target. Huang et al [165] found that sublingual microcirculation was abnormal (microcirculatory flow index < 2.6) in 34 of 228 patients (15%) with preserved CRT. Therefore, future research should evaluate whether using advanced physiological metrics such as MAPopt

may confer additional benefits for selected patients above clinical markers of perfusion and how they can be incorporated into contemporary resuscitation protocols.

Our findings align with previous literature on microvascular dysfunction in ICU patients, emphasizing its prevalence [9], [166]. While static (e.g., tissue oxygen saturation) and dynamic (e.g., vascular occlusion test) NIRS-derived indices correlate with ICU outcomes in sepsis [167], integrating these metrics into treatment protocols has not consistently improved survival, and resulted in more days of mechanical ventilation and RBC transfusion [168]. Recently, Bruno et al [169] randomized patients with shock to provide clinicians with an assessment of sublingual microcirculation, but this did not confer a survival benefit despite frequent changes to management; this study was criticized for not connecting these sublingual measurements with a specified intervention [170]. In this regard, skeletal muscle MAPopt presented in our study may overcome some of these limitations, as this will also define a specific treatment—titration of vasoactive medications to achieve the target MAPopt.

The heterogeneity of MAPopt values in this cohort underscores the importance of individualized care. Our data suggests that skeletal muscle MAPopt targets can guide vasoactive therapy tailored to the patient's specific microvascular needs. Moreover, the variability observed between skeletal muscle and brain MAPopt highlights the need for organ-specific considerations in managing circulatory shock. This personalized approach could address limitations in current resuscitation protocols, which often apply universal MAP thresholds without accounting for patient or organ variability.

As for the wavelet study, the findings highlight the significant clinical potential of wavelet-derived metrics for improving the management and monitoring of critically ill patients. The observed difference in microvascular power between ICU patients and healthy controls highlights the sensitivity of these metrics in detecting microvascular dysfunction, which often occurs before overt systemic changes become apparent. Ince (2015) emphasized the necessity of monitoring microcirculation in critically ill patients to uncover perfusion impairments that systemic parameters frequently fail to capture [7]. This aligns with our findings, suggesting that wavelet-derived microvascular power metrics could not only serve as diagnostic tools but also provide clinicians with an opportunity to intervene early, potentially preventing irreversible tissue damage.

In addition to diagnostic utility, wavelet-derived metrics have the potential to refine resuscitation strategies. Current protocols in critical care often rely on fixed targets for systemic parameters, such as maintaining a mean arterial pressure (MAP) above 65 mm Hg. The association between reduced microvascular power and the need for vasopressors observed in this study emphasizes the value of tailoring resuscitation goals to each patient's microvascular status. Evidence from previous studies highlights the risks associated with vasopressor therapy. While norepinephrine is essential for stabilizing MAP, high doses have been linked to increased fluid requirements, fewer ventilator-free days, and adverse hemodynamic effects without consistently improving survival [171]. Similarly, cumulative vasopressor loads have been shown to increase mortality and contribute to organ injury and dysregulated perfusion [172]. These findings underscore the importance of minimizing vasopressor exposure and prioritizing resuscitation strategies that balance systemic perfusion with microvascular and organ-specific outcomes. Developing adjunctive approaches to reduce vasopressor reliance could mitigate these risks and improve overall patient outcomes. Monitoring wavelet-derived metrics during interventions could guide dynamic adjustments, ensuring that therapies are optimized to restore tissue-level perfusion rather than simply meeting systemic targets.

Wavelet analysis also offers a unique perspective by capturing the frequency-specific dynamics of microvascular and cardiac power. These insights complement conventional systemic monitors, bridging the gap between macro-hemodynamic parameters and microcirculation. For example, integrating wavelet-derived metrics with other tools, such as lactate levels or tissue oxygen saturation, could provide a more comprehensive understanding of a patient's circulatory status. This holistic approach may reveal critical discrepancies between macro- and microcirculation, which are often missed in routine monitoring but are crucial for guiding targeted interventions [7], [161].

The role of wavelet-derived metrics in managing septic shock is particularly noteworthy. Patients receiving vasopressors exhibited lower microvascular power, reflecting the severity of their circulatory dysfunction. This finding supports the use of wavelet-derived metrics to identify patients who may benefit from more aggressive resuscitation or tailored therapeutic strategies aimed at optimizing tissue perfusion. Conversely, patients with relatively preserved microvascular power could potentially avoid unnecessary interventions, minimizing the risks associated with excessive fluids or vasopressors.

6.3. Study Limitations

This study was exploratory and had several limitations. The use of research-grade hr-NIRS equipment allowed for high temporal resolution (10 Hz) but was vulnerable to motion artifacts, and the absence of a short-distance channel may have influenced cerebral measurements. The relatively short monitoring periods did not allow for assessment of MAPopt evolution throughout ICU admission, as has been done with cerebral monitoring. Furthermore, our use of a fixed-window MAPopt derivation was suitable for short monitoring sessions, but newer algorithms are currently being evaluated in the literature, both within existing software (e.g., optimal flex window methodology [145]) or designed de novo by research groups [173]; newer methodology is still required to derive MAPopt from continuous physiologic data in real time at the bedside.

The choice of HbT- or TSI-derived indices of MA to best determine MAPopt is not established; a comprehensive study in a swine model of cardiac arrest compared many indices [174], and human studies in traumatic brain injury show that these indices behave similarly [175]. The small sample size of this cohort is meant to demonstrate the ability to calculate MAPopt in skeletal muscle and is not intended to make general claims about specific target values. Larger studies may also help elucidate the contribution of chronic comorbidities (e.g., diabetes, peripheral arterial disease) to the observed microvascular dysfunction. Last, it should be noted that, unlike for cerebral monitoring, impaired MA in skeletal muscle has not yet been associated with adverse ICU outcomes, nor is the threshold for abnormal MA of 0.3 identified in skeletal muscle. This will be a focus for our future research.

The wavelet study, while demonstrating feasibility and clinical relevance, also has limitations. The inclusion of 43 ICU patients provided meaningful data but limits broader generalizability. Larger studies with more diverse cohorts, including intermediate clinical states, will be essential for establishing normative ranges and defining thresholds for clinical application. Although research-grade hr-NIRS equipment allowed for high temporal resolution, the absence of a short-distance channel and the impact of motion artifacts reduced the proportion of analyzable data. Future studies should incorporate real-time artifact detection and complementary modalities to enhance reliability.

The study's relatively short monitoring periods limited the ability to assess temporal trends and recovery patterns over the course of ICU admission. Furthermore, systemic factors such

as vasopressors, fluid balance, and sedation, which are known to influence microvascular function, were not explicitly controlled for in this analysis. Finally, skeletal muscle wavelet-derived microvascular metrics have not yet been directly correlated with clinical outcomes, representing an important avenue for future research.

6.4. Comparative Literature and Future Directions

Our findings align with studies that document microvascular dysfunction as a key factor in critical illness. Static measures like tissue oxygen saturation (StO2%) and dynamic indices such as vascular occlusion tests have shown associations with ICU outcomes but have not consistently improved survival when used in treatment protocols. More recently, researchers have emphasized the need for targeted interventions linked to advanced physiological monitoring, such as the integration of skeletal muscle MAPopt into resuscitation strategies.

Future work should focus on longitudinal studies that track MAPopt evolution throughout ICU admission, as has been done with cerebral autoregulation. Additionally, expanding the cohort size would allow for more robust comparisons and correlations with clinical outcomes. Investigating the optimal choice between HbT and TSI-derived indices is another critical area, as is the development of real-time MAPopt derivation algorithms. Lastly, correlating skeletal muscle MA with specific ICU outcomes will be essential to fully establish its clinical relevance.

The findings of the wavelet study build upon prior research demonstrating the clinical importance of microvascular monitoring in critical illness. Previous studies have established that microvascular dysfunction is prevalent in shock states and often persists despite normalization of systemic parameters such as MAP. The use of wavelet-derived metrics to quantify microvascular power provides a novel approach, complementing earlier efforts using static (StO2%) and dynamic (vascular occlusion test) indices. Mendelson et al. (2021) demonstrated the feasibility of using wavelet analysis to characterize frequency-specific microvascular dynamics, and this study extends those insights to a critically ill ICU population, emphasizing its clinical relevance.

Future research should prioritize expanding the patient cohort to include diverse critical illness states and larger sample sizes to enable robust statistical comparisons and subgroup analyses. Additionally, incorporating a multimodal approach by combining wavelet-derived

microvascular metrics with systemic and metabolic parameters could provide a more comprehensive understanding of perfusion in critical illness. Such integrative strategies could refine the monitoring and treatment of septic shock patients, addressing the complexity of circulatory dysfunction [161]. Longitudinal studies are essential to assess the evolution of wavelet-derived microvascular metrics over the course of ICU stays and during recovery. These studies could provide insights into whether changes in microvascular power correlate with therapeutic interventions or predict clinical outcomes. Another important direction for future research is to undertake controlled interventions in ICU patients, such as altering MAP, introducing inotropes, or administering blood transfusions, and evaluating how microvascular power changes over time in response. Such studies would help elucidate the relationship between therapeutic strategies and microvascular function, paving the way for more targeted interventions.

Additionally, integrating wavelet-derived metrics with other advanced monitoring techniques, such as MAPopt, could offer a more comprehensive understanding of the interplay between macro- and microcirculatory systems. Developing real-time wavelet analysis tools for bedside implementation would further enhance their clinical utility, allowing dynamic adjustments to resuscitation strategies based on evolving patient needs.

Finally, validating thresholds and defining normative ranges for wavelet-derived microvascular metrics remain critical challenges. Establishing clinically actionable cutoffs will require multicenter studies and comparisons across varied patient populations, including septic and non-septic cohorts. As skeletal muscle microvascular power becomes more widely studied, correlating these metrics with ICU outcomes, such as survival, organ failure, or weaning from vasopressors, will be crucial to fully realize its clinical impact.

6.5. Conclusion

This thesis investigated two independent but complementary approaches to individualized microvascular monitoring in critically ill patients using high-resolution near-infrared spectroscopy (hr-NIRS):

(1) the derivation of optimal mean arterial pressure (MAPopt) from skeletal muscle autoregulation signals, and

(2) the application of wavelet-based signal analysis to assess microvascular and cardiac power. These techniques were evaluated for their ability to reflect patient-specific circulatory physiology and clinical outcomes.

MAPopt Study Conclusions

The first objective was to assess the technical feasibility of calculating MAPopt from skeletal muscle using hr-NIRS and ABP signals in critically ill patients. The study demonstrated that MAPopt could be derived in the majority of patients using muscle autoregulation indices, with sufficient data quality and curve fitting to enable reliable estimation. This confirms that skeletal muscle is a viable site for real-time autoregulation monitoring using non-invasive optical methods. However, several challenges were encountered, including signal noise, movement artifacts, and non-U-shaped correlations, which occasionally limited interpretability. These results establish the method's feasibility, while also highlighting the need for standardized preprocessing and binning protocols before clinical implementation.

The second objective was to determine whether the MAPopt values derived from skeletal muscle differed from the standard ICU MAP target of 65 mmHg. In a large proportion of cases, the MAPopt derived from skeletal muscle was lower than 65 mmHg, suggesting that fixed targets may not reflect individualized perfusion needs. This finding aligns with previous research questioning the universality of a one-size-fits-all MAP threshold. The observed discrepancies support the rationale for a more personalized approach to hemodynamic management in critically ill patients. Still, the occasional need for manual adjustment of bin sizes and variability in curve shape underscore the importance of refining the MAPopt estimation process for routine clinical use.

The third objective was to examine the correlation between skeletal muscle- and brain-derived MAPopt values to assess whether peripheral measurements could serve as surrogates for cerebral autoregulation. A moderate positive correlation was found between muscle- and brain-derived MAPopt in patients where both signals were available, suggesting some physiological overlap. However, the variability in individual responses indicated that cerebral and peripheral autoregulation are not always aligned. This supports the concept that autoregulatory function may be organ-specific and challenges the assumption that a single

MAP target can optimize perfusion across all tissues. These findings reinforce the need for organ-specific monitoring and individualized hemodynamic targets.

Wavelet Study Conclusions

The fourth objective was to evaluate differences in wavelet-derived microvascular and cardiac power between critically ill patients and healthy controls using hr-NIRS signals. The results confirmed that microvascular power was significantly lower in ICU patients compared to healthy individuals, consistent with the hypothesis that critical illness impairs vascular oscillatory behavior. This supports prior findings that sepsis and circulatory shock are associated with reduced vasomotor activity and impaired autoregulation. However, cardiac power did not differ significantly between groups, suggesting that wavelet-derived cardiac components may be less sensitive to disease severity or require more targeted signal analysis. Overall, this objective confirmed the physiological relevance of wavelet-derived microvascular power but also pointed to limitations in its specificity for cardiac function.

The fifth objective was to assess whether wavelet-derived microvascular power could distinguish between survivors and non-survivors and between septic and non-septic patients. Contrary to the hypothesis, no significant differences in microvascular or cardiac power were observed between these clinical subgroups. While microvascular power was clearly reduced in the ICU population overall, it did not correlate with survival or sepsis status within the ICU cohort. This suggests that while wavelet-derived power reflects global microvascular impairment, it may not serve as a reliable prognostic biomarker when used alone. These findings emphasize the complexity of outcome prediction in critical care and highlight the need for multimodal approaches that integrate additional physiological and clinical variables.

The sixth objective was to investigate whether changes in wavelet-derived microvascular power over time were associated with patient outcomes. Specifically, the study examined whether survivors exhibited increasing microvascular power between day 1 and day 3 of ICU admission. This hypothesis was not supported, as no consistent or statistically significant temporal trends were observed between outcome groups. While some survivors showed improving power and some non-survivors showed declining trends, the overall variability was high and lacked a clear pattern. These findings indicate that microvascular recovery does not

follow a uniform trajectory and that short-term changes in wavelet-derived metrics may not be sufficient to predict clinical outcomes.

Although the core hypothesis that microvascular power would predict outcomes was not supported, subgroup analysis based on vasopressor use yielded additional insights. Patients who required vasopressors on both day 1 and day 3 exhibited the lowest microvascular power on day 1, followed by a modest increase by day 3. This pattern may reflect delayed hemodynamic recovery in the most severely ill patients and suggests that wavelet-derived microvascular power is responsive to therapeutic interventions. While not prognostic on its own, microvascular power may have potential as a marker of treatment response when interpreted alongside other clinical indicators.

Final Remarks

In summary, this study demonstrated the feasibility of deriving MAPopt from skeletal muscle autoregulation and confirmed that ICU patients exhibit significant microvascular impairment compared to healthy controls. While wavelet-derived microvascular power captured meaningful physiological differences, it did not correlate reliably with survival or sepsis status. The variability in MAPopt across tissues and the inconsistent prognostic utility of microvascular power highlight the complexity of circulatory regulation in critical illness.

These findings support the growing recognition that fixed resuscitation targets may not meet the needs of all patients and underscore the potential of individualized monitoring approaches. Future research should focus on refining signal processing methods, extending monitoring durations, and integrating multiple physiological metrics to improve the clinical utility of NIRS-based monitoring. With further development, techniques such as skeletal muscle MAPopt and wavelet-derived power analysis may contribute to more precise, patient-specific care in the ICU.

References

[1] Vincent Jean-Louis and De Backer Daniel, "Circulatory Shock," *New England Journal of Medicine*, vol. 369, no. 18, pp. 1726–1734, 2013, doi: 10.1056/NEJMra1208943.

[2] M. Cecconi *et al.*, "Consensus on circulatory shock and hemodynamic monitoring. Task force of the European Society of Intensive Care Medicine," *Intensive Care Med*, vol. 40, no. 12, pp. 1795–1815, 2014, doi: 10.1007/s00134-014-3525-z.

[3] S. M *et al.*, "The Third International Consensus Definitions for Sepsis and Septic Shock (Sepsis-3)," *JAMA*, vol. 315, no. 8, Feb. 2016, doi: 10.1001/jama.2016.0287.

[4] P. Asfar *et al.*, "High versus Low Blood-Pressure Target in Patients with Septic Shock," *New England Journal of Medicine*, vol. 370, no. 17, pp. 1583–1593, Apr. 2014, doi: 10.1056/NEJMoa1312173.

[5] G. Hernandez, R. Bellomo, and J. Bakker, "The ten pitfalls of lactate clearance in sepsis.," *Intensive Care Medicine*, vol. 45, no. 1, pp. 82–86, Jan. 2019, doi: 10.1007/s00134-018-5213-x.

[6] Y. Sakr, M.-J. Dubois, D. De Backer, J. Creteur, and J.-L. Vincent, "Persistent microcirculatory alterations are associated with organ failure and death in patients with septic shock," *Crit Care Med*, vol. 32, no. 9, pp. 1825–1831, Sep. 2004, doi: 10.1097/01.ccm.0000138558.16257.3f.

[7] C. Ince, "Hemodynamic coherence and the rationale for monitoring the microcirculation," *Crit Care*, vol. 19, no. 3, Art. no. 3, Dec. 2015, doi: 10.1186/cc14726.

[8] D. De Backer, D. Orbegozo Cortes, K. Donadello, and J.-L. Vincent, "Pathophysiology of microcirculatory dysfunction and the pathogenesis of septic shock," *Virulence*, vol. 5, no. 1, pp. 73–79, Jan. 2014, doi: 10.4161/viru.26482.

[9] A. Donati *et al.*, "Near-infrared spectroscopy for assessing tissue oxygenation and microvascular reactivity in critically ill patients: a prospective observational study," *Crit Care*, vol. 20, no. 1, Art. no. 1, Dec. 2016, doi: 10.1186/s13054-016-1500-5.

[10] K. Rosenblatt *et al.*, "Cerebral Autoregulation–Guided Optimal Blood Pressure in Sepsis-Associated Encephalopathy: A Case Series," *J Intensive Care Med*, vol. 35, no. 12, pp. 1453–1464, Dec. 2020, doi: 10.1177/0885066619828293.

[11] O. Hamzaoui and R. Shi, "Microcirculation and mean arterial pressure: friends or foes?," *Annals of Translational Medicine*, vol. 8, no. 12, Art. no. 12, Jun. 2020, doi: 10.21037/atm.2020.01.70.

[12] H. Merdji, B. Levy, C. Jung, C. Ince, M. Siegemund, and F. Meziani, "Microcirculatory dysfunction in cardiogenic shock," *Annals of Intensive Care*, vol. 13, no. 1, p. 38, May 2023, doi: 10.1186/s13613-023-01130-z.

[13] D. Mladinov, R. C. Godwin, D. Benz, I. M. Folorunso, D. E. Berkowitz, and R. L. Melvin, "The Impact of Blood Pressure Below Personalized Lower Cerebral Autoregulation Limit on Outcomes After Cardiac Surgery: A Retrospective Study," *Journal of Cardiothoracic and Vascular Anesthesia*, vol. 0, no. 0, Dec. 2024, doi: 10.1053/j.jvca.2024.12.019.

[14] Q. Guo, D. Liu, X. Wang, and Chinese Critical Ultrasound Study Group (CCUSG), "Early peripheral perfusion monitoring in septic shock," *European Journal of Medical Research*, vol. 29, no. 1, p. 477, Sep. 2024, doi: 10.1186/s40001-024-02074-1.
[15] A. A. Mendelson *et al.*, "Dynamic tracking of microvascular hemoglobin content for continuous perfusion monitoring in the intensive care unit: pilot feasibility study," *J Clin Monit Comput*, vol. 35, no. 6, pp. 1453–1465, Dec. 2021, doi: 10.1007/s10877-020-00611-x.
[16] M. E. Astiz, E. C. Rackow, and M. H. Weil, "Pathophysiology and Treatment of Circulatory Shock," *Critical Care Clinics*, vol. 9, no. 2, pp. 183–203, Apr. 1993, doi: 10.1016/S0749-0704(18)30192-1.
[17] J.-L. Vincent, "Circulatory Shock: Definition, Assessment, and Management," in *Resuscitation: Translational Research, Clinical Evidence, Education, Guidelines*, A. Gullo and G. Ristagno, Eds., Milano: Springer Milan, 2014, pp. 219–227. doi: 10.1007/978-88-470-5507-0_21.
[18] V. S *et al.*, "[Circulatory shock: early diagnosis and therapy].," *G Ital Cardiol (Rome)*, vol. 24, no. 2, pp. 110–121, Feb. 2023, doi: 10.1714/3963.39418.
[19] E. PMC, "Circulatory shock: a symposium on advances in the understanding of mechanisms and treatment.," *California Medicine*, vol. 106, no. 1, p. 1, Jan. 1967.
[20] J.-L. Vincent, C. Ince, and J. Bakker, "Clinical review: Circulatory shock - an update: a tribute to Professor Max Harry Weil," *Critical Care*, vol. 16, no. 6, p. 239, Nov. 2012, doi: 10.1186/cc11510.
[21] "The History and Evolution of Circulatory Shock," *Critical Care Clinics*, vol. 25, no. 1, pp. 1–29, Jan. 2009, doi: 10.1016/j.ccc.2008.12.013.
[22] F. H. Millham, "A brief history of shock," *Surgery*, vol. 148, no. 5, pp. 1026–1037, Nov. 2010, doi: 10.1016/j.surg.2010.02.014.
[23] D. Blumlein and I. Griffiths, "Shock: aetiology, pathophysiology and management: British Journal of Nursing," *BR J NURS*, vol. 31, no. 8, pp. 422–428, Apr. 2022, doi: 10.12968/bjon.2022.31.8.422.
[24] J. Ross, R. J. Murtaugh, and K. Moore, "Shock I: Pathophysiology," in *Critical Care*, Routledge, 2002.
[25] L. Teba, D. E. Banks, and M. R. Balaan, "Understanding circulatory shock: Is it hypovolemic, cardiogenic, or vasogenic?," *Postgraduate Medicine*, vol. 91, no. 7, pp. 121–129, May 1992, doi: 10.1080/00325481.1992.11701349.
[26] L. Kobayashi, T. W. Costantini, and R. Coimbra, "Hypovolemic Shock Resuscitation," *Surgical Clinics*, vol. 92, no. 6, pp. 1403–1423, Dec. 2012, doi: 10.1016/j.suc.2012.08.006.
[27] D. M. Kelley, "Hypovolemic Shock: An Overview," *Critical Care Nursing Quarterly*, vol. 28, no. 1, p. 2, Mar. 2005.
[28] S. M. Hollenberg, C. J. Kavinsky, and J. E. Parrillo, "Cardiogenic Shock," *Ann Intern Med*, vol. 131, no. 1, pp. 47–59, Jul. 1999, doi: 10.7326/0003-4819-131-1-199907060-00010.
[29] C. Vahdatpour, D. Collins, and S. Goldberg, "Cardiogenic Shock," *Journal of the American Heart Association*, vol. 8, no. 8, p. e011991, Apr. 2019, doi: 10.1161/JAHA.119.011991.

[30] C. Morgan and D. S. Wheeler, “Obstructive Shock,” *The Open Pediatric Medicine Journal*, vol. 7, no. 1, Feb. 2013, Accessed: Apr. 22, 2024. [Online]. Available: https://benthamopen.com/ABSTRACT/TOPEDJ-7-35

[31] V. Zotzmann, F. A. Rottmann, K. Müller-Pelzer, C. Bode, T. Wengenmayer, and D. L. Staudacher, “Obstructive Shock, from Diagnosis to Treatment,” *RCM*, vol. 23, no. 7, Art. no. 7, Jun. 2022, doi: 10.31083/j.rcm2307248.

[32] A. Hussain, V. V. Kuzkov, and M. Y. Kirov, “Distributive Shock,” in *Advanced Hemodynamic Monitoring: Basics and New Horizons*, M. Y. Kirov, V. V. Kuzkov, and B. Saugel, Eds., Cham: Springer International Publishing, 2021, pp. 245–255. doi: 10.1007/978-3-030-71752-0_25.

[33] J. Chong, T. Dumont, L. Francis-Frank, and M. Balaan, “Sepsis and Septic Shock: A Review,” *Critical Care Nursing Quarterly*, vol. 38, no. 2, p. 111, Jun. 2015, doi: 10.1097/CNQ.0000000000000052.

[34] D. G. Remick, “Pathophysiology of Sepsis,” *The American Journal of Pathology*, vol. 170, no. 5, pp. 1435–1444, May 2007, doi: 10.2353/ajpath.2007.060872.

[35] R. S. Hotchkiss, L. L. Moldawer, S. M. Opal, K. Reinhart, I. R. Turnbull, and J.-L. Vincent, “Sepsis and septic shock,” *Nat Rev Dis Primers*, vol. 2, no. 1, pp. 1–21, Jun. 2016, doi: 10.1038/nrdp.2016.45.

[36] R. Habimana, I. Choi, H. J. Cho, D. Kim, K. Lee, and I. Jeong, “Sepsis-induced cardiac dysfunction: a review of pathophysiology,” *Acute Crit Care*, vol. 35, no. 2, pp. 57–66, May 2020, doi: 10.4266/acc.2020.00248.

[37] Y. Sakr *et al.*, “Does dopamine administration in shock influence outcome? Results of the Sepsis Occurrence in Acutely Ill Patients (SOAP) Study*:,” *Critical Care Medicine*, vol. 34, no. 3, pp. 589–597, Mar. 2006, doi: 10.1097/01.CCM.0000201896.45809.E3.

[38] O. A. Khalil, M. M. Sakr, F. O. Selim, and I. M. Mohammed Salem, “PREVALENCE, PATTERN AND CLINICAL OUTCOME OF CIRCULATORY SHOCK IN CRITICALLY ILL PATIENTS IN MEDICAL ICU,” *Zagazig University Medical Journal*, vol. 24, no. 4, pp. 329–337, Jul. 2018, doi: 10.21608/zumj.2018.13226.

[39] D. Berg, J. Katz, E. Bohula, S. Van Diepen, and D. Morrow, “EPIDEMIOLOGY OF SHOCK IN CONTEMPORARY CARDIAC INTENSIVE CARE UNITS: DATA FROM THE CRITICAL CARE CARDIOLOGY TRIALS NETWORK (CCCTN) REGISTRY,” *Journal of the American College of Cardiology*, vol. 73, no. 9, Supplement 1, p. 666, Mar. 2019, doi: 10.1016/S0735-1097(19)31274-4.

[40] F. B. Mayr, S. Yende, and D. C. Angus, “Epidemiology of severe sepsis,” *Virulence*, vol. 5, no. 1, pp. 4–11, Jan. 2014, doi: 10.4161/viru.27372.

[41] C. J. Paoli, M. A. Reynolds, M. Sinha, M. Gitlin, and E. Crouser, “Epidemiology and Costs of Sepsis in the United States-An Analysis Based on Timing of Diagnosis and Severity Level,” *Crit Care Med*, vol. 46, no. 12, pp. 1889–1897, Dec. 2018, doi: 10.1097/CCM.0000000000003342.

[42] M. Bauer, H. Gerlach, T. Vogelmann, F. Preissing, J. Stiefel, and D. Adam, “Mortality in sepsis and septic shock in Europe, North America and Australia between 2009 and 2019— results from a systematic review and meta-analysis,” *Critical Care*, vol. 24, no. 1, p. 239, May 2020, doi: 10.1186/s13054-020-02950-2.

[43] M. Shankar-Hari, D. A. Harrison, G. D. Rubenfeld, and K. Rowan, “Epidemiology of sepsis and septic shock in critical care units: comparison between sepsis-2 and sepsis-3 populations using a national critical care database,” *BJA: British Journal of Anaesthesia*, vol. 119, no. 4, pp. 626–636, Oct. 2017, doi: 10.1093/bja/aex234.

[44] J.-L. Vincent and A. Rapotec, “Circulatory Shock: Hypovolemic, Distributive, Cardiogenic, Obstructive,” in *Perioperative Critical Care Cardiology*, J. L. Atlee, A. Gullo, G. Sinagra, and J.-L. Vincent, Eds., Milano: Springer Milan, 2007, pp. 211–224. doi: 10.1007/978-88-470-0558-7_13.

[45] A. Hendy and Ş.-I. Bubenek-Turconi, “The Diagnosis and Hemodynamic Monitoring of Circulatory Shock: Current and Future Trends,” *The Journal of Critical Care Medicine*, vol. 2, no. 3, pp. 115–123, Jul. 2016, doi: 10.1515/jccm-2016-0018.

[46] M. Garcia-Alvarez, P. Marik, and R. Bellomo, “Sepsis-associated hyperlactatemia,” *Critical Care*, vol. 18, no. 5, p. 503, Sep. 2014, doi: 10.1186/s13054-014-0503-3.

[47] M. E. Mikkelsen *et al.*, “Serum lactate is associated with mortality in severe sepsis independent of organ failure and shock*,” *Critical Care Medicine*, vol. 37, no. 5, p. 1670, May 2009, doi: 10.1097/CCM.0b013e31819fcf68.

[48] J. T. Y. Soong and N. Soni, “Circulatory shock,” *Medicine*, vol. 41, no. 2, pp. 64–69, Feb. 2013, doi: 10.1016/j.mpmed.2012.11.012.

[49] J.-L. Vincent, “Definition, Monitoring, and Management of Shock States,” in *Intensive and Critical Care Medicine: WFSICCM World Federation of Societies of Intensive and Critical Care Medicine*, A. Gullo, P. D. Lumb, J. Besso, and G. F. Williams, Eds., Milano: Springer Milan, 2009, pp. 143–150. doi: 10.1007/978-88-470-1436-7_13.

[50] C. Darreau *et al.*, “Use, timing and factors associated with tracheal intubation in septic shock: a prospective multicentric observational study,” *Ann. Intensive Care*, vol. 10, no. 1, p. 62, May 2020, doi: 10.1186/s13613-020-00668-6.

[51] J.-L. Vincent and M. H. Weil, “Fluid challenge revisited,” *Critical Care Medicine*, vol. 34, no. 5, p. 1333, May 2006, doi: 10.1097/01.CCM.0000214677.76535.A5.

[52] R. D. Berry, “Management of shock in trauma,” *Anaesthesia & Intensive Care Medicine*, vol. 9, no. 9, pp. 390–393, Sep. 2008, doi: 10.1016/j.mpaic.2008.07.006.

[53] D. VanValkinburgh, C. C. Kerndt, and M. F. Hashmi, “Inotropes and Vasopressor,” 2023, Accessed: May 05, 2024. [Online]. Available: https://www.ncbi.nlm.nih.gov/books/NBK482411

[54] M. H. Weil, H. Shubin, and R. Carlson, “Treatment of Circulatory Shock: Use of Sympathomimetic and Related Vasoactive Agents,” *JAMA*, vol. 231, no. 12, pp. 1280–1286, Mar. 1975, doi: 10.1001/jama.1975.03240240050030.

[55] R. J. Beale, S. M. Hollenberg, J.-L. Vincent, and J. E. Parrillo, “Vasopressor and inotropic support in septic shock: An evidence-based review,” *Critical Care Medicine*, vol. 32, no. 11, p. S455, Nov. 2004, doi: 10.1097/01.CCM.0000142909.86238.B1.

[56] R. P. Dellinger *et al.*, “Surviving Sepsis Campaign guidelines for management of severe sepsis and septic shock,” *Critical Care Medicine*, vol. 32, no. 3, p. 858, Mar. 2004, doi: 10.1097/01.CCM.0000117317.18092.E4.

[57] R. K. Kayambankadzanja *et al.*, “Towards definitions of critical illness and critical care using concept analysis,” *BMJ Open*, vol. 12, no. 9, p. e060972, Sep. 2022, doi: 10.1136/bmjopen-2022-060972.

[58] D. M. Maslove *et al.*, “Redefining critical illness,” *Nat Med*, vol. 28, no. 6, pp. 1141–1148, Jun. 2022, doi: 10.1038/s41591-022-01843-x.
[59] A. Garland, K. Olafson, C. D. Ramsey, M. Yogendran, and R. Fransoo, “Epidemiology of critically ill patients in intensive care units: a population-based observational study,” *Crit Care*, vol. 17, no. 5, p. R212, Sep. 2013, doi: 10.1186/cc13026.
[60] “Hemodynamic Monitoring in the Intensive Care Unit - Muller - 2012 - Nutrition in Clinical Practice - Wiley Online Library.” Accessed: Jul. 12, 2024. [Online]. Available: https://aspenjournals.onlinelibrary.wiley.com/doi/10.1177/0884533612443562
[61] A. E. Laher *et al.*, “A review of hemodynamic monitoring techniques, methods and devices for the emergency physician,” *The American Journal of Emergency Medicine*, vol. 35, no. 9, pp. 1335–1347, Sep. 2017, doi: 10.1016/j.ajem.2017.03.036.
[62] E. J. Couture, P. Laferrière-Langlois, and A. Denault, “New Developments in Continuous Hemodynamic Monitoring of the Critically Ill Patient,” *Canadian Journal of Cardiology*, vol. 39, no. 4, pp. 432–443, Apr. 2023, doi: 10.1016/j.cjca.2023.01.012.
[63] “Monitorización hemodinámica integrada: clínica, gasométrica y ecocardiográfica,” *RUC*, vol. 37, Mar. 2021, doi: 10.29277/cardio.38.1.4.
[64] M. R. Pinsky *et al.*, “Effective hemodynamic monitoring,” *Critical Care*, vol. 26, no. 1, p. 294, Sep. 2022, doi: 10.1186/s13054-022-04173-z.
[65] G. de Takats, “Microcirculation: The Third Force,” *JAMA*, vol. 195, no. 4, pp. 302–304, Jan. 1966, doi: 10.1001/jama.1966.03100040108028.
[66] N. E. Hendricks, “The microcirculation,” *Southern African Journal of Anaesthesia and Analgesia*, vol. 26, no. 6, pp. S62-65, Nov. 2020.
[67] B. Fagrell and M. Intaglietta, “Microcirculation: its significance in clinical and molecular medicine,” *Journal of Internal Medicine*, vol. 241, no. 5, pp. 349–362, 1997, doi: 10.1046/j.1365-2796.1997.125148000.x.
[68] A. Bauer, D. Bruegger, and F. Christ, “[Microcirculatory monitoring of sepsis].,” *Der Anaesthesist*, 2005, Accessed: Jul. 12, 2024. [Online]. Available: https://www.semanticscholar.org/paper/%5BMicrocirculatory-monitoring-of-sepsis%5D.-Bauer-Bruegger/aef2d20e9da88ca36ac0bdc6f9cbcb74ff6529fe
[69] C. Liu, H. Gomez, S. Narasimhan, A. Dubrawski, M. R. Pinsky, and B. Zuckerbraun, “Real-time visual analysis of microvascular blood flow for critical care,” in *2015 IEEE Conference on Computer Vision and Pattern Recognition (CVPR)*, Jun. 2015, pp. 2217–2225. doi: 10.1109/CVPR.2015.7298834.
[70] D. De Backer and A. Durand, “Monitoring the microcirculation in critically ill patients,” *Best Practice & Research Clinical Anaesthesiology*, vol. 28, no. 4, pp. 441–451, Dec. 2014, doi: 10.1016/j.bpa.2014.09.005.
[71] D. D. Backer, F. Ricottilli, and G. A. Ospina-Tascón, “Septic shock: a microcirculation disease.,” *Current Opinion in Anaesthesiology*, vol. 34, Feb. 2021, doi: 10.1097/aco.0000000000000957.
[72] D. D. Backer, J. Creteur, M.-J. Dubois, Y. Sakr, and J.-L. Vincent, “Microvascular alterations in patients with acute severe heart failure and cardiogenic shock,” *American Heart Journal*, vol. 147, Dec. 2003, doi: 10.1016/j.ahj.2003.07.006.

[73] D. De Backer, J. Creteur, J.-C. Preiser, M.-J. Dubois, and J.-L. Vincent, “Microvascular Blood Flow Is Altered in Patients with Sepsis,” *Am J Respir Crit Care Med*, vol. 166, no. 1, pp. 98–104, Jul. 2002, doi: 10.1164/rccm.200109-016OC.
[74] A. Kara, S. Akin, and C. Ince, “Monitoring microcirculation in critical illness,” *Current Opinion in Critical Care*, vol. 22, no. 5, p. 444, Oct. 2016, doi: 10.1097/MCC.0000000000000335.
[75] E. Kattan, M. Ibarra-Estrada, G. Hernández, and G. Ospina-Tascón, “Perspectives on peripheral perfusion assessment.,” *Current Opinion in Critical Care*, vol. 29, Apr. 2023, doi: 10.1097/mcc.0000000000001038.
[76] G. Hernández *et al.*, “Effect of a Resuscitation Strategy Targeting Peripheral Perfusion Status vs Serum Lactate Levels on 28-Day Mortality Among Patients With Septic Shock: The ANDROMEDA-SHOCK Randomized Clinical Trial,” *JAMA*, vol. 321, no. 7, pp. 654–664, Feb. 2019, doi: 10.1001/jama.2019.0071.
[77] G. Francony, P. Bouzat, and J.-F. Payen, “Monitorage par spectroscopie de proche infrarouge en neuroréanimation,” *Annales Françaises d’Anesthésie et de Réanimation*, vol. 31, no. 6, pp. e133–e136, Jun. 2012, doi: 10.1016/j.annfar.2012.04.017.
[78] N. S. Ghanayem and G. M. Hoffman, “Near Infrared Spectroscopy as a Hemodynamic Monitor in Critical Illness,” *Pediatric Critical Care Medicine*, vol. 17, no. 8, p. S201, Aug. 2016, doi: 10.1097/PCC.0000000000000780.
[79] A. Lima and J. Bakker, “Near-infrared spectroscopy for monitoring peripheral tissue perfusion in critically ill patients.,” *Revista Brasileira de terapia intensiva*, 2011, Accessed: Jun. 23, 2024. [Online]. Available: https://www.semanticscholar.org/paper/Near-infrared-spectroscopy-for-monitoring-tissue-in-Lima-Bakker/0e35be56b243aa9c1d80b180045126be23ae5df7
[80] M. S. Green, S. Sehgal, and R. Tariq, “Near-Infrared Spectroscopy: The New Must Have Tool in the Intensive Care Unit?,” *Semin Cardiothorac Vasc Anesth*, vol. 20, no. 3, pp. 213–224, Sep. 2016, doi: 10.1177/1089253216644346.
[81] Z. A. Vesoulis, J. P. Mintzer, and V. Y. Chock, “Neonatal NIRS monitoring: recommendations for data capture and review of analytics,” *J Perinatol*, vol. 41, no. 4, pp. 675–688, Apr. 2021, doi: 10.1038/s41372-021-00946-6.
[82] “Optical Absorption of Hemoglobin.” Accessed: Mar. 06, 2025. [Online]. Available: https://omlc.org/spectra/hemoglobin/
[83] H. Owen-Reece, M. Smith, C. E. Elwell, and J. C. Goldstone, “Near infrared spectroscopy,” *British Journal of Anaesthesia*, vol. 82, no. 3, pp. 418–426, Mar. 1999, doi: 10.1093/bja/82.3.418.
[84] G. Strangman, M. A. Franceschini, and D. A. Boas, “Factors affecting the accuracy of near-infrared spectroscopy concentration calculations for focal changes in oxygenation parameters,” *NeuroImage*, vol. 18, no. 4, pp. 865–879, Apr. 2003, doi: 10.1016/S1053-8119(03)00021-1.
[85] P. Rolfe, “In vivo near infra-red spectroscopy instrumentation combining spatially-resolved and intensity modulation techniques,” in *IEEE EMBS Asian-Pacific Conference on Biomedical Engineering, 2003.*, Oct. 2003, pp. 304–305. doi: 10.1109/APBME.2003.1302705.

[86] “PortaMon User Manual,” Artinis Medical Systems, version 06.2019.
[87] S. Takatani and J. Ling, “Optical oximetry sensors for whole blood and tissue,” *IEEE Engineering in Medicine and Biology Magazine*, vol. 13, no. 3, pp. 347–357, Jun. 1994, doi: 10.1109/51.294005.
[88] A. N. S. M.d, S. P. G. M.d, and C. S. R. M.d, “Clinical application of near-infrared spectroscopy in patients with traumatic brain injury: a review of the progress of the field,” *NPh*, vol. 3, no. 3, p. 031409, Apr. 2016, doi: 10.1117/1.NPh.3.3.031409.
[89] M. M. M.d and I. M. M.d, “Review of functional near-infrared spectroscopy in neurorehabilitation,” *NPh*, vol. 3, no. 3, p. 031414, Jul. 2016, doi: 10.1117/1.NPh.3.3.031414.
[90] M. Smith, “Shedding light on the adult brain: a review of the clinical applications of near-infrared spectroscopy,” *Philosophical Transactions of the Royal Society A: Mathematical, Physical and Engineering Sciences*, vol. 369, no. 1955, pp. 4452–4469, Nov. 2011, doi: 10.1098/rsta.2011.0242.
[91] Y. Minagawa-Kawai, “[Current status and future perspectives of near-infrared spectroscopy: clinical applications and neurocognitive findings].,” *Brain and nerve = Shinkei kenkyu no shinpo*, Sep. 2012, Accessed: Jul. 03, 2024. [Online]. Available: https://www.semanticscholar.org/paper/%5BCurrent-status-and-future-perspectives-of-clinical-Minagawa-Kawai/08a02fb909a725db0215d98068a8a406ddb60f85
[92] J. Mesquida, G. Gruartmoner, and C. Espinal, “Skeletal Muscle Oxygen Saturation (StO2) Measured by Near-Infrared Spectroscopy in the Critically Ill Patients,” *BioMed Research International*, vol. 2013, no. 1, p. 502194, 2013, doi: 10.1155/2013/502194.
[93] E. Varis, V. Pettilä, and E. Wilkman, “Near-Infrared Spectroscopy in Adult Circulatory Shock: A Systematic Review,” *J Intensive Care Med*, vol. 35, no. 10, pp. 943–962, Oct. 2020, doi: 10.1177/0885066620907307.
[94] J. M. Kainerstorfer, A. Sassaroli, K. T. Tgavalekos, and S. Fantini, “Cerebral Autoregulation in the Microvasculature Measured with Near-Infrared Spectroscopy,” *J Cereb Blood Flow Metab*, vol. 35, no. 6, pp. 959–966, Jun. 2015, doi: 10.1038/jcbfm.2015.5.
[95] F. A. Zeiler *et al.*, “Continuous cerebrovascular reactivity monitoring in moderate/severe traumatic brain injury: a narrative review of advances in neurocritical care,” *British Journal of Anaesthesia*, vol. 124, no. 4, pp. 440–453, Apr. 2020, doi: 10.1016/j.bja.2019.11.031.
[96] D. Lidington, H. Wan, and S.-S. Bolz, “Cerebral Autoregulation in Subarachnoid Hemorrhage,” *Front. Neurol.*, vol. 12, Jul. 2021, doi: 10.3389/fneur.2021.688362.
[97] F. A. Zeiler, M. Aries, M. Czosnyka, and P. Smielewski, “Cerebral Autoregulation Monitoring in Traumatic Brain Injury: An Overview of Recent Advances in Personalized Medicine,” *Journal of Neurotrauma*, vol. 39, no. 21–22, pp. 1477–1494, Nov. 2022, doi: 10.1089/neu.2022.0217.
[98] D. Hori *et al.*, “Optimal blood pressure during cardiopulmonary bypass defined by cerebral autoregulation monitoring,” *The Journal of Thoracic and Cardiovascular Surgery*, vol. 154, no. 5, pp. 1590-1598.e2, Nov. 2017, doi: 10.1016/j.jtcvs.2017.04.091.

[99] D. S. DeWitt and D. S. Prough, “Cerebral Blood Flow and Blood Pressure: Dependent or Codependent?*,” *Critical Care Medicine*, vol. 47, no. 7, p. 1007, Jul. 2019, doi: 10.1097/CCM.0000000000003784.
[100] N. A. Lassen, “Cerebral Blood Flow and Oxygen Consumption in Man,” *Physiological Reviews*, vol. 39, no. 2, pp. 183–238, Apr. 1959, doi: 10.1152/physrev.1959.39.2.183.
[101] P. Brassard *et al.*, “Losing the dogmatic view of cerebral autoregulation,” *Physiological Reports*, vol. 9, no. 15, p. e14982, 2021, doi: 10.14814/phy2.14982.
[102] C. Small *et al.*, “What are we measuring? A refined look at the process of disrupted autoregulation and the limitations of cerebral perfusion pressure in preventing secondary injury after traumatic brain injury,” *Clin Neurol Neurosurg*, vol. 221, p. 107389, Oct. 2022, doi: 10.1016/j.clineuro.2022.107389.
[103] J. A. H. R. Claassen, D. H. J. Thijssen, R. B. Panerai, and F. M. Faraci, “Regulation of cerebral blood flow in humans: physiology and clinical implications of autoregulation,” *Physiological Reviews*, vol. 101, no. 4, pp. 1487–1559, Oct. 2021, doi: 10.1152/physrev.00022.2020.
[104] M. J. Cipolla, “Regulation of Cerebrovascular Tone,” in *The Cerebral Circulation*, Morgan & Claypool Life Sciences, 2009. Accessed: Feb. 24, 2025. [Online]. Available: https://www.ncbi.nlm.nih.gov/books/NBK53080/
[105] A. Silverman and N. H. Petersen, “Physiology, Cerebral Autoregulation,” in *StatPearls*, Treasure Island (FL): StatPearls Publishing, 2024. Accessed: Jul. 10, 2024. [Online]. Available: http://www.ncbi.nlm.nih.gov/books/NBK553183/
[106] D. D. Vaulina, D. Y. Butko, A. A. Karpov, and M. M. Galagudza, “Neurogenic Regulation of Cerebral Blood Flow,” *J Evol Biochem Phys*, vol. 59, no. 6, pp. 2196–2209, Nov. 2023, doi: 10.1134/S0022093023060236.
[107] Y. Rikitake and J. K. Liao, “Rho GTPases, Statins, and Nitric Oxide,” *Circ Res*, vol. 97, no. 12, pp. 1232–1235, Dec. 2005, doi: 10.1161/01.RES.0000196564.18314.23.
[108] S. Sulhan, K. A. Lyon, L. A. Shapiro, and J. H. Huang, “Neuroinflammation and Blood-Brain Barrier Disruption Following Traumatic Brain Injury: Pathophysiology and Potential Therapeutic Targets,” *Journal of neuroscience research*, vol. 98, no. 1, p. 19, Sep. 2018, doi: 10.1002/jnr.24331.
[109] “Targeting Autoregulation-Guided Cerebral Perfusion Pressure after Traumatic Brain Injury (COGiTATE): A Feasibility Randomized Controlled Clinical Trial | Journal of Neurotrauma.” Accessed: Jul. 11, 2024. [Online]. Available: https://www.liebertpub.com/doi/full/10.1089/neu.2021.0197
[110] L. Meng, Y. Wang, L. Zhang, and D. L. McDonagh, “Heterogeneity and Variability in Pressure Autoregulation of Organ Blood Flow: Lessons Learned Over 100+ Years,” *Critical Care Medicine*, vol. 47, no. 3, p. 436, Mar. 2019, doi: 10.1097/CCM.0000000000003569.
[111] R. A. De Blasi *et al.*, “Microvascular dysfunction and skeletal muscle oxygenation assessed by phase-modulation near-infrared spectroscopy in patients with septic shock,” *Intensive Care Med*, vol. 31, no. 12, pp. 1661–1668, Dec. 2005, doi: 10.1007/s00134-005-2822-y.

[112] A. Subasi, “Chapter 3 - Biomedical Signal Processing Techniques,” *Practical Guide for Biomedical Signals Analysis Using Machine Learning Techniques*, Jan. 2019, doi: 10.1016/b978-0-12-817444-9.00003-9.
[113] A. Braga *et al.*, “Applied Pervasive Patient Timeline in Intensive Care Units,” https://services.igi-global.com/resolvedoi/resolve.aspx?doi=10.4018/978-1-7998-2451-0.ch028. Accessed: Oct. 14, 2024. [Online]. Available: https://www.igi-global.com/gateway/chapter/www.igi-global.com/gateway/chapter/246266
[114] S. Yang *et al.*, “A Novel Continuous Real-Time Vital Signs Viewer for Intensive Care Units: Design and Evaluation Study,” *JMIR Human Factors*, vol. 11, no. 1, p. e46030, Jan. 2024, doi: 10.2196/46030.
[115] R. Liu, “Utilizing fast Fourier transform in the processing of biomedical signals: An analytical approach,” *Theoretical and Natural Science*, vol. 38, Jun. 2024, doi: 10.54254/2753-8818/38/20240589.
[116] J. U. Anugom and A. M. Grigoryan, “Multiresolution signal processing by Fourier transform time-frequency correlation analysis,” in *2006 IEEE Region 5 Conference*, Apr. 2006, pp. 296–301. doi: 10.1109/TPSD.2006.5507413.
[117] D. Toweill, B. Kimberly, S. Lai, B. Goldstein, and K. Sonnenthal, “Linear and nonlinear analysis of hemodynamic signals during sepsis and septic shock.,” *Critical Care Medicine*, vol. 28, Jun. 2000, doi: 10.1097/00003246-200006000-00063.
[118] M. Farge, “WAVELET TRANSFORMS AND THEIR APPLICATIONS TO TURBULENCE,” *Annual Review of Fluid Mechanics*, vol. 24, no. Volume 24, 1992, pp. 395–458, Jan. 1992, doi: 10.1146/annurev.fl.24.010192.002143.
[119] B. Nasih and P. D. Assitant, “Application of Wavelet Transform and Its Advantages Compared To Fourier Transform,” 2016. Accessed: Jul. 11, 2024. [Online]. Available: https://www.semanticscholar.org/paper/Application-of-Wavelet-Transform-and-Its-Advantages-Nasih-Assitant/5fb6976ac9ccf8588b516d34f1a5be59c24e0634
[120] J.-S. Yu, X.-Q. Wang, and X.-D. Chen, “Wavelet Transform in Physiological Signal Analysis: A Survey,” in *2020 Cross Strait Radio Science & Wireless Technology Conference (CSRSWTC)*, Dec. 2020, pp. 1–3. doi: 10.1109/CSRSWTC50769.2020.9372629.
[121] A. Figliola and E. Serrano, “Analysis of physiological time series using wavelet transforms,” *IEEE Engineering in Medicine and Biology Magazine*, vol. 16, no. 3, pp. 74–79, May 1997, doi: 10.1109/51.585521.
[122] S. Brasil, D. J. F. Solla, R. de C. Nogueira, M. J. Teixeira, L. M. S. Malbouisson, and W. da S. Paiva, “A Novel Noninvasive Technique for Intracranial Pressure Waveform Monitoring in Critical Care,” *Journal of Personalized Medicine*, vol. 11, no. 12, Art. no. 12, Dec. 2021, doi: 10.3390/jpm11121302.
[123] H.-W. Yien, S.-S. Hseu, L.-C. Lee, T. B. J. Kuo, T.-Y. Lee, and S. H. H. Chan, “Spectral analysis of systemic arterial pressure and heart rate signals as a prognostic tool for the prediction of patient outcome in the intensive care unit,” *Critical Care Medicine*, vol. 25, no. 2, p. 258, Feb. 1997.
[124] V. Pukhova, E. Gorelova, G. Ferrini, and S. Burnasheva, “Time-frequency representation of signals by wavelet transform,” in *2017 IEEE Conference of Russian*

Young Researchers in Electrical and Electronic Engineering (ElConRus), Feb. 2017, pp. 715–718. doi: 10.1109/EIConRus.2017.7910658.
[125] Z. G. Yin, "The Research of the Spectral Features of Vibration Signals from Underground Railway Based on Wavelet Transform," *Advanced Materials Research*, vol. 243–249, May 2011, doi: 10.4028/www.scientific.net/amr.243-249.3463.
[126] Z. Y. Chen, X. P. Guo, X. L. Zhang, W. J. Cram, and Z. W. Li, "A novel method for analysis of single ion channel signal based on wavelet transform," *Computers in Biology and Medicine*, vol. 37, Sep. 2006, doi: 10.1016/j.compbiomed.2006.08.006.
[127] F. Li, H. Wu, N. Liu, Y. Hu, and B. Wu, "Seismic Time–Frequency Analysis via Adaptive Mode Separation-Based Wavelet Transform," *IEEE Geoscience and Remote Sensing Letters*, vol. 17, Aug. 2019, doi: 10.1109/lgrs.2019.2930583.
[128] R. X. Gao and R. Yan, "Continuous Wavelet Transform," in *Wavelets: Theory and Applications for Manufacturing*, R. X. Gao and R. Yan, Eds., Boston, MA: Springer US, 2011, pp. 33–48. doi: 10.1007/978-1-4419-1545-0_3.
[129] W. K. Ngui, M. S. Leong, L. M. Hee, and A. M. Abdelrhman, "Wavelet Analysis: Mother Wavelet Selection Methods," *Applied Mechanics and Materials*, vol. 393, pp. 953–958, 2013, doi: 10.4028/www.scientific.net/AMM.393.953.
[130] P. S. Addison, "A Review of Wavelet Transform Time–Frequency Methods for NIRS-Based Analysis of Cerebral Autoregulation," *IEEE Reviews in Biomedical Engineering*, vol. 8, pp. 78–85, 2015, doi: 10.1109/RBME.2015.2436978.
[131] V. E. Papaioannou, I. G. Chouvarda, N. K. Maglaveras, and I. A. Pneumatikos, "Temperature variability analysis using wavelets and multiscale entropy in patients with systemic inflammatory response syndrome, sepsis, and septic shock," *Critical Care*, vol. 16, no. 2, p. R51, Mar. 2012, doi: 10.1186/cc11255.
[132] M. Saeed and R. G. Mark, "Multiparameter trend monitoring and intelligent displays using wavelet analysis," in *Computers in Cardiology 2000. Vol.27 (Cat. 00CH37163)*, Sep. 2000, pp. 797–800. doi: 10.1109/CIC.2000.898645.
[133] Z. Li, Y. Wang, Y. Li, Y. Wang, J. Li, and L. Zhang, "Wavelet analysis of cerebral oxygenation signal measured by near infrared spectroscopy in subjects with cerebral infarction," *Microvascular Research*, vol. 80, no. 1, pp. 142–147, Jul. 2010, doi: 10.1016/j.mvr.2010.02.004.
[134] R. Doobay, "ICU Survival guide," *SUNY Upstate Medical University*.
[135] S. L. Hiser, K. Casey, P. Nydahl, C. L. Hodgson, and D. M. Needham, "Intensive care unit acquired weakness and physical rehabilitation in the ICU," *BMJ*, vol. 388, p. e077292, Jan. 2025, doi: 10.1136/bmj-2023-077292.
[136] J. M. Khan *et al.*, "Cerebral autoregulation-based mean arterial pressure targets and delirium in critically ill adults without brain injury: a retrospective cohort study," *Can J Anesth/J Can Anesth*, vol. 71, no. 1, pp. 107–117, Jan. 2024, doi: 10.1007/s12630-023-02609-w.
[137] J. Diedler, E. Santos, S. Poli, and M. Sykora, "Optimal cerebral perfusion pressure in patients with intracerebral hemorrhage: an observational case series," *Critical Care*, vol. 18, no. 2, p. R51, Mar. 2014, doi: 10.1186/cc13796.

[138] J. Duranteau *et al.*, "The future of intensive care: the study of the microcirculation will help to guide our therapies," *Crit Care*, vol. 27, p. 190, May 2023, doi: 10.1186/s13054-023-04474-x.
[139] M. Thanaj, A. J. Chipperfield, and G. F. Clough, "Complexity-Based Analysis of Microvascular Blood Flow in Human Skin," in *Physics of Biological Oscillators*, Springer, Cham, 2021, pp. 291–310. doi: 10.1007/978-3-030-59805-1_19.
[140] J. K. Lee *et al.*, "Cerebrovascular reactivity measured by near-infrared spectroscopy," *Stroke*, vol. 40, no. 5, pp. 1820–1826, May 2009, doi: 10.1161/STROKEAHA.108.536094.
[141] M. J. H. Aries *et al.*, "Continuous determination of optimal cerebral perfusion pressure in traumatic brain injury," *Crit Care Med*, vol. 40, no. 8, pp. 2456–2463, Aug. 2012, doi: 10.1097/CCM.0b013e3182514eb6.
[142] C. Zweifel *et al.*, "Continuous assessment of cerebral autoregulation with near-infrared spectroscopy in adults after subarachnoid hemorrhage," *Stroke*, vol. 41, no. 9, pp. 1963–1968, Sep. 2010, doi: 10.1161/STROKEAHA.109.577320.
[143] L. Froese *et al.*, "Continuous Determination of the Optimal Bispectral Index Value Based on Cerebrovascular Reactivity in Moderate/Severe Traumatic Brain Injury: A Retrospective Observational Cohort Study of a Novel Individualized Sedation Target," *Crit Care Explor*, vol. 4, no. 3, p. e0656, Mar. 2022, doi: 10.1097/CCE.0000000000000656.
[144] L. A. Steiner *et al.*, "Continuous monitoring of cerebrovascular pressure reactivity allows determination of optimal cerebral perfusion pressure in patients with traumatic brain injury," *Crit Care Med*, vol. 30, no. 4, pp. 733–738, Apr. 2002, doi: 10.1097/00003246-200204000-00002.
[145] E. Beqiri *et al.*, "Optimal Cerebral Perfusion Pressure Assessed with a Multi-Window Weighted Approach Adapted for Prospective Use: A Validation Study," *Acta Neurochir Suppl*, vol. 131, pp. 181–185, 2021, doi: 10.1007/978-3-030-59436-7_36.
[146] G. Zhang *et al.*, "Effect of Parametric Variation of Center Frequency and Bandwidth of Morlet Wavelet Transform on Time-Frequency Analysis of Event-Related Potentials," in *Proceedings of 2017 Chinese Intelligent Systems Conference*, Y. Jia, J. Du, and W. Zhang, Eds., Singapore: Springer, 2018, pp. 693–702. doi: 10.1007/978-981-10-6496-8_63.
[147] S.-C. Wooh and K. Veroy, "Time-frequency analysis of broadband dispersive waves using the wavelet transform," *AIP Conference Proceedings*, vol. 509, no. 1, pp. 831–838, May 2000, doi: 10.1063/1.1306132.
[148] D. De Backer *et al.*, "A plea for personalization of the hemodynamic management of septic shock," *Crit Care*, vol. 26, no. 1, Art. no. 1, Dec. 2022, doi: 10.1186/s13054-022-04255-y.
[149] R. Kato and M. R. Pinsky, "Personalizing blood pressure management in septic shock," *Ann. Intensive Care*, vol. 5, no. 1, Art. no. 1, Dec. 2015, doi: 10.1186/s13613-015-0085-5.
[150] "Feasibility of individualised severe traumatic brain injury management using an automated assessment of optimal cerebral perfusion pressure: the COGiTATE phase

II study protocol | BMJ Open." Accessed: Jan. 16, 2025. [Online]. Available: https://bmjopen.bmj.com/content/9/9/e030727.abstract
[151] J. Donnelly *et al.*, "Individualizing Thresholds of Cerebral Perfusion Pressure Using Estimated Limits of Autoregulation," *Critical Care Medicine*, vol. 45, no. 9, p. 1464, Sep. 2017, doi: 10.1097/CCM.0000000000002575.
[152] F. A. Zeiler *et al.*, "Comparison of Performance of Different Optimal Cerebral Perfusion Pressure Parameters for Outcome Prediction in Adult Traumatic Brain Injury: A Collaborative European NeuroTrauma Effectiveness Research in Traumatic Brain Injury (CENTER-TBI) Study," *J Neurotrauma*, vol. 36, no. 10, pp. 1505–1517, May 2019, doi: 10.1089/neu.2018.6182.
[153] P. Bagher and S. S. Segal, "Regulation of blood flow in the microcirculation: role of conducted vasodilation," *Acta Physiologica*, vol. 202, no. 3, pp. 271–284, 2011, doi: 10.1111/j.1748-1716.2010.02244.x.
[154] C. K. Willie, Y.-C. Tzeng, J. A. Fisher, and P. N. Ainslie, "Integrative regulation of human brain blood flow," *The Journal of Physiology*, vol. 592, no. 5, pp. 841–859, 2014, doi: 10.1113/jphysiol.2013.268953.
[155] A. Lima and J. Bakker, "Clinical monitoring of peripheral perfusion: there is more to learn," *Crit Care*, vol. 18, no. 1, Art. no. 1, Feb. 2014, doi: 10.1186/cc13738.
[156] L. Froese *et al.*, "Temporal relationship between vasopressor and sedative administration and cerebrovascular response in traumatic brain injury: a time-series analysis," *ICMx*, vol. 11, no. 1, Art. no. 1, Dec. 2023, doi: 10.1186/s40635-023-00515-5.
[157] D. A. Hartmann, V. Coelho-Santos, and A. Y. Shih, "Pericyte Control of Blood Flow Across Microvascular Zones in the Central Nervous System," *Annual Review of Physiology*, vol. 84, no. Volume 84, 2022, pp. 331–354, Feb. 2022, doi: 10.1146/annurev-physiol-061121-040127.
[158] B. A. MacVicar and E. A. Newman, "Astrocyte Regulation of Blood Flow in the Brain," *Cold Spring Harb Perspect Biol*, vol. 7, no. 5, p. a020388, May 2015, doi: 10.1101/cshperspect.a020388.
[159] D. De Backer, "Is microcirculatory assessment ready for regular use in clinical practice?," *Current Opinion in Critical Care*, vol. 25, no. 3, p. 280, Jun. 2019, doi: 10.1097/MCC.0000000000000605.
[160] Z. Zhang, G. Zhang, H. Goyal, L. Mo, and Y. Hong, "Identification of subclasses of sepsis that showed different clinical outcomes and responses to amount of fluid resuscitation: a latent profile analysis," *Crit Care*, vol. 22, no. 1, p. 347, Dec. 2018, doi: 10.1186/s13054-018-2279-3.
[161] G. Hernandez, A. Bruhn, R. Castro, and T. Regueira, "The holistic view on perfusion monitoring in septic shock," *Current Opinion in Critical Care*, vol. 18, no. 3, p. 280, Jun. 2012, doi: 10.1097/MCC.0b013e3283532c08.
[162] A. Dubin *et al.*, "Increasing arterial blood pressure with norepinephrine does not improve microcirculatory blood flow: a prospective study," *Crit Care*, vol. 13, no. 3, Art. no. 3, Jun. 2009, doi: 10.1186/cc7922.
[163] J.-Y. Xu *et al.*, "A high mean arterial pressure target is associated with improved microcirculation in septic shock patients with previous hypertension: a prospective

open label study," *Crit Care*, vol. 19, no. 1, Art. no. 1, Dec. 2015, doi: 10.1186/s13054-015-0866-0.
[164] E. Kattan *et al.*, "Hemodynamic phenotype-based, capillary refill time-targeted resuscitation in early septic shock: The ANDROMEDA-SHOCK-2 Randomized Clinical Trial study protocol," *Rev. bras. ter. intensiva*, vol. 34, pp. 96–106, Jun. 2022, doi: https://doi.org/10.5935/0103-507X.20220004-en.
[165] W. Huang *et al.*, "Association of Sublingual Microcirculation Parameters and Capillary Refill Time in the Early Phase of ICU Admission*," *Critical Care Medicine*, vol. 51, no. 7, p. 913, Jul. 2023, doi: 10.1097/CCM.0000000000005851.
[166] D. De Backer *et al.*, "Microcirculatory Alterations in Patients With Severe Sepsis: Impact of Time of Assessment and Relationship With Outcome*," *Critical Care Medicine*, vol. 41, no. 3, p. 791, Mar. 2013, doi: 10.1097/CCM.0b013e3182742e8b.
[167] A. S. Neto, V. G. M. Pereira, J. A. Manetta, D. C. Espósito, and M. J. Schultz, "Association between static and dynamic thenar near-infrared spectroscopy and mortality in patients with sepsis: A systematic review and meta-analysis," *Journal of Trauma and Acute Care Surgery*, vol. 76, no. 1, p. 226, Jan. 2014, doi: 10.1097/TA.0b013e3182a9221f.
[168] O. Nardi *et al.*, "Targeting skeletal muscle tissue oxygenation (StO2) in adults with severe sepsis and septic shock: a randomised controlled trial (OTO-StS Study)," *BMJ Open*, vol. 8, no. 3, p. e017581, Mar. 2018, doi: 10.1136/bmjopen-2017-017581.
[169] R. R. Bruno *et al.*, "Direct assessment of microcirculation in shock: a randomized-controlled multicenter study," *Intensive Care Med*, vol. 49, no. 6, pp. 645–655, Jun. 2023, doi: 10.1007/s00134-023-07098-5.
[170] M. P. Hilty, J. Duranteau, J. Montomoli, T. Y.-C. Yeh, and C. Ince, "A microcirculation-guided trial doomed to fail," *Intensive Care Med*, vol. 49, no. 12, pp. 1557–1558, Dec. 2023, doi: 10.1007/s00134-023-07223-4.
[171] H. Yamamura, Y. Kawazoe, K. Miyamoto, T. Yamamoto, Y. Ohta, and T. Morimoto, "Effect of norepinephrine dosage on mortality in patients with septic shock," *j intensive care*, vol. 6, no. 1, Art. no. 1, Dec. 2018, doi: 10.1186/s40560-018-0280-1.
[172] M. W. Dünser *et al.*, "Association of arterial blood pressure and vasopressor load with septic shock mortality: a post hoc analysis of a multicenter trial," *Crit Care*, vol. 13, no. 6, Art. no. 6, Dec. 2009, doi: 10.1186/cc8167.
[173] K. F. Lee, M. D. Wood, D. M. Maslove, J. G. Muscedere, and J. G. Boyd, "Dysfunctional cerebral autoregulation is associated with delirium in critically ill adults," *J Cereb Blood Flow Metab*, vol. 39, no. 12, pp. 2512–2520, Dec. 2019, doi: 10.1177/0271678X18803081.
[174] R. B. Govindan *et al.*, "Comparison of Frequency- and Time-Domain Autoregulation and Vasoreactivity Indices in a Piglet Model of Hypoxia-Ischemia and Hypothermia," *Developmental Neuroscience*, vol. 40, no. 5–6, pp. 547–559, May 2019, doi: 10.1159/000499425.
[175] F. A. Zeiler *et al.*, "Continuous Autoregulatory Indices Derived from Multi-Modal Monitoring: Each One Is Not Like the Other," *Journal of Neurotrauma*, vol. 34, no. 22, pp. 3070–3080, Nov. 2017, doi: 10.1089/neu.2017.5129.